

APPLICATION OF A GLOBAL SOLAR  
WIND/PLANETARY OBSTACLE INTERACTION  
COMPUTATIONAL MODEL: EARTH,  
VENUS, MARS, JUPITER AND SATURN STUDIES

by

Stephen S. Stahara

NEAR TR 322

May 1984

Prepared Under Contract No. NASW-3791

for

NATIONAL AERONAUTICS & SPACE ADMINISTRATION  
Washington, D.C. 20546

by

NIELSEN ENGINEERING & RESEARCH, INC.  
510 Clyde Avenue, Mountain View, CA 94043  
Telephone (415) 968-9457

1. Report No.	2. Government Accession No.	3. Recipient's Catalog No.	
4. Title and Subtitle APPLICATION OF A GLOBAL SOLAR WIND/PLANETARY OBSTACLE INTERACTION COMPUTATIONAL MODEL: EARTH, VENUS, MARS, JUPITER, AND SATURN STUDIES.		5. Report Date May 1984	
		6. Performing Organization Code 850/C	
7. Author(s) Stephen S. Stahara		8. Performing Organization Report No. NEAR TR 322	
		10. Work Unit No.	
9. Performing Organization Name and Address Nielsen Engineering & Research, Inc. 510 Clyde Avenue Mountain View, CA 94043		11. Contract or Grant No. NASW-3791	
		13. Type of Report and Period Covered Contractor Report 6/83 - 6/84	
12. Sponsoring Agency Name and Address National Aeronautics & Space Administration Washington, D.C. 20546		14. Sponsoring Agency Code	
		15. Supplementary Notes	
16. Abstract  A summary report is provided of the work performed under NASA Contract No. NASW-3791. This work relates to a series of collaborative investigations involving the application of a computational model for the determination of the detailed plasma and magnetic field properties associated with the global interaction of the solar wind with various planetary obstacles throughout the solar system. The theoretical method is based on an established single fluid, steady, dissipationless, magneto-hydrodynamic continuum model, and is appropriate for the calculation of supersonic, super-Alfvénic solar wind flow past planetary obstacles. The investigations undertaken relate to studies of various solar wind interaction phenomena with Venus, Earth, Mars, Jupiter, and Saturn. This report provides a concise description of the problems studied, a summary of all the important research results, and copies of the publications.			
17. Key Words (Suggested by Author(s))  Solar wind/planetary interaction Frozen magnetic field		18. Distribution Statement  Unclassified - Unlimited	
19. Security Classif. (of this report) Unclassified	20. Security Classif. (of this page) Unclassified	21. No. of Pages 178	22. Price*

\*For sale by the National Technical Information Service, Springfield, Virginia 22161

## TABLE OF CONTENTS

<u>Section</u>	<u>Page</u>
SUMMARY	1
1.0 INTRODUCTION	2
2.0 STATEMENT OF PROBLEMS INVESTIGATED	2
3.0 SUMMARY OF RESEARCH RESULTS	3
3.1 Terrestrial Planet Applications - Venus, Earth and Mars	3
3.2 Outer Planet Applications - Jupiter and Saturn	7
3.3 References	9
4.0 PUBLICATIONS LIST	10
APPENDIX	A

APPLICATION OF A GLOBAL SOLAR WIND/PLANETARY  
OBSTACLE INTERACTION COMPUTATIONAL MODEL:  
EARTH, VENUS, MARS, JUPITER, AND SATURN STUDIES

SUMMARY

A summary report is provided of the work performed under NASA Contract No. NASW-3791. This work relates to a series of collaborative investigations involving the application of a computational model for the determination of the detailed plasma and magnetic field properties associated with the global interaction of the solar wind with various planetary obstacles throughout the solar system. The theoretical method is based on an established single fluid, steady, dissipationless, magnetohydrodynamic continuum model, and is appropriate for the calculation of supersonic, super-Alfvénic solar wind flow past planetary obstacles. The investigations undertaken relate to studies of various solar wind interaction phenomena with Venus, Earth, Mars, Jupiter, and Saturn. This report provides a concise description of the problems studied, a summary of all the important research results, and copies of the publications.

## 1. INTRODUCTION

This is the final summary report under Contract No. NASW-3791 for the National Aeronautics and Space Administration. All of the important results from the research performed under this contract have been reported in the open literature, both in scientific journals and as technical papers at scientific meetings with appropriate acknowledgement of NASA support. This summary report provides a description of the problems studied, a summary of the most important results obtained, and a reference list and copies of all publications resulting from the research.

## 2. STATEMENT OF PROBLEMS INVESTIGATED

The problems toward which the research under this contract was directed involved the application of a previously developed computational model (references 1-3) capable of determining the detailed plasma and magnetic field properties in the magnetosheath region associated with the three-dimensional global interaction of the solar wind with various planetary obstacles throughout the solar system. A series of collaborative investigations were undertaken which used the model to provide a theoretical understanding of various solar wind interaction phenomena.

The theoretical method employed is based on an established, continuum, single fluid, steady, dissipationless magnetohydrodynamic model that is appropriate for the calculation of supersonic, super-Alfvénic solar wind flow past magneto/ionopause obstacle shapes typical of terrestrial planets. The overall objective was the enablement of rational quantitative modeling studies to be performed on different interaction phenomena related to the global solar wind interaction problem with the planetary obstacles associated with Venus, Earth, Mars, Jupiter, and Saturn. Predictive results from the model enable the

investigation of plasma and field properties in the interaction region in a detail heretofore impossible, and thereby provide the necessary theoretical comparative basis for interpreting the observations.

A series of eight investigations were undertaken as follows:

- Distant planetary Mach cone and bow shock studies for Venus, Earth, and Mars
- Magnetospheric source of energetic particles upstream of Earth's bow shock.
- Locations of magnetic field merging sites on the Earth's magnetopause
- Asymmetries in magnetic field merging sites on the Earth's magnetopause.
- Magnetic field draping on the Earth's magnetopause.
- Intrinsic magnetic field of Mars
- Venusian ionopause studies
- Bow shock studies of Jupiter and Saturn.

### 3. SUMMARY OF RESEARCH RESULTS

#### 3.1 Terrestrial Planet Applications - Venus, Earth and Mars

With regard to terrestrial planetary applications of the model, a series of seven collaborative investigations were undertaken with other space scientists in which theoretical

predictions from the present models were employed to interpret observational plasma and field results and to augment other theoretical analyses. These studies are described below.

An investigation, made with Dr. J. A. Slavin of J.P.L. and Professor R. E. Holzer of the Institute of Geophysics and Planetary Physics, U.C.L.A., employed the flow field predictive capability of the model to investigate the asymptotic behavior of planetary Mach cones. Mach cone angles determined from observational distant bow shock shapes and positions for solar wind flows past Venus, Earth, and Mars were compared in reference 4 with far downstream predictions from the gas dynamic model. The results verified that the model, which is already known to predict good results in regions ahead of and up to the terminator, also yields good results downstream beyond the terminator to certain distances for each the planets. These downstream distances were found to be  $-4 R_{Ob}$  at Venus,  $-6 R_{Ob}$  at Earth, and  $-10 R_{Ob}$  at Mars, where  $R_{Ob}$  denotes the particular obstacle nose radius.

For each of the planets discrepancies appear farther downstream of these points, however, presumably due to the difference between the MHD fast mode Mach number and the sonic Mach number inherent in the present gas dynamic model. The tendency to achieve better agreement between gasdynamic theory and observation at larger downstream distances for these various obstacles as the planetary distance from the sun increases (i.e., Venus, Earth, Mars) is attributed to the increase in accuracy of the gas dynamic approximation with decreasing IMF strength. These results suggest that gas dynamic theory predictions for far downstream flows about planetary obstacles will be very accurate for flows past the large bodies (Jupiter, Saturn) in the outer solar system.

A series of collaborative efforts were next carried out which focused primarily on employing the magnetic field predictive capability of the present model to study a variety of

different solar wind magnetic interaction phenomena. These studies were carried out in collaboration mainly with Dr. J. G. Luhmann, Professor C. T. Russell, and Dr. N. U. Crooker of the Institute of Geophysics and Planetary Studies, U.C.L.A.

In reference 5 a study was made of the magnetospheric source of energetic particles observed upstream of the Earth's bow shock. Calculations were performed in which those magnetosheath field lines predicted by the model to drape over the magnetopause were traced from the magnetopause to the bow shock. This was done to locate regions at the shock that should be populated with magnetospheric particles. Subsets of those fields lines that connect to potential sites of magnetic merging on the magnetopause were also traced in the event that leakage occurs preferentially where normal components of the field are present across the boundary.

In reference 6 the predictive model was employed to investigate patterns of magnetic field merging sites on the Earth's magnetopause. Predictions of the magnetospheric field based on the Hedgecock and Thomas model and predictions of the magnetosheath field based on the current model were used to determine the relative orientations between the two fields at locations in the vicinity of the dayside magnetopause. Areas on the magnetopause with various degrees of antiparallelness between the two fields for various orientations of the IMF were obtained for the purpose of locating potential field merging sites and displayed as contour diagrams. The results suggest that large fractions of the magnetopause surface are suitable for merging for IMF's that are primarily southward or radial in direction.

In reference 7 a study was made of asymmetries in magnetic field merging sites for the Earth's magnetopause. Employing the same ideas as developed in reference 6, the model was employed to investigate, as a function of IMF orientation, the degree of asymmetry induced in merging site locations on the magnetopause. These regions where the draped magnetosheath magnetic

field is nearly antiparallel to the model geomagnetic field are shown to be asymmetric for an interplanetary magnetic field (IMF) at the garden hose angle, as suggested by Heelis. When the IMF has a southward component, the asymmetry favors the dawn region for both IMF polarities. The dusk region is favored when the IMF has a northward component. If the regions of antiparallel fields are assumed to be sites of maximum magnetic merging, then the asymmetry is consistent with observed seasonal variations of geomagnetic activity and with dawn-displaced magnetospheric phenomena. In the alternate merging geometry of a line passing through the subsolar region, the asymmetry is predominantly north-south rather than dawn-dusk. Merging line geometry is consistent with the seasonal variations but not with the dawn-displaced phenomena. However, in view of available direct observations of merging signatures in the subsolar region, it is suggested that merging sites may be determined by some combination of the antiparallel and merging line hypotheses.

In reference 8 the model was employed to study magnetic field draping against the Earth's dayside magnetopause. Interplanetary magnetic fields observed upstream of Earth's magnetosphere at ISEE 3 provided input to the model. Model results near the magnetopause were compared with appropriately lagged observations at ISEE 1. In 16 of 24 cases, the angle between the transverse component of the model and observed fields is less than  $20^\circ$ . The agreement is surprisingly good in view of the uncertainty introduced by the large distances between ISEE 1 and ISEE 3. The results indicate that magnetohydrodynamic and energy transfer processes at the magnetopause do not cause large distortions of the magnetosheath magnetic field. In addition, a comparison between observed and model field magnitudes indicates that immediately outside the magnetopause the observed field behaves like the model field at a distance of  $0.5 R_E$  from the magnetopause, outside the region where magnetohydrodynamic effects made the gasdynamic model inapplicable. Patterns of model magnetic field orientation at the magnetopause are presented for practical application.

In reference 9 the predictive model was employed to investigate the continuing question of whether the Mars-3 spacecraft observation of January 21, 1982 was of a Martian magnetosphere or of a compressed IMF in the magnetosheath. In this study, the gas dynamic model was first employed to generate the global flow field. Then the magnetic field computational module was repeatedly employed to investigate whether an appropriate IMF could be determined which would produce the same time history variation of magnetic field that was observed. Based upon the results, it was found that a good simulation of the observed magnetic variation could be made purely on the basis of a magnetosheath field without invoking an entry into a putative Martian magnetosphere to explain the observations.

A final terrestrial planet collaborative study is underway involving Dr. William Knudsen of Lockheed Palo Alto Research Laboratories regarding Pioneer-Venus velocity potential analyzer observations and interpretations of the Venusian ionopause boundary shape. The present model is being employed to examine a more accurate shape determination of the Venusian ionopause based on measured ionospheric properties at axial locations from the subsolar point downstream beyond the terminator and into the wake region. Employment of the flow field predictive capability of the model to provide details of the plasma and magnetic field properties in those regions near the ionopause is essential for understanding the shape of the boundary and the key physical phenomena present in the data. Presently, flowfield determinations from the model have been made for a series of new and different ionopause shapes.

### 3.2 Outer Planet Applications - Jupiter and Saturn

In reference 10, a study was made with Drs. J. A. Slavin and E. J. Smith of J.P.L. employing the flow field predictive capability of the present model to provide the theoretical basis

of an examination of solar wind flows past Jupiter and Saturn. The model was applied to study the mean bow shock shapes and positions for solar wind flows past these planets. Observations from Pioneers 10, 11 and Voyagers 1, 2 were used to characterize the solar wind conditions near the orbits of Jupiter and Saturn and create pressure corrected models of their bow shock and magnetopause surfaces. The present computational model was then applied to examine bow shock location. The results, based upon typical oncoming solar wind Mach numbers for the outer solar system, indicated that the subsolar Jovian and Saturnian magnetosheaths are, respectively, 45% and 20% thinner than predicted. It is suggested that the most plausible cause for this result is the polar flattening of these magnetospheres which is not accounted for in the present axisymmetric flow field model.

### 3.3 References

1. Stahara, S. S., Klenke, D., Trudinger, B. C., and Spreiter, J. R.: Application of Advanced Computational Procedures for Modeling Solar-Wind Interactions with Venus - Theory and Computer Code. NASA CR 3267, May 1980.
2. Spreiter, J. R. and Stahara, S. S.: A New Predictive Model for Determining Solar Wind - Terrestrial Planet Interactions. Journal of Geophysics Research, Vol. 85, No. A12, pp. 6769-6777, December 1, 1980.
3. Spreiter, J. R. and Stahara, S. S.: Solar Wind Past Venus: Theory and Comparisons. Journal of Geophysics Research, Vol. 85, No. A13, pp. 7715-7738, December 30, 1980.
4. Slavin, J. A., Holzer, R. E., Spreiter, J. R., and Stahara, S. S.: Planetary Mach Cones: Theory and Observation. Accepted for publication by Journal of Geophysics Research.
5. Luhmann, J. G., Walker, R. J., Russell, C. T., Crooker, N. U., Spreiter, J. R., Stahara, S. S., and Williams, D. J.: Characteristics of the Magnetospheric Source of Interplanetary Energetic Particles. Institute of Geophysics and Planetary Physics, U.C.L.A. Publication No. 2442, May 1983. Accepted for publication by Journal of Geophysics Research.
6. Luhmann, J. G., Walker, R. J., Russell, C. T., Crooker, N. U., Spreiter, J. R., and Stahara, S. S.: Patterns of Magnetic Field Merging Sites on the Magnetopause. Institute of Geophysics and Planetary Physics, U.C.L.A. Publication No. 2443, May 1983. Accepted for publication by Journal of Geophysics Research.
7. Crooker, N. U., Luhmann, J. G., Spreiter, J. R., and Stahara, S. S.: Magnetopause Merging Site Asymmetries, Institute of Geophysics and Planetary Physics, U.C.L.A. Publication, March 1984. Submitted to Journal of Geophysics Research.
8. Crooker, N. U., Luhmann, J. G., Russell, C. T., Smith, E. J., Spreiter, J.R., and Stahara, S.S.: Magnetic Field Draping Against the Dayside Magnetopause. Institute of Geophysics and Planetary Physics, U.C.L.A. Publication, March 1984. Submitted to Journal of Geophysics Research.
9. Russell, C. T., Luhmann, J. G., Spreiter, J. R., and Stahara, S. S.: The Magnetic Field of Mars: Implications from Gas Dynamic Modeling. Institute of Geophysics and Planetary Physics, U.C.L.A. Publication No. 2468, July 1983. Accepted for publication by Journal of Geophysics Research.

10. Slavin, J. A., Smith, E. J., Spreiter, J. R., and Stahara, S. S.: Solar Wind Flow Past the Outer Planets: Gas Dynamic Modeling of the Jupiter and Saturn Bow Shocks. Submitted to Journal of Geophysics Research.

#### 4. PUBLICATIONS LIST

1. Slavin, J.A., Holzer, R. E., Spreiter, J. R., and Stahara, S.S.: Planetary Mach Cones: Theory and Observation. Accepted for publication by Journal of Geophysics Research.
2. Luhmann, J. G., Walker, R. J., Russell, C. T., Crooker, N. U., Spreiter, J. R., Stahara, S. S., and Williams, D. J.: Characteristics of the Magnetospheric Source of Interplanetary Energetic Particles. Institute of Geophysics and Planetary Physics, U.C.L.A. Publication No. 2442, May 1983. Accepted for publication by Journal of Geophysics Research.
3. Luhmann, J. G., Walker, R. J., Russell, C. T., Crooker, N. U., Spreiter, J. R., and Stahara, S. S.: Patterns of Magnetic Field Merging Sites on the Magnetopause. Institute of Geophysics and Planetary Physics, U.C.L.A. Publication No. 2443, May 1983. Accepted for publication by Journal of Geophysics Research.
4. Crooker, N. U., Luhmann, J. G., Spreiter, J. R., and Stahara, S. S.: Magnetopause Merging Site Asymmetries, Institute of Geophysics and Planetary Physics, U.C.L.A. Publication, March 1984. Submitted to Journal of Geophysics Research.
5. Crooker, N. U., Luhmann, J. G., Russell, C. T., Smith, E. J., Spreiter, J.R., and Stahara, S.S.: Magnetic Field Draping Against the Dayside Magnetopause. Institute of Geophysics and Planetary Physics, U.C.L.A. Publication, March 1984. Submitted to Journal of Geophysics Research.
6. Russell, C. T., Luhmann, J. G., Spreiter, J. R., and Stahara, S. S.: The Magnetic Field of Mars: Implications from Gas Dynamic Modeling. Institute of Geophysics and Planetary Physics, U.C.L.A. Publication No. 2468, July 1983. Accepted for publication by Journal of Geophysics Research.
7. Slavin, J. A., Smith, E. J., Spreiter, J. R., and Stahara, S. S.: Solar Wind Flow Past the Outer Planets: Gas Dynamic Modeling of the Jupiter and Saturn Bow Shocks. Submitted to Journal of Geophysics Research.

APPENDIX

COPIES OF PUBLICATIONS

APPENDIX

TABLE OF CONTENTS

	<u>Page</u>
Planetary Mach Cones: Theory and Observation	A-1
Patterns of Magnetic Field Merging Sites on the Magnetopause	A-24
Characteristics of the Magnetospheric Source	A-33
Magnetopause Merging Site Asymmetries	A-51
Magnetic Field Draping Against the Dayside Magnetopause	A-74
The Magnetic Field of Mars: Implications from Gasdynamic Modeling	A-92
Gasdynamic Modeling of the Jupiter and Saturn Bow Shocks: Solar Wind Flow About the Outer Planets	A-116

PLANETARY MACH CONES: THEORY AND OBSERVATION

J.A. Slavin<sup>1</sup>, R.E. Holzer<sup>2</sup>, J.R. Spreiter<sup>3</sup>, and S.S. Stahara<sup>4</sup>

Submitted to J. Geophys. Res.

July, 1983

Revised October, 1983

<sup>1</sup> Jet Propulsion Laboratory, California Institute of Technology,  
Pasadena, CA 91109

<sup>2</sup> Institute of Geophysics and Planetary Physics, University of  
California, Los Angeles, CA 90024

<sup>3</sup> Division of Applied Mechanics, Stanford University, Stanford,  
CA 94305

<sup>4</sup> Nielsen Engineering and Research, Mountain View, CA 94035

## ABSTRACT

This study uses observations by a number of spacecraft to investigate the asymptotic behavior of planetary bow shocks. Toward this end a single standard method has been used to model distant bow shock position and shape. Mach cone angles of  $13.9 \pm 2^\circ$ ,  $11.4 \pm 3^\circ$ , and  $8.1 \pm 4^\circ$  at Venus, Earth, and Mars, respectively, were determined from the observational shock models. These cone angles and their decrease with growing distance from the sun are generally consistent with downstream bow shock position being limited by the MHD fast mode Mach number. Gasdynamic solutions for solar wind flow about Venus, Earth, and Mars were computed up to  $50 R_{OB}$  (i.e. obstacle radii) behind each planet and compared with observed bow shock location. In each case the position of the shock was well predicted up to a certain distance downstream:  $-4 R_{OB}$  at Venus,  $-6 R_{OB}$  at Earth, and  $-10 R_{OB}$  at Mars. Beyond this point the observed shock position lies farther from the aberrated sun-planet line than the gasdynamic model with the discrepancy greatest at Venus and least at Mars. The better agreement between gasdynamic theory and observation with growing distance from the sun is attributed to an increase in the accuracy of the gasdynamic approximation with decreasing IMF strength.

## Introduction

Previous studies (Fairfield, 1971; Slavin et al., 1983) have shown that the position and shape of planetary bow shocks forward of about one obstacle radius behind the planet are well predicted by single fluid gasdynamic theory (Spreiter et al., 1966; Dryer and Faye-Petersen, 1966; Spreiter and Stahara, 1980). In these theoretical models the presence of the interplanetary magnetic field is neglected on the grounds of its smallness in the sense  $M_A^2 = v^2 / (B^2 / 8\pi) \approx 100$ . The flow field is then completely determined by upstream sonic Mach number,  $M_s$ , adiabatic exponent,  $\gamma$ , and the obstacle shape/position.

While this approach is mathematically valid in the large Alfvén Mach number limit as an approximation to the MHD equations, the requirement that the ambient magnetic field be negligible is not met everywhere. For example, investigations of the regions just exterior to the Venus ionopause (Elphic et al., 1980), Earth magnetopause (Crooker et al., 1979), and Saturn magnetopause (Smith et al., 1980; Slavin et al., 1982) have discovered a thin layer of compressed magnetic field adjacent to these obstacles from which the solar wind plasma has been lost via field aligned flows. These layers are not present in gasdynamic theory, but were predicted by one dimensional (Lees, 1964) and quasi-two dimensional (Zwan and Wolf, 1976) MHD studies of the stagnation region.

Another place where the gasdynamic approximation may be a poor representation is near the distant downstream bow shock. In this region the characteristic lines start to approach the shock at small angles, as shown in Figure 1, indicating that the shock is approaching its "Mach cone" limit (e.g. Landau and Lifshitz, 1959; Spreiter et al., 1966). While the effect of the magnetic field on the downstream flow is small at any given point, the differences between the gasdynamic and magnetohydrodynamic characteristics can accumulate by the time they intersect the distant shock. The result is a fast mode MHD Mach cone that may be significantly larger than the gasdynamic sonic Mach cone.

This study investigates the asymptotic behavior of planetary bow shocks and the ability of gasdynamic theory to describe it. Spacecraft observations at Venus, Earth, and Mars are used to model the shapes and positions of their distant bow waves. The measured planetary Mach cone angles are compared with the mean sonic and MHD fast wave Mach numbers at 0.7, 1.0, and 1.5 AU to assess the downstream influence of the interplanetary magnetic field. Finally, numerical gasdynamic flow solutions extending to 50 obstacle radii behind each planet are obtained and tested against the observed location of the downstream bow shock.

## Modeling Bow Shock Position

The bow shocks of Venus and Mars have been modeled using the three parameter second order method of Slavin et al. (1980) and Slavin and Holzer (1981). The terrestrial shock was not modeled because the techniques applied by Fairfield (1971) have already been shown to be largely equivalent to those employed here (Slavin and Holzer, 1981). The fitting parameters are the surface eccentricity,  $\epsilon$ , the semi-latus

rectum,  $L$ , and the location of the focus along the  $x'$  axis,  $x_0$ . The shock itself is assumed to possess cylindrical symmetry about the solar wind direction which is taken to be opposite the aberrated planet centered solar ecliptic  $x$  axis (i.e.  $\vec{V}_{sw}/|V_{sw}| = -\hat{x}'$ ). All modeling is performed in the aberrated coordinates using either in situ solar wind speed or a mean value of 430 km/sec. A more detailed discussion of this modeling method in comparison with other possible approaches is contained in Slavin and Holzer (1981).

The near planet bow shock has been found previously to be highly symmetric about the  $x'$  direction in agreement with the predictions of gasdynamic for flow about an axisymmetric obstacle (Slavin et al., 1980; Slavin and Holzer, 1981; Tatrallyay et al., 1983). Farther downstream the asymmetric nature of the MHD fast wave Mach cone may become significant. However, the effect should be small for most solar wind conditions and there are too few distant shock observations to model this region as a function of the upstream IMF orientation. Uncertainties introduced by our assumption of cylindrical symmetry for the downstream shock will be discussed in a later section.

The equation for a second order model surface in polar form is (see Slavin and Holzer, 1981)

$$r = L/(1 + \epsilon \cos \theta) \quad (1)$$

where  $r$  is radial distance from the focus (i.e.  $x' = x_0$ ) and  $\theta$  is measured about the focus from the positive  $x'$  axis direction. When the eccentricity in (1) is greater than unity, as is usually the situation for studies of the distant shock, the resultant curve is a hyperbola. For any hyperbola asymptotes exist which bound its position and correspond to the shock wave's Mach cone. They depend only upon the eccentricity and yield an expression for experimentally determined Mach cone angle

$$\alpha_{OBS} = \tan^{-1}((\epsilon^2 - 1)^{1/2}) \quad (2)$$

This expression can be differentiated to obtain the uncertainty in Mach cone angle as a function of the error in the model eccentricity

$$\delta \alpha_{OBS} = (\delta \epsilon / \epsilon) / (\epsilon^2 - 1)^{1/2} \quad (3)$$

Figure 2 displays typical orbits for Venera 9,10 and the Pioneer Venus Orbiter, PVO, in relationship to an extrapolated near planet model surface (Slavin et al., 1980). While PVO provides some excellent coverage of the forward shock when periapsis is on the nightside, it is a poor source of information on the location of the distant bow wave because of its tendency to parallel the shock (Slavin and Holzer, 1981; Tatrallyay et al., 1983). Small variations in the flare angle of the shock appear in the PVO observations as boundary crossings at larger or smaller values of the  $x'$  coordinate. The result is a model surface which tends to follow the spacecraft trajectory. For this reason we have not used the PVO observations in modeling the downstream Venus shock. The lower inclination and less eccentric nature of their orbits make the Venera 9 and 10 shock crossings (Smirnov et al., 1980) better

suited for modeling the distant Venus shock. Near planet shock crossings by Pioneer Venus were not included because of the solar cycle variations in the altitude of the forward Cytherean shock discovered by Slavin et al. (1979;1980). With the exception of the Mariner 5 and Venera 4,6 crossings, the Venus bow shock model produced by this study is based on solar minimum measurements.

In  $1/r, \cos(\theta)$  coordinates centered on the geometric focus, second order curves become straight lines (see equation 1) and linear least square fitting techniques may be applied. Figure 3 displays Mariner 5 (Bridge et al., 1967; Russell, 1977), Venera 4 and 6 (Gringauz et al., 1970), Mariner 10 (Bridge et al., 1974; Russell, 1977), and Venera 9 and 10 (Smirnov et al., 1980) bow shock crossings in these "conic" coordinates along with a least square best fit. Despite the goodness of the fit there is a clear tendency for the distribution of points to curve over below  $\cos(\theta) = -0.5$  and above  $+0.5$ . The focus location on the  $x'$  axis was then systematically varied until the root-mean-square deviation of the crossings measured normal to the best fit surface was minimized. Figure 4 plots the Venus crossings in the conic coordinates again, but with the focus now centered on the optimum  $x_0 = +0.45 R_V$ . The rms deviation in  $x', (y'^2 + z'^2)^{1/2}$  space is decreased by a factor of 2.6 in going from  $x_0 = 0$  to  $x_0 = 0.45 R_V$ . Figure 5 displays the shock crossings and best fit model surface in the more usual aberrated cylindrical coordinates. The uncertainties in the model eccentricity and semi-latus rectum are approximately  $\pm 1\%$ . This is somewhat less than was found for the near planet Venera 9,10 and Pioneer Venus models by Slavin and Holzer (1981) because the inclusion the downstream observations permits less variation in the fitting parameters. The Mach cone determined from our shock model and equations (2) and (3) is  $13.9^\circ \pm 2^\circ$ . To test the sensitivity of our modeling to data selection and modeling techniques, we have calculated Mach cone angles from two other Venus shock modeling studies. Given the results of our error analysis, there is reasonable agreement between the  $13.9^\circ \pm 2^\circ$  obtained in this study and the  $10.8^\circ$  and  $15.4^\circ$  cone angles implied by the Pioneer Venus models of Tatrallyay et al. (1983) and Venera 9,10 shock surfaces generated by Smirnov et al. (1980). The next section will compare this result to the sonic and MHD Mach cones expected on the basis of average solar wind parameters.

Observations of the terrestrial bow shock downstream of  $x' = -60 R_e$  have been made by only a few missions: Explorer 33 (Howe and Binsack, 1972; Mihalov, 1974), Pioneer 7 (Villante, 1976), and Pioneer 8 (Bavassano et al., 1971). The shock crossings in the better sampled  $x' > -60 R_e$  region have been modeled by Fairfield (1971) with a second order method comparable to the procedure employed here. As discussed in Slavin and Holzer (1981), the Fairfield best fit to the aberrated shock data was a hyperbola with  $\Sigma = 1.02$ ,  $L = 22.3 R_e$ , and  $x_0 = +3.4 R_e$ . The corresponding Mach cone angle is  $11.4^\circ \pm 3^\circ$  (assuming  $\pm 1\%$  fitting errors) or  $2.5^\circ$  less than observed for Venus. The only other model of the distant shock is that of Howe and Binsack (1972) derived from Explorer 33 and 35 observations up to  $120 R_e$  behind the earth. The modeling method used in that study was never fully discussed and the fit to their data shows a clear tendency to underestimate the altitude of the forward shock. The result is a  $17.7^\circ$  cone angle which is greater than any of the other planetary Mach cones derived from surface models. It

corresponds to a solar wind Mach number of only 3.3 which is about half of the smallest solar wind Mach numbers in Table 1. Large cone angles of about  $20^\circ$  (i.e. Mach numbers of 3) were also inferred from shock normal studies conducted on the Pioneer 7,8 distant shock encounters by Villante (1976) and Bavassano et al. (1971). However, the determination of shock normals from the observed jump conditions can be subject to large errors (Russell et al., 1983), particularly when the shocks are weak as was the case for the distant crossings of Pioneer 7,8. In addition, the trajectories of these slow moving spacecraft (i.e. relative to the size of the downstream shock and time scales for shock motion) may have favored shock encounters during intervals of lower than average solar wind Mach number. For these reasons we have chosen to use the bow shock model and associated cone angle of Fairfield (1971) for the comparisons to be made in this study.

The Martian bow shock has been observed by the ~~Mariner 2,3~~ Mars 2,3, and 5 orbiters, and the Mariner 4 fly-by (see reviews by Intriligator and Smith, 1979; Russell, 1979; Gringauz, 1980; Slavin and Holzer, 1982). Sample trajectories for the three Soviet orbiters are displayed in Figure 6 along with the locations at which they crossed the Martian bow shock. While the Mars 2,3 orbits parallel the downstream shock surface, the more perpendicular crossings of Mars 5 at about  $x' = -5 R_{OB}$  allow us to model the distant shock. Mariner 4 also provides an additional shock encounter at approximately twice that distance (Smith, 1969). Normally, a single crossing at such a large distance would be excluded due to the great leverage it could exert on the best fit. In this case, however, the differences in eccentricity between the final fits obtained with and without the Mariner 4 crossings were small.

Figure 7 displays our best fit to all of the Mars shock encounters. The shape and location of the model surface is well determined with  $\epsilon = 1.01 (\pm 1\%)$ ,  $L = 1.68 R_{MS} (\pm 1\%)$ , and  $x_0 = +0.7 R_{MS}$ . The Mach cone angle is  $8.1^\circ \pm 4^\circ$  which is  $3.3^\circ$  less than the Earth value and  $5.8^\circ$  degrees below the Venus result. No other Martian shock model using observations from all four of these missions has been published. However, comparison with the Bogdanov and Vaisberg (1975) Mars 2,3 and Mariner 4 model demonstrates the importance of the Mars 5 crossings. In the absence of the intermediate distance Mars 5 shock data, their model eccentricity was approximately 7% larger and far more uncertain than determined here.

### Mach Cone Angles

Table 1 compares the Mach cone angles at Venus, Earth, and Mars determined in the preceding section with conditions in the interplanetary medium. In particular, the radial scalings for solar wind sonic and Alfvénic Mach number discussed in Slavin and Holzer (1981) have been adopted and the 0.7, 1.0, and 1.5 AU values listed. These numbers are average values based on observations made between the late 1960's and mid-1970's. While probably not optimum for all of the shock models generated in this study, most of the shock and solar wind observations took place during the "flat" portion of solar cycle 20 which saw little long term variation in the mean solar wind conditions (e.g. Slavin and Smith, 1983). The uncertainty in these average solar wind Mach cones is estimated to be less than  $0.5^\circ$ .

The limiting Mach cone angle in gasdynamic theory is that associated with the sonic wave speed

$$\alpha_s = \sin^{-1}(1/M_s) \quad (4)$$

Following Table 1, as mean sonic Mach number increases from 6.6 to 7.9 the cone angle decreases from  $8.7^\circ$  at 0.7 AU to  $7.3^\circ$  near 1.5 AU. While no general three dimensional MHD solutions for flow about a blunt obstacle have been found (Shen, 1972; Spreiter and Rizzi, 1974), Mach cone type arguments using the MHD fast wave speed may be applied to predict asymptotic bow shock position in MHD theory (Michel, 1965). Unlike the situation for compressional disturbances in an unmagnetized isotropic plasma, fast mode wave speed is a function of propagation direction relative to the ambient magnetic field. The fast mode propagates faster perpendicular to B than parallel to it. Mach number based on the perpendicular fast mode speed is (Spreiter et al., 1966)

$$M_{ms} = M_A M_s / (M_A^2 + M_s^2)^{1/2} \quad (5)$$

with an associated Mach cone angle

$$\alpha_\perp = \sin^{-1}((M_A^2 + M_s^2)^{1/2} / M_A M_s) \quad (6)$$

Since the perpendicular fast mode speed is significantly larger than the sonic speed, the  $\alpha_\perp$  values are  $2-3^\circ$  greater than  $\alpha_s$  as shown in Table 1. The parallel fast mode propagation speed is the greater of the sonic and Alfvén speeds. Hence, the parallel MHD Mach number,  $M_{ms\parallel}$ , is simply equal to  $M_s$  due to the average  $M_A > M_s$  conditions in the solar wind. At oblique propagation angles the fast mode speed lies in between the  $0^\circ$  and  $90^\circ$  values listed in the table. Thus, for any given  $M_s$  and  $M_A$  the minimum and maximum Mach cone angles for all orientations of the IMF are given by  $\alpha_s$  and  $\alpha_\perp$ .

A third MHD Mach number appropriate to intervals when the the IMF and solar wind velocity vectors are aligned also exists (Dryer and Heckman; 1967; Shen, 1972; Spreiter and Rizzi, 1974)

$$M_* = M_A M_s / (M_A^2 + M_s^2 - 1)^{1/2} \quad (7)$$

Since the field is everywhere parallel to the flow in this case, the Mach cone is symmetric about the upstream flow direction as in gasdynamics. In fact, the MHD equations for aligned flow can be reduced to those of gasdynamics and solved using the same techniques (Spreiter and Rizzi, 1974). Numerically,  $M_*$  is nearly identical in magnitude to  $M_{ms\perp}$  and will not be considered further here due to the rarity of aligned flow in the solar wind.

The angle the local shock propagation direction (i.e. the shock normal) makes with the magnetic field is function of location on the shock surface. Both the mean spiral configuration of the IMF and the three dimensional curved nature of the bow shock contribute to the lack of symmetry. Over the poles and on the dusk side of the shock surface, the tendency is toward quasi-perpendicular geometries with limiting

angles approaching  $\alpha_1$ . Quasi-parallel conditions are more probable on the dawn side where the cone angle should be closer to  $\alpha_{11}$ ,  $\approx \alpha_s$ . These asymmetries in the MHD Mach cone were first quantitatively modeled by Michel (1965). It was his conclusion that the variations in MHD Mach cone angle with respect to the  $x'$  axis are about  $1^\circ$  overall, but generally less than  $0.5^\circ$  for the regions near the ecliptic where most of the spacecraft observations used in this study were made. For this reason it does not appear that any significant additional errors have been introduced by our earlier assumption of axial symmetry, given the  $2-4^\circ$  uncertainties in the observational determinations of Mach cone angle.

The observed Mach cone angles in Table 1 decrease with distance from the sun as predicted by both gasdynamic and MHD theory although the variation is somewhat larger than expected. The observed Mach cone angles are all significantly greater than the sonic angles predicted by gasdynamic theory. Given the uncertainties in both the observed and bow shock and average solar wind Mach cone angles, there is reasonably good support for shock location being limited by the MHD fast mode Mach number. While not unexpected, this result does provide another piece of experimental evidence for the applicability of magnetohydrodynamic theory to high speed flow problems in space plasmas.

#### Gasdynamic Models

The Spreiter and Stahara (1980; Stahara et al., 1980) gasdynamic code has been modified to produce solutions up to  $x = -50 R_{OB}$  as shown in Figure 1. Figures 8, 9, and 10 display the calculated bow shock locations for the Venus, earth, and Mars body shapes determined by the Slavin et al. (1983) study and sonic Mach numbers of 4 and 8. These two Mach numbers were chosen because they bracket the expected Mach number range from the perpendicular fast mode to the gasdynamic sonic value. The ability of the gasdynamic solutions to predict forward shock position has already been demonstrated (Fairfield, 1971; Slavin et al., 1983). However, the planetary Mach cones inferred from the shock observations in the preceding section indicate that downstream the bow shocks are limited by larger Mach cones than predicted by gasdynamic theory. Below we investigate where these departures start and their magnitude.

The gasdynamic models of flow past Venus are displayed in Figure 8. The near shock is well represented by the  $M_s=8$  theoretical shock forward of approximately  $x' = -4 R_{OB}$ . Farther downstream the bow shock continues to flare outward until its slope nearly matches that of the  $M_s=4$  gasdynamic shock. Figure 9 performs this same comparison with the earth shock model of Fairfield (1971). The results are similar, but with the disagreement between theory and observation being less severe and starting farther behind the planet near  $x' = -6 R_{OB}$ . Finally, Figure 10 presents the Mars observations. In this case the  $M_s=8$  theoretical model does not begin to seriously diverge from the observational model until  $x' = -10 R_{OB}$  is reached, and then only by a modest amount.

These results are generally consistent with both the expected limitations of the gasdynamic approximation and the uncertainties in the experimentally determined Mach cones. In all three cases the planetary bow shocks approach Mach cones that are greater than predicted by gasdynamic theory, but by only a small amount at Mars where  $\alpha_{||} < \alpha_{OBS} < \alpha_{\perp}$ . The trend as a function of distance from the sun is much as would be expected from Table 1. Gasdynamic theory is more accurate and may be used farther downstream at greater distances from the sun where the IMF is weaker and the Alfvénic Mach number higher. The larger the Alfvénic Mach number the smaller the errors introduced by the gasdynamic approximation and the closer the agreement with MHD theory and observation. The implications are that gasdynamic theory will be least useful at Mercury, but highly accurate for describing the flow of solar wind about Jupiter, Saturn, and other large bodies in the outer solar system.

### Conclusions

The distant bow shocks of Venus, Earth, and Mars have been modeled using a single standard method. Mach cone angles determined from the best fit shock models are generally consistent with the MHD fast mode speeds measured in the solar wind as a function of distance from the sun. The finding by earlier studies that gasdynamic theory can accurately predict the location and shape of the forward bow shock has been extended and quantified. At Venus the bow shock position and orientation is poorly represented by gasdynamic theory much beyond  $x' = -4 R_{OB}$ . The disagreement is smaller at the Earth and begins farther downstream near  $x' = -6 R_{OB}$ . Finally, at Mars the gasdynamic bow wave lies quite close to the observed shock surface with small discrepancies becoming evident only downstream of  $x' = -10 R_{OB}$ . The better agreement between gasdynamic theory and observation with increasing distance from the sun is attributed to the decrease in IMF strength with distance making the gasdynamic approximation more accurate.

Acknowledgement. One of the authors (JAS) would like to thank the NASA/NRC research associate program for financial support. We also wish to thank O.L. Vaisberg and V.N. Smirnov for providing listings of the Mars and Venera bow shock times and locations. The research described in this report was carried out for NASA under contract to the Jet Propulsion Laboratory and Stanford University (NAGW-286).

## References

- Bavassano, B., F. Mariani, U. Villante, and N.F. Ness, Multiple crossings of the earth's bow shock at large geocentric distances, *J. Geophys. Res.*, 76, 5970, 1971.
- Bridge, H.S., A.J. Lazarus, C.W. Snyder, E.J. Smith, L. Davis, Jr., P.J. Coleman, Jr., and D.E. Jones, Plasma and magnetic fields observed near Venus, *Science*, 158, 1669, 1967.
- Bridge, H.S., A.J. Lazarus, J.D. Scudder, K.W. Ogilvie, R.E. Hartle, J.R. Asbridge, S.J. Bame, W.C. Feldman, and G.L. Siscoe, Observations at Venus encounter by the plasma science experiment on Mariner 10, *Science*, 183, 1293, 1974.
- Crooker, N.U., T.E. Eastman, and G.S. Stiles, Observations of plasma depletion in the magnetosheath at the dayside magnetopause, *J. Geophys. Res.*, 84, 869, 1979.
- Dryer, M., and R. Faye-Petersen, Magneto-gasdynamic boundary condition for self-consistent solution to closed magnetopause, *AIAA J.*, 4, 246, 1966.
- Elphic, R.C., C.T. Russell, J.A. Slavin, and L.H. Brace, Observations of the dayside ionopause and ionosphere of Venus, *J. Geophys. Res.*, 85, 7679, 1980.
- Fairfield, D.H., Average and unusual locations of the earth's magnetopause and bow shock, *J. Geophys. Res.*, 76, 6700, 1971.
- Gringauz, K.I., V.V. Bezrukikh, G.I. Volkov, L.S. Mustov, and T.K. Breus, Interplanetary disturbances near Venus determined from Venera 4 and 6 data, *Cosmic Res.*, 8, 1970.
- Gringauz, K.I., A comparison of the magnetospheres of Mars, Venus, and Mars, *Adv. Space Sci.*, 1, 5, 1981.
- Howe, H.C., Jr., and J.H. Binsack, Explorer 33 and 35 plasma observations of magnetosheath flow, *J. Geophys. Res.*, 77, 3334, 19.
- Landau, L.D., and E.M. Lifshitz, *Fluid Mechanics*, pp. 310-313, Pergamon Press, New York, 1959.
- Lees, L., Interaction between the solar plasma wind and the geomagnetic cavity, *AIAA J.*, 2, 1576, 1964.
- Michel, F.C., Detectability of disturbances in the solar wind, *J. Geophys. Res.*, 70, 1, 1965.
- Mihalov, J.D., Distant bow shock observations by Explorer 33, *Astrophys. and Space Sci.*, 30, 447, 1974.
- Russell, C.T., On the relative locations of the bow shocks of the terrestrial planets, *Geophys. Res. Lett.*, 4, 387, 1977.
- Russell, C.T., The interaction of the solar wind with Mars, Venus, and Mercury, *Solar Wind Plasma Physics*, eds. C.F. Kennel, L.J. Lanzerotti, and E.N. Parker, pp. 208-252, North-Holland Pub., Amsterdam, 1979.
- Russell, C.T., M.M. Mellott, E.J. Smith, and J.H. King, Multiple spacecraft observations of interplanetary shocks: Four spacecraft determinations of shock normals, *J. Geophys. Res.*, 88, 4739, 1983.
- Shen, W.-W., The earth's bow shock in an oblique magnetic field, *Cosmic Electrodyn.*, 2, 381, 1972.
- Slavin, J.A., R.C. Elphic, and C.T. Russell, A comparison of Pioneer Venus and Venera observations: Evidence for a solar cycle variation, *Geophys. Res. Lett.*, 6, 905, 1979.
- Slavin, J.A., R.C. Elphic, C.T. Russell, F.L. Scarf, J.H. Wolfe,

- J.D. Mihalov, D.S. Intriligator, L.H. Brace, H.A. Taylor, Jr., and R.E. Daniell, Jr., The solar wind interaction with Venus: Pioneer Venus observations of bow shock location and structure, J. Geophys. Res., 85, 7625, 1980.
- Slavin, J.A., and R.E. Holzer, Solar wind flow about the terrestrial planets 1. Modeling bow shock position and shape, J. Geophys. Res., 86, 11,401, 1981.
- Slavin, J.A., and R.E. Holzer, The solar wind interaction with Mars Revisited, J. Geophys. Res., 87, 10,285, 1982.
- Slavin, J.A., and E.J. Smith, Solar cycle variations in the interplanetary magnetic field, in press, Proceedings of Solar Wind 5, 1983.
- Slavin, J.A., E.J. Smith, P.R. Gazis, and J.D. Mihalov, A Pioneer - Voyager study of the solar wind interaction with Saturn, Geophys. Res. Lett., 10, 9, 1983.
- Slavin, J.A., R.E. Holzer, J.R. Spreiter, S.S. Stahara, and D.S. Chaussee, Solar wind flow about the terrestrial planets 2. Comparison with gasdynamic theory and implications for solar-planetary interactions, J. Geophys. Res., 88, 19, 1983.
- Smirnov, V.N., O.L. Vaisberg, and D.S. Intriligator, An empirical model of the Venusian outer environment 2. Shape and location of the bow shock, J. Geophys. Res., 85, 7651, 1980.
- Smith, E.J., Planetary magnetic field experiments, Advanced Space Environments, eds. O.L. Tiffany and E.M. Zaitzeff, American Astronautical Society, Tarzana, California, 1969.
- Smith, E.J., L. Davis, Jr., D.E. Jones, P.J. Coleman, Jr., D.S. Colburn, P. Dyal, and C.P. Sonett, Saturn's magnetosphere and its interaction with the solar wind, J. Geophys. Res., 85, 5655, 1980.
- Spreiter, J.R., and A.W. Rizzi, Aligned MHD solution for solar wind flow past the earth's magnetosphere, Acta Astronautica, 1, 15, 1974.
- Spreiter, J.R., A.L. Summers, and A.Y. Alksne, Hydromagnetic flow around the magnetosphere, Planet. Space Sci., 14, 223, 1966.
- Spreiter, J.R., and S.S. Stahara, A new predictive model for determining solar wind-terrestrial planet interactions, J. Geophys. Res., 85, 6769, 1980.
- Stahara, S.S., D. Klenke, B.C. Trudinger, and J.R. Spreiter, Application of Advanced Computational Procedures for Modeling Solar Wind Interactions with Venus - Theory and Computer Code, NASA Contract Rep. 3267, 1980.
- Tatrallyay, M., C.T. Russell, J.D. Mihalov, and A. Barnes, Factors controlling the location of the Venus bow shock, submitted to J. Geophys. Res., 1983.
- Villante, U., Evidence for a bow shock structure at 400  $R_e$ : Pioneer 7, J. Geophys. Res., 81, 1441, 1976.
- Zwan, B.J., and R.A. Wolf, Depletion of solar wind plasma near a planetary boundary, J. Geophys. Res., 81, 1636, 1976.

### Figure Captions

1. Gasdynamic models of flow about the earth for an adiabatic exponent of 2 and sonic Mach numbers of 4 and 8 are displayed. Obstacle shape in the Spreiter and Stahara (1980) numerical codes is parameterized in terms a quantity  $H/R_0$ . The coordinates used are aberrated geo - centric solar ecliptic (i.e.  $\hat{x}' = -\hat{x} \cdot \mathbf{v}_{sw}/|\mathbf{v}_{sw}|$ ) in units of obstacle radii,  $R_{OB}$ .
2. Sample Venera 9, 10 and Pioneer Venus orbits are shown in Venus solar ecliptic coordinates relative to the bow shock.
3. Mariner 5, Venera 4, Venera 6, Mariner 10, and Venera 9, 10 bow shock crossings are displayed in planet-centered "conic" coordinates along with a linear best fit.
4. The same as the preceding figure, but with the conic focus moved to  $x_0 = +0.45 R_V$  to improve the fit.
5. The Venus bow shock crossings and best fit are displayed in aberrated planet centered solar ecliptic coordinates.
6. Sample Mars 2, 3, and 5 orbital trajectories are plotted in relation to the observed crossings of the bow shock.
7. Mariner 4, Mars 2, Mars 3, and Mars 5 bow shock crossings are plotted in planet centered solar ecliptic coordinates. The best 3 parameter second order least square fit to the boundary is also displayed.
8. The observed location of the Venus bow shock is compared with two gasdynamic models of flow about the planet.
9. The terrestrial bow shock model of Fairfield (1971) is compared with two models of flow about the earth.
10. The observed location of the Mars bow shock is compared with two models of flow about the planet.

TABLE 1. Predicted and Observed Mach Cones

Planet	R	MA	M <sub>S</sub>	M <sub>MSL</sub>	$\alpha_S = \alpha_{ij}$	$\alpha_L$	$\alpha_{OBS}$
Venus	0.7 AU	7.9	6.6	5.1	8.7°	11.3°	13.9° ± 2°
Earth	1.0 AU	9.4	7.2	5.7	8.0°	10.1°	11.4° ± 3°
Mars	1.5 AU	11.1	7.9	6.4	7.3°	9.0°	8.1° ± 4°

# GASDYNAMIC MODEL OF FLOW PAST A PLANETARY OBSTACLE

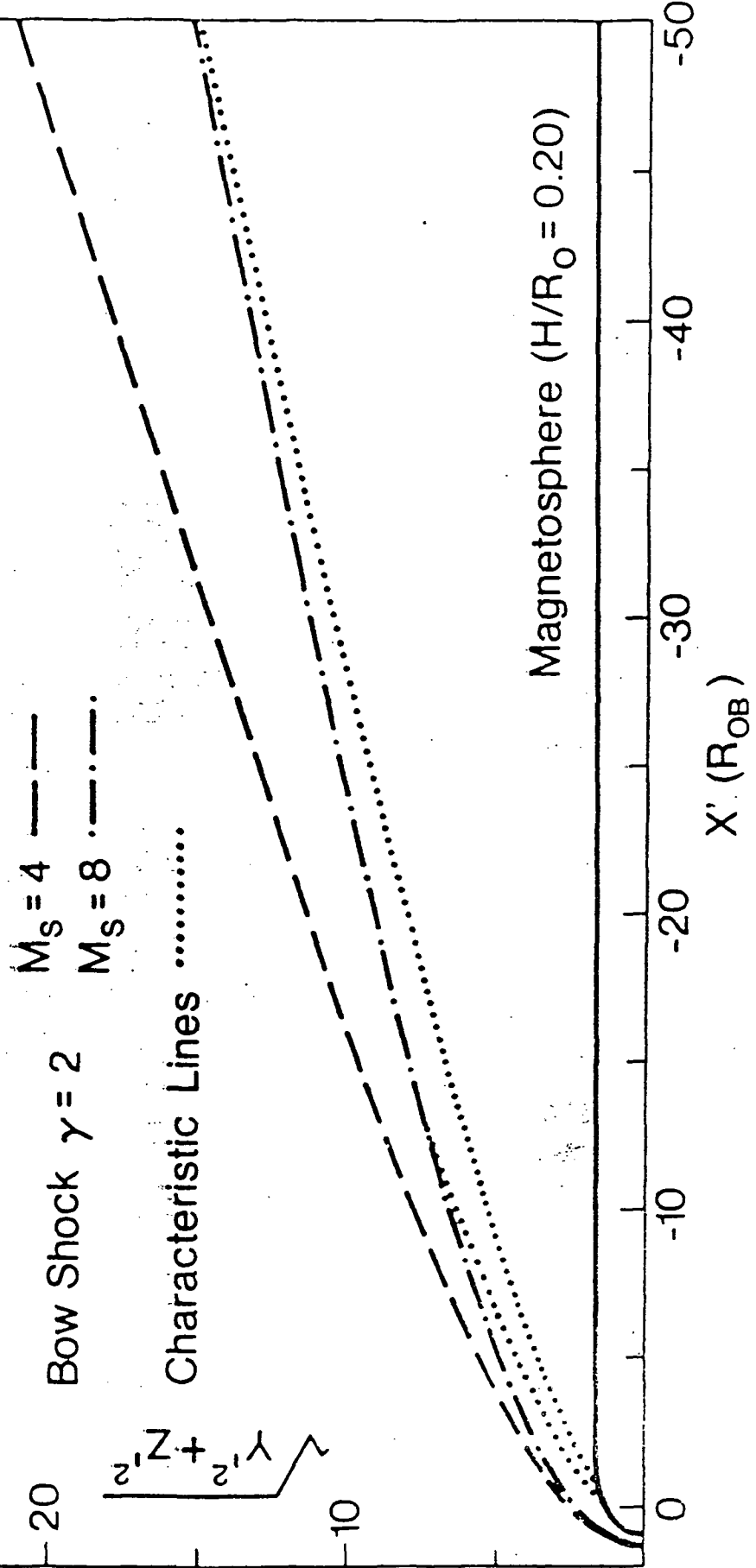


FIG. 1

# VENUS ORBITER MISSIONS

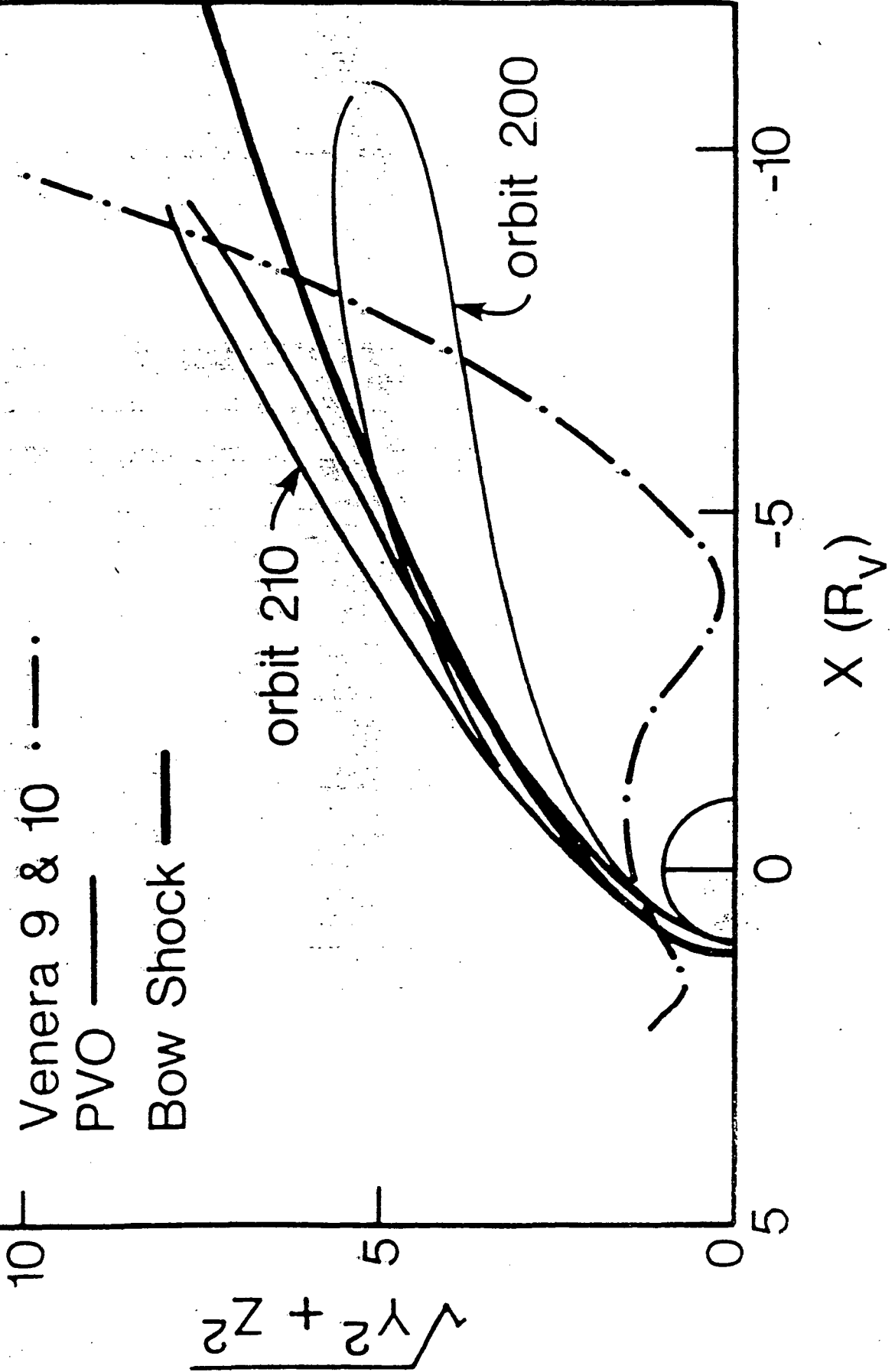


FIG. 2

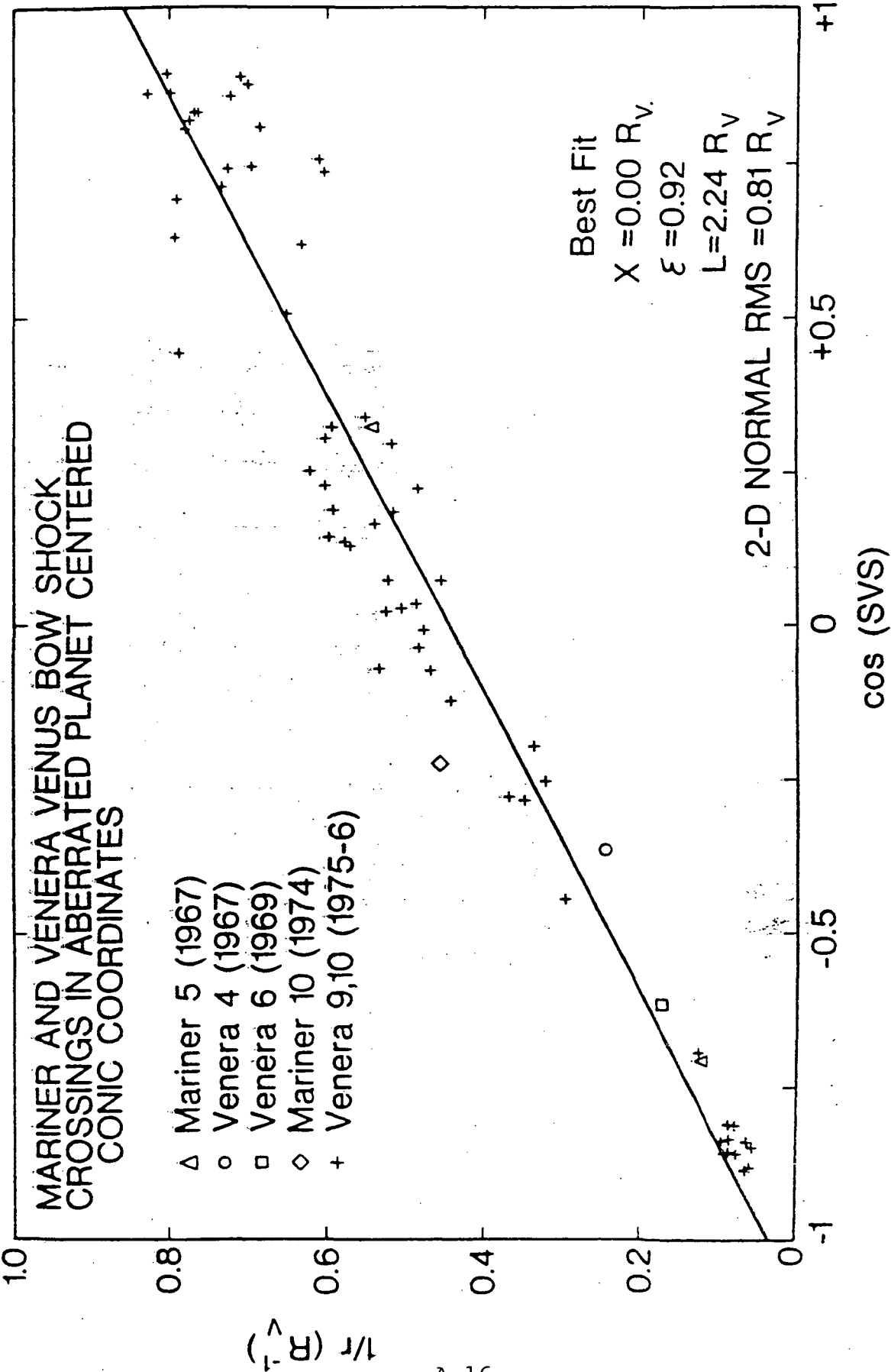


FIG. 3

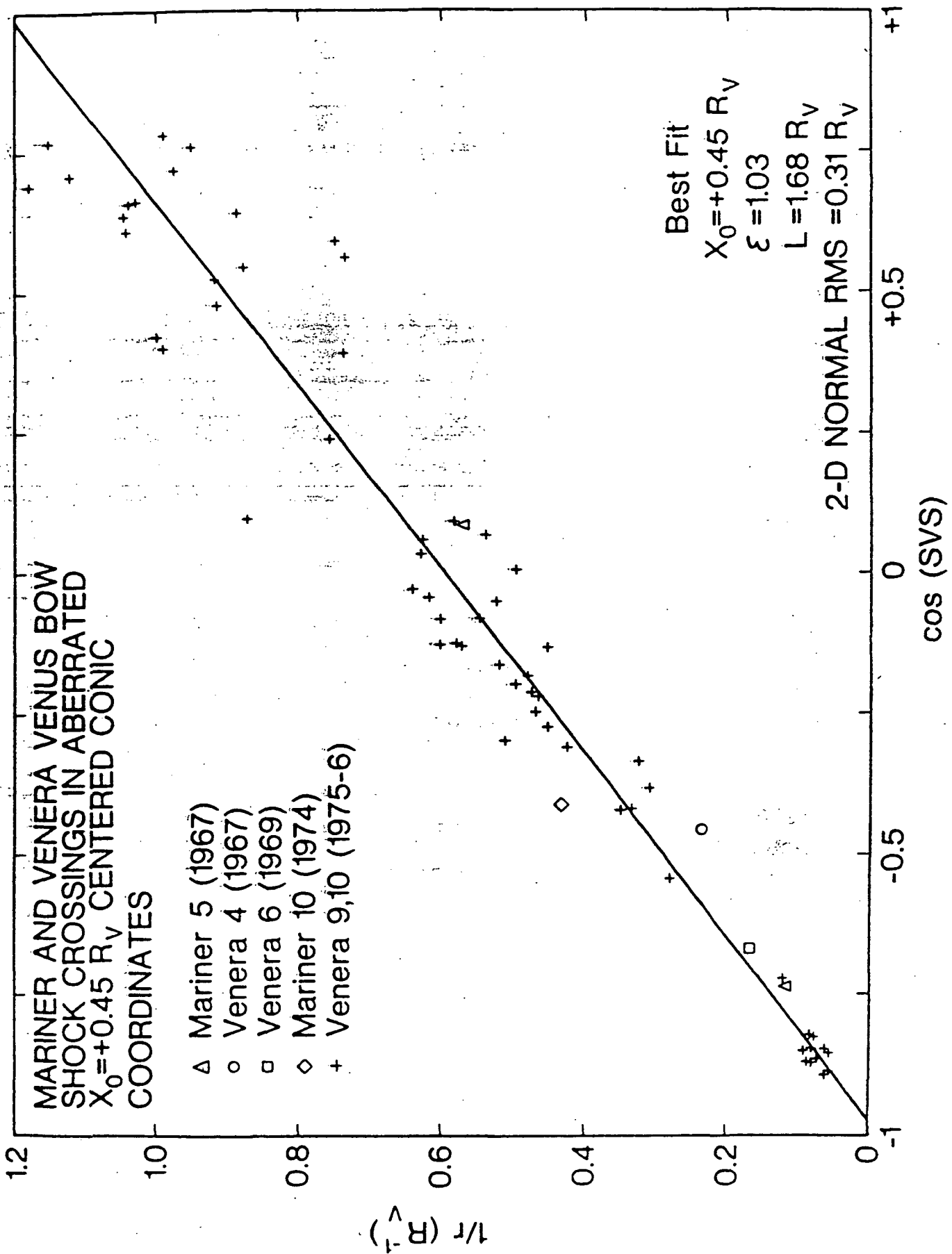


FIG. 4

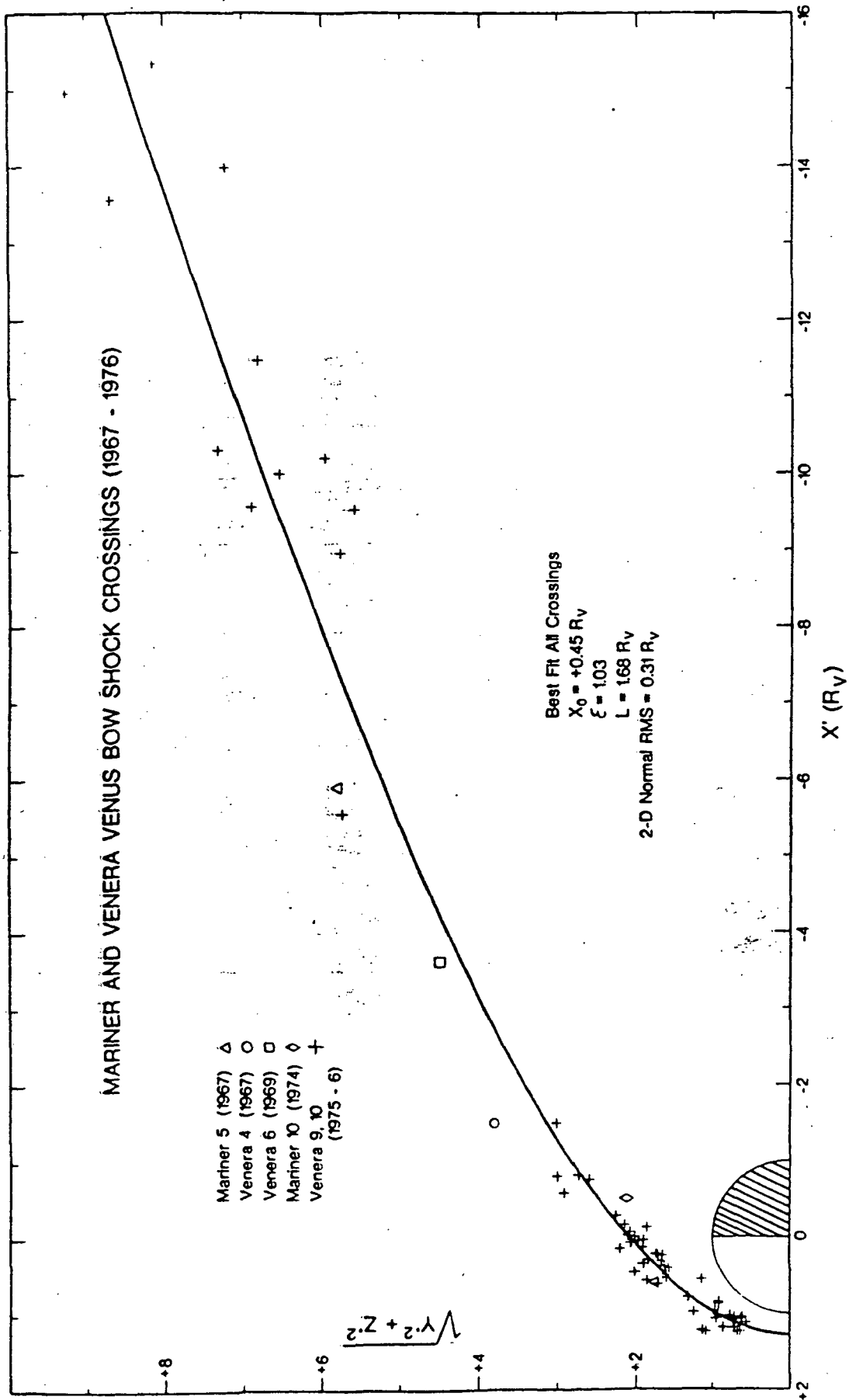


FIG. 5

# MARS ORBITER BOW SHOCK CROSSINGS

Mars 2 (1971-2)  $\Delta$   
Mars 3 (1971-2)  $\circ$   
Mars 5 (1974)  $\square$

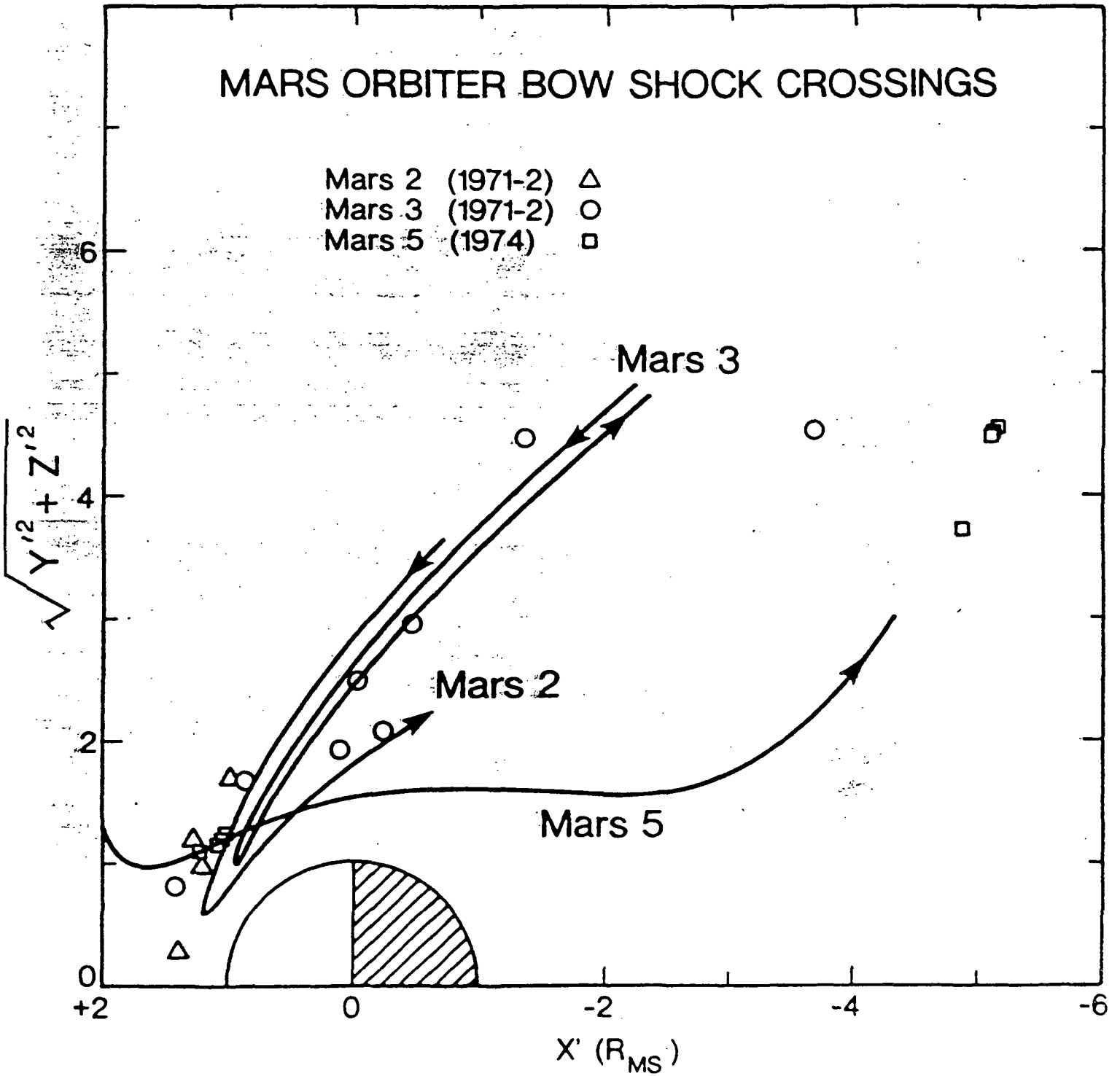


FIG. 6  
A-19

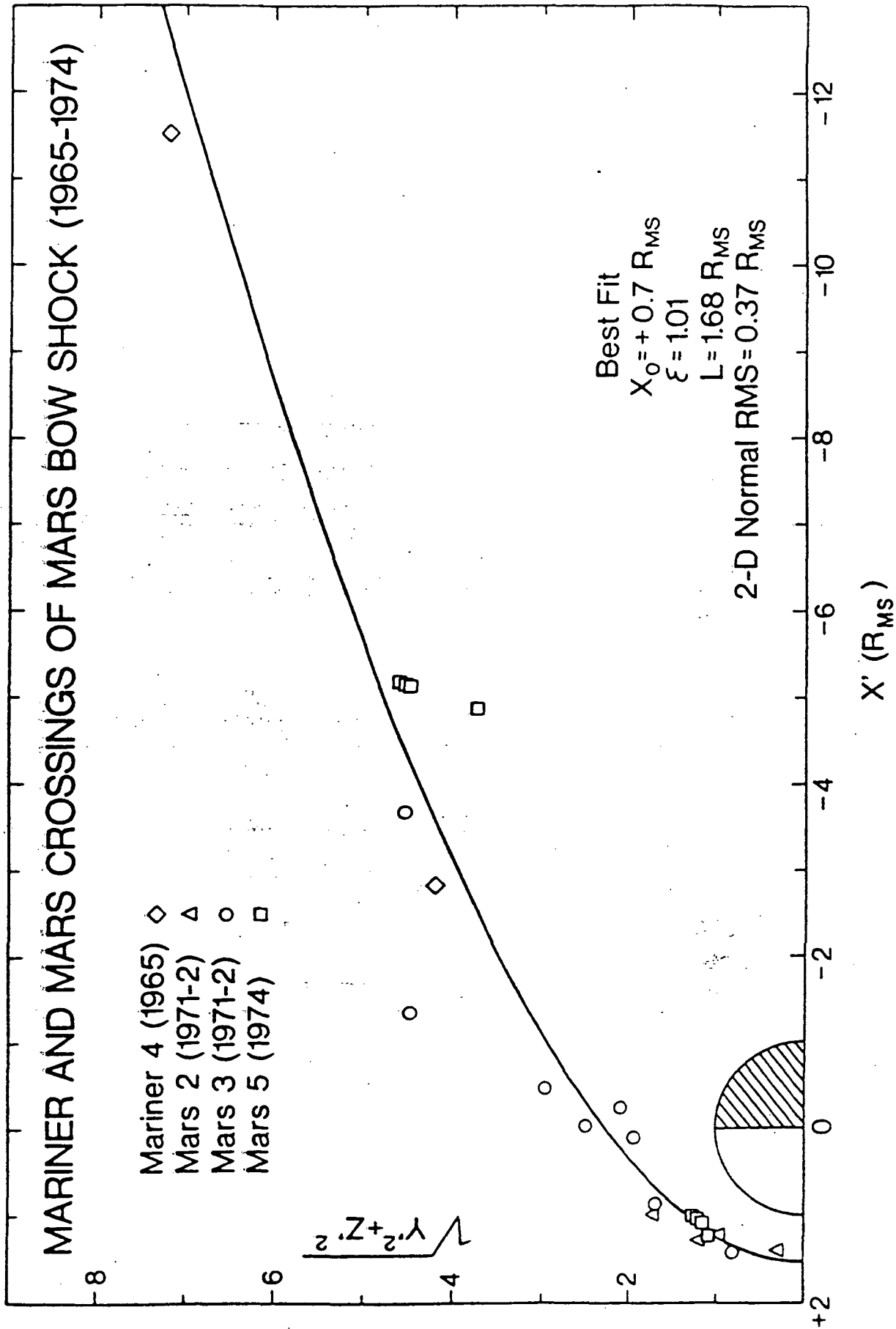


FIG. 7

# VENUS BOW SHOCK : 1967-76

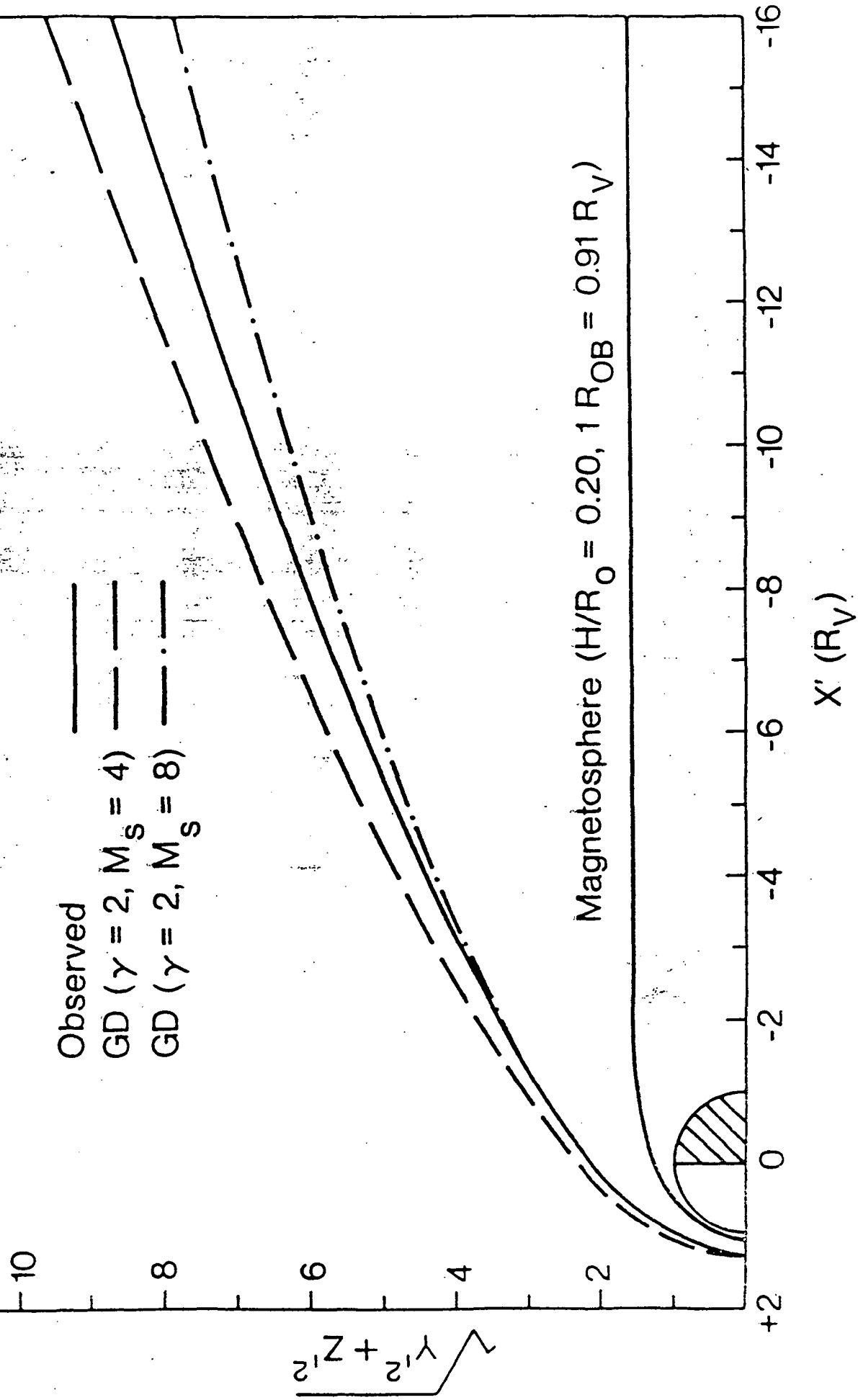


FIG. 8

# EARTH BOW SHOCK: 1963-68

Observed (Fairfield, 1971) —

GD ( $\gamma = 2, M_S = 4$ ) - - -

GD ( $\gamma = 2, M_S = 8$ ) ·····

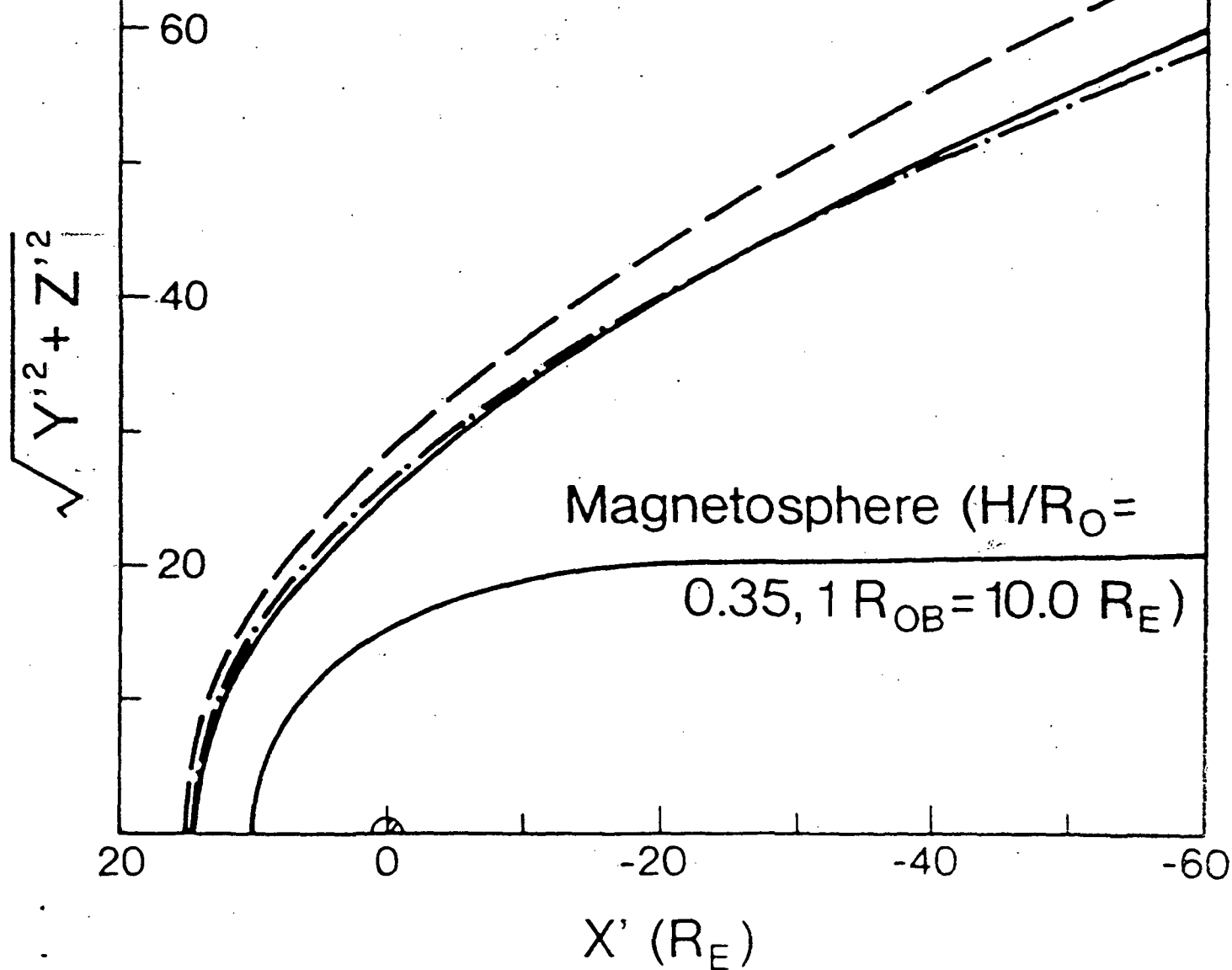


FIG. 9

# MARS BOW SHOCK: 1965 - 1974

- Observed ———
- GD ( $\gamma = 2, M_S = 4$ ) - - -
- GD ( $\gamma = 2, M_S = 8$ ) - · -

$$\sqrt{Y^2 + Z^2}$$

Magnetosphere ( $H/R_0 = 0.05, 1 R_{OB} = 1.15 R_{MS}$ )

+2 -4 -6 -8 -10

$X' (R_{MS})$

FIG. 10

Patterns of Magnetic Field Merging Sites  
on the Magnetopause

J.G. Luhmann, R.J. Walker, C.T. Russell

Institute of Geophysics and Planetary Physics

University of California

Los Angeles, California 90024

N.U. Crooker

Department of Atmospheric Sciences

University of California

Los Angeles, California 90024

J.R. Spreiter

Department of Applied Mechanics

Stanford University

Stanford, California 94305

S.S. Stahara

Heilsen Engineering and Research, Inc.

Mountain View, California 94043

IGPP Publication #2443

May, 1983

## Abstract

Models of the magnetospheric and magnetosheath magnetic fields are used to determine the relative orientations of the two near the dayside magnetopause for the purpose of locating potential merging sites. Areas on the magnetopause with various degrees of antiparallelness for different interplanetary field orientations are displayed as contour diagrams. For southward and GSE-Y interplanetary field, the patterns obtained are consistent with those envisioned by Crooker in an earlier analysis which used simplified representations for the magnetic field geometry. Here, the application of realistic models shows the locations of areas where any antiparallel component occurs. Merging sites for radial interplanetary fields are also illustrated. The results suggest that the geometrical configuration of the field is suitable for merging over a large fraction of the magnetopause for interplanetary fields that are either primarily southward, GSE-Y, or radial (GSE-X) in direction.

## Introduction

There is considerable interest in the question of where reconnection or magnetic field merging occurs in the magnetosphere (cf. Russell, 1976). Several years ago Crooker (1979) presented a qualitative model of the sites of magnetic field merging on the magnetopause. This analysis was based on a conceptual picture of the magnetopause and a superposed overlying uniform field, perpendicular to the earth-sun line, which was taken to represent the magnetosheath field at its inner boundary. The latter was rotated to mimic the effect of different interplanetary field directions. Reconnection or merging lines were defined as the locus of points for which these approximate magnetospheric and magnetosheath fields were antiparallel when projected onto a plane (the GSE Y-Z plane). The major point arising from this analysis was the role of the cusp in locating potential merging sites. However, the author also qualified the results by pointing out that merging can occur where only components of the two fields are antiparallel (cf. Cowley, 1976), and that the draping geometry of the magnetosheath field over the magnetopause is not necessarily well represented by a uniform field in the GSE Y-Z plane projected onto the magnetopause. The present study extends the ideas put forth in this earlier effort by employing realistic models of the magnetospheric and magnetosheath fields to locate antiparallel fields at their magnetopause interface. The new aspects of this analysis include the location of fields with only components that are antiparallel, and the treatment of radial (GSE-X) interplanetary fields which were not considered previously.

## Description of the Model

The Hedgecock and Thomas model (cf. Walker, 1976) was selected to represent the magnetospheric field at the dayside magnetosheath because it has a fairly realistic cusp geometry. This model also has north-south asymmetries caused by the uneven distribution of the data that went into its construction, rather than by true

asymmetry. It was therefore assumed that the more heavily sampled northern section was the more accurate, and a mirror image of the model north of the equator was used to represent the southern magnetosphere. Possibly real dawn-dusk asymmetries in this northern section were retained. The dipole axis of the model was assumed to coincide with the GSE-Z axis for this study. Although the seasonal variation of the dipole tilt with respect to this axis will modify the magnetospheric field at the magnetopause, the complication introduced by the use of a tilted model precluded the study of this effect.

The magnetosheath field was modeled using the assumption that the interplanetary field is frozen into the medium in the gasdynamic treatment of supersonic flow around an axisymmetric obstacle (cf. Spreiter and Stahara, 1982). The shape of the obstacle was presumed to follow the shape of the Hedgecock and Thomas model magnetopause in the noon-midnight meridian. For the purpose of the present analysis, the aberration of the solar wind flow was neglected. A free-stream sonic Mach number of 6.0 was used in the gasdynamic code, with which magnetosheath fields at a distance of approximately .5 earth radii from the surface of the obstacle were computed for a variety of interplanetary field orientations. (The field determined with the gasdynamic code becomes inaccurate near the stagnation streamline that bathes the obstacle surface.)

The angle between the two modeled fields was found over the surface of the dayside magnetopause at the grid points shown in Figure 1. Contour diagrams of the cosine of this angle were then constructed to display the regions of different degrees of antiparallelness as viewed from the Sun.

### Results

Figure 2 contains the contour diagrams described above for various interplanetary magnetic field orientations (ie. magnetosheath models). The shaded areas, representing fields that are within  $10^\circ$  of being antiparallel, are roughly consistent with

Crooker's (1979) merging lines for interplanetary field orientations perpendicular to the solar wind velocity. New sites arise when there is a substantial GSE-X or radial component of the interplanetary field. As expected, the southward directed interplanetary field produces the largest area of nearly antiparallel fields on the magnetopause, while the northward interplanetary field produces the smallest area. However, the regions for which there is some component of the magnetosphere and magnetosheath fields antiparallel cover a large region of the magnetopause for most interplanetary field orientations.

### Discussion and Conclusions

For several reasons, the patterns shown in Figure 2 must be considered with some measure of caution when comparing with observations at the magnetopause. First, the interplanetary field is typically variable on the time scale of plasma convection through the dayside magnetosheath. Except under circumstances of exceptionally steady interplanetary field orientation, the actual pattern of antiparallel fields projected on the magnetopause must be predicted from the field observed in the solar wind at earlier times. (The convection time is several minutes from the subsolar shock to the nose of the magnetopause.) Second, currents near the magnetopause and MHD effects such as that described by Zwan and Wolf (1979) will affect the field geometry at that boundary. Third, the possible dependence of the merging rate on the local plasma velocity has not been folded into these patterns. If slow flow is necessary for merging then those regions near the subsolar stagnation point will be favored. Similarly, the possible role of the field magnitudes was neglected here. Finally, reconnection itself may cause the reconnected field lines to be pulled over the magnetopause, disrupting any pattern imposed purely by the magnetospheric and magnetosheath fields. (The boundary layer may be a manifestation of the latter process.) Yet, the patterns shown in Figure 2 may provide a picture of the initial conditions set up by a sudden change in interplanetary field orientation.

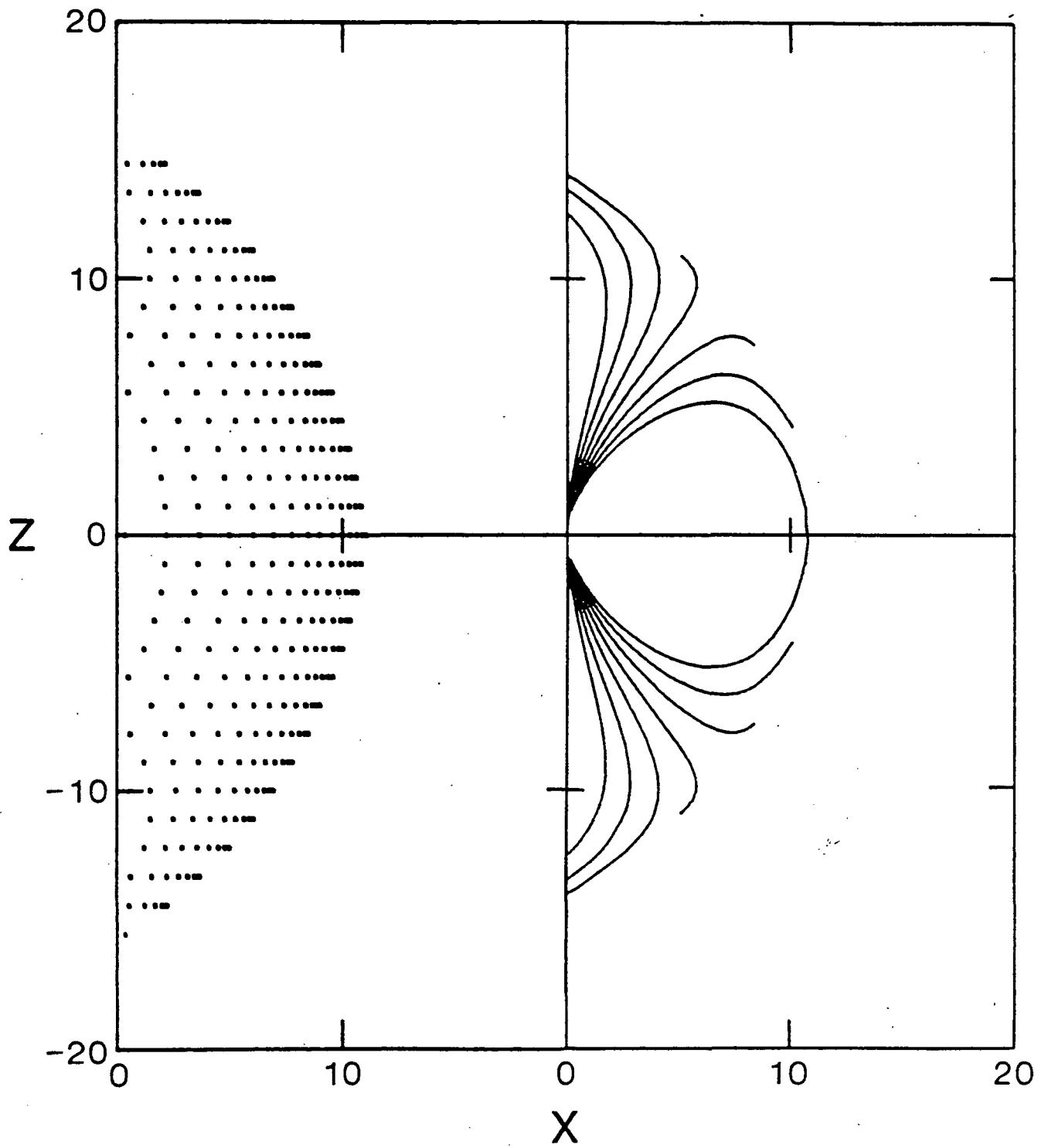
Recent statistical studies of the spatial distribution of flux transfer events near the magnetopause (Berchem and Russell, 1983) show a double-banded distribution which flanks the equator. These authors have argued that their results are consistent with the preferred occurrence of reconnection at the equator where quasi-steady merging has been predicted for southward interplanetary field (Dungey, 1961, Sonnerup, 1976). However, their distributions are also consistent with a superposition of the patterns for southward field and for GSE-Y fields as shown in Figure 2. In fact, in their study, some events occurred in association with practically GSE-Y directed fields. Also, because the highest geomagnetic latitudes were not covered in their sample, the merging poleward of the cusps predicted for northward directed fields (see Fig. 2) could not have been observed. Still, separation of their data into events associated with steady, primarily southward interplanetary fields and GSE-Y fields may produce the distinctive patterns shown in Figure 2 for these two cases. One would expect the GSE-Y fields to produce events in opposing corners along a diagonal through the subsolar point, while southward fields would produce a broad latitudinal band including the equator.

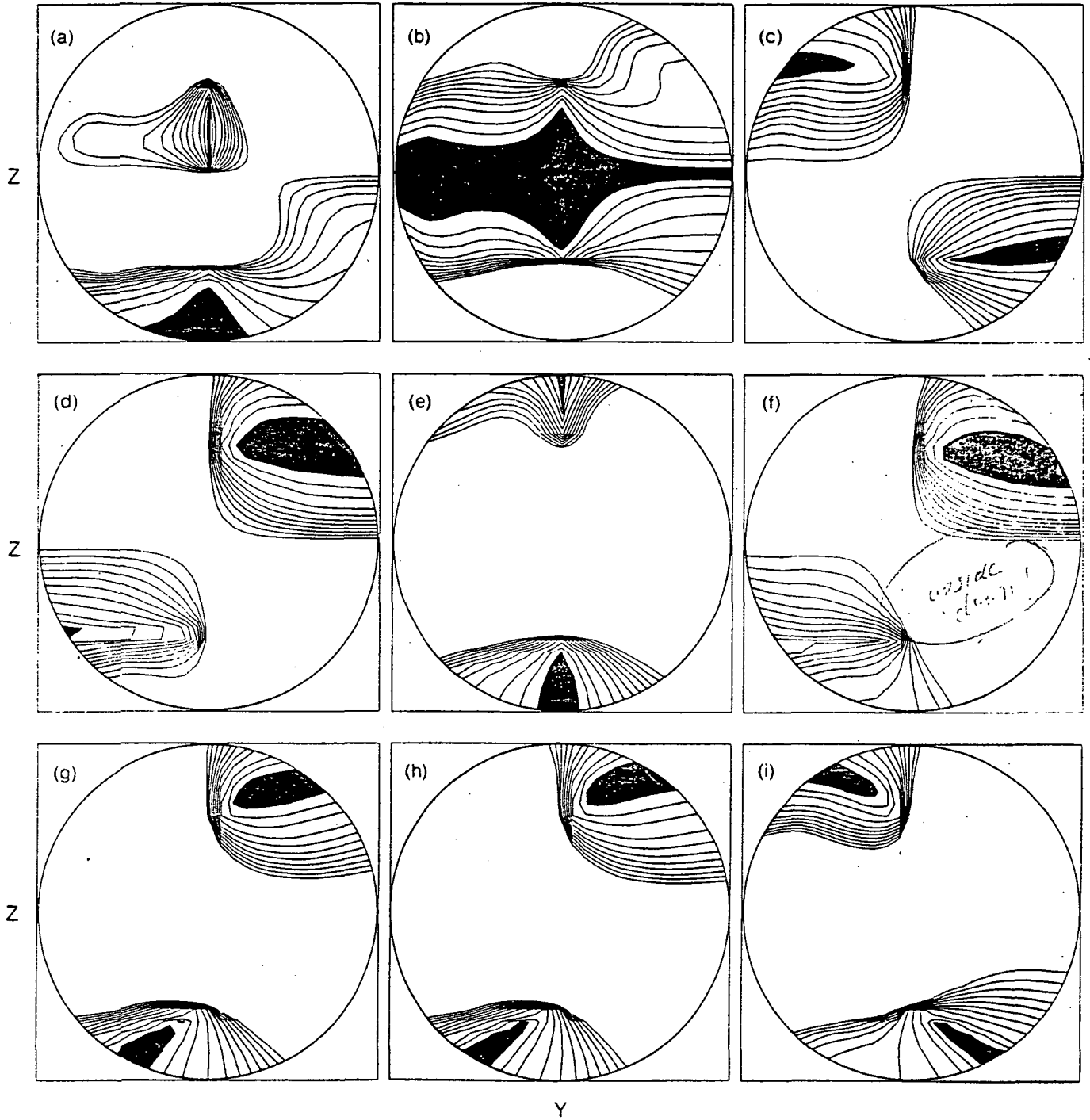
In conclusion, the present analysis represents the extent to which one can practically go in using static magnetic field models to understand the global picture of reconnection sites on the magnetopause. Time-dependent, 3-dimensional MHD models of the solar wind interaction with the magnetosphere, such as that developed by Wu et al. (1980) and Fedder et al. (1981) will, of course, be the ultimate tool for the investigation of merging sites.

### Figure Captions

Figure 1. A view, in the GSE X-Z plane, of the grid points on the Hedgecock-Thomas model magnetopause at which the dot-product of the magnetospheric field model and the gasdynamic magnetosheath field model was computed in this analysis. Also shown are the magnetospheric model field lines in the noon meridian.

Figure 2. Contours on the magnetopause (viewed from the sun, i.e., the GSE Y-Z plane projection) of equal value of the cosine of the angle between the magnetospheric and magnetosheath model fields. Only contours with negative values, implying some antiparallel component, are shown. Values at the contours, starting with the contour filled with shading, are -.98, -.95, -.9, -.8, -.7, -.6, -.5, -.4, -.3, -.2, -.1, 0. The interplanetary field orientations are as follows: (a) radial (+X-directed), (b) southward, (c) Y-directed (toward dusk), (d) Parker Spiral toward, (e) northward, (f) Parker Spiral away, (g) equal Y and Z components, no X-component, (h) equal X, Y, and Z components, (i) equal and opposite Y and Z components, no X-component.





Characteristics of the Magnetospheric Source  
of Interplanetary Energetic Particles

J.G. Luhmann, R.J. Walker, C.T. Russell

Institute of Geophysics and Planetary Physics  
University of California  
Los Angeles, California 90024

N.U. Crooker

Department of Atmospheric Sciences  
University of California  
Los Angeles, California 90024

J.R. Spreiter

Department of Applied Mechanics  
Stanford University  
Stanford, California 94305

S.S. Stahara

Neilsen Engineering and Research, Inc.  
Mountain View, California 94043

D.J. Williams

Applied Physics Laboratory  
Johns Hopkins University  
Laurel, Maryland 20707

IGPP Publication No. 2442

## Abstract

The earth's bow shock is frequently cited as an example of an astrophysical shock where particle acceleration is observed. However, because energetic particles observed upstream of the bow shock may be accelerated within the magnetosphere, it is important to understand the properties of the magnetospheric source. A first order picture of the spatial distribution of magnetospheric particles in the magnetosheath and upstream is obtained by mapping those magnetic field lines which drape over the magnetopause through the bow shock. Subsets of these field lines that connect to potential sites of magnetic merging on the magnetopause are also traced in the event that leakage occurs preferentially where normal components of the field are present across that boundary. The results can be used to determine whether the so-called "diffuse" particles observed upstream are accelerated locally or within the magnetosphere.

## Introduction

The energetic particles that are observed in interplanetary space are attributed to a variety of sources, both nonlocal and local. The primary nonlocal sources are the as yet uncertain sources of the galactic cosmic rays, while the more numerous local sources include solar flares, corotating interaction regions, interplanetary shocks, and planetary bow shocks. In recent years, much attention has been focussed on the  $\sim 50$  keV ions detected upstream of the earth's bow shock because of their implications for shock acceleration of galactic cosmic rays in the interstellar medium (cf. Axford, 1981). While the question of the contribution of magnetospheric particles to this population has been addressed by a number of authors (i.e., Scholer et al., 1981), it is still a relatively unsettled issue. Yet, if planetary bow shocks are to be used as astrophysical laboratories, it is important to understand the nature of the magnetospheric source.

Ions and electron beams with energies a few times that of solar wind particles have been traced back to the quasiperpendicular bow shock (cf. Gosling et al., 1981). The origin of these few keV particles is most likely related to the reflection of a small fraction of the incident solar wind from the bow shock as first suggested by Sonnerup (1969). These beams are probably also responsible for the generation by a beam-plasma instability of the MHD waves that are observed in the same upstream region (Barnes, 1970; Gary, 1981; Russell and Hoppe, 1983). A more energetic, ( $>50$  keV) less directed population, the so-called "diffuse" particles which are observed downstream of these beams (cf. Ipavich et al., 1981; Anderson, 1981; Mitchell et al., 1983) has been explained as beam particles which are stochastically accelerated by the Fermi process in the regions where the upstream magnetic field fluctuations produced by the beam are convected against the shock (cf. Jokipii, 1967; Lee, 1982). Indeed, both West and Buck (1976) and Crooker et al. (1981) found an energetic ion population in the magnetosheath that appeared to be convected, together

with fluctuating magnetic fields, along plasma stream lines from the region of the bow shock where the diffuse particles are observed upstream.

On the other hand, very energetic (MeV) Jovian electrons observed in the interplanetary medium have been attributed to a magnetospheric source (McDonald et al., 1975), and Zwickl et al. (1981) found heavy ions of unmistakably magnetospheric origin in the upstream particles near Jupiter. Still, it may be argued that the region of space near the planets is contaminated by cold planetary ions which are then accelerated at the planetary bow shock, as proposed for the earth's upstream diffuse particles.

These things considered, it is relevant to review what has been observed near the terrestrial magnetopause through which the particles must exit the magnetosphere. Williams et al. (1981) have examined the behavior of energetic particles at the magnetopause boundary. These authors demonstrated that bite-outs occur in the trapped pitch angle distributions at large pitch angles, which is what one expects if some of the drifting trapped population is lost to the magnetosheath. Also, West and Buck (1976), Asbridge et al. (1978) and Bieber and Stone (1981) have all reported observations of layers of energetic particles in the magnetosheath near the magnetopause. Scholer et al. (1981) showed that the flux in the magnetosheath is comparable to the  $90^\circ$  trapped flux which is feeding the leakage. At least some of these particles observed near the magnetopause must end up in interplanetary space.

The distinction between magnetospheric particles and those accelerated upstream of the terrestrial bow shock was attempted experimentally by Scholer et al. (1981) who argued that magnetospheric ions are more energetic and are accompanied by electrons. In another observational study, Bieber and Stone (1981) pointed out that upstream magnetospheric electron events usually occur in conjunction with geomagnetic activity on the ground. Yet it seems that some of the confusion surrounding this matter of magnetospheric sources can be cleared up most effectively by a model that describes where those particles which are observed to leak out of the magnetopause go.

A global picture of the magnetospheric particle source can be expected to exhibit certain characteristics. The particles are presumably accelerated within the magnetosphere either in the routine manner of the permanently trapped outer zone population, or in transient events in the magnetotail. Proceeding outward, there are two mechanisms by which these particles can exit the magnetopause based on the current understanding of its structure. One possibility is that a turbulent boundary layer (cf. Russell and Greenstadt, 1983) can scatter an adiabatically drifting trapped magnetospheric particle onto magnetosheath field lines. Provided that the boundary layer is large in areal extent, this type of leakage would occur over practically the entire magnetopause, with perhaps a preference for dawn and dusk where the sunward drifting electrons and protons, respectively, cross the terminator. Alternatively, the particles may leak out preferentially at areas on the magnetopause where merging of the magnetospheric and magnetosheath fields occurs (Crooker, 1979; Luhmann et al., 1983) because there normal components of the magnetic field allow adiabatic motion from one region to the other (Speiser et al., 1981; Daly, 1983).

Next, one must trace the particle motion through the magnetosheath from the magnetopause to the bow shock. Here there is a question of whether the particle motion is adiabatic or diffusive. If along its path a particle encounters magnetic fluctuations of substantial amplitude which satisfy the condition for gyroresonance when Doppler shifted to the particle's reference frame (cf. Jokipii, 1967), it will be scattered by the fluctuations. In this case the magnetospheric particles will "diffuse" outwards towards the shock. Moreover, if the magnetic fluctuations have some net motion, say in the direction of the convecting magnetosheath plasma, the isotropized particles will exhibit a similar bulk motion. If the scattering is strong, few magnetospheric particles will be able to reach the upstream region.

Rather, they will be carried antisunwards along the flanks of the magnetopause with the magnetosheath plasma in which the magnetic fluctuations are embedded. However, if the magnetic fluctuations are in a frequency range that does not affect the particles of interest, or if the magnetic field is fairly undisturbed, the gyrocenters of the energetic particles will approximately follow magnetosheath field lines through the bow shock to interplanetary space. While displacement of the gyrocenters from the field lines will be caused by the motional (VXB) electric field drift associated with the convection of the magnetized magnetosheath and solar wind plasma, this can probably be neglected for  $>50$  keV ions (cf. Anderson, 1981; Mitchell et al., 1983). Thus, field line tracing from the magnetopause through the magnetosheath will, under conditions of nearly adiabatic particle motion, give information (to within a gyroradius) about the volume that should be populated with magnetospheric particles.

While some combination of diffusive and adiabatic behavior is probably a more realistic description of the particle motion in the magnetosheath, several studies (i.e., Palmer, 1981) suggest that the mean free path for scattering in the magnetosheath can be long. In this paper emphasis is placed on the characteristics of the magnetospheric source that would be expected for adiabatic behavior of the particles within the magnetosheath, although some discussion of the effects of magnetosheath turbulence is included in the final section. Toward this end, magnetosheath magnetic field lines that either pass within  $\sim 1 R_e$  ( $\sim 1$  particle gyroradius) of the magnetopause (for modeling widespread leakage) or at potential sites of magnetopause reconnection where the magnetosheath and magnetosphere fields are antiparallel, are traced outward to interplanetary space. The magnetosheath field model used here is derived from the gasdynamic treatment of the solar wind flow around the magnetosphere (Spreiter and Stahara, 1964, 1982). In this model, the

magnetic field configuration is calculated on the assumption that the interplanetary magnetic field is frozen in the diverted solar wind plasma. Thus, the "beams" of magnetospheric particles are found to have distinctive shapes and locations that depend on the interplanetary field orientation.

#### Description of the Model

The gasdynamic magnetosheath magnetic field model has been described elsewhere by its originators (Spreiter and Stahara, 1964, 1982). As mentioned above, this model assumes that the interplanetary magnetic field is frozen in the flow. Although few comparisons of this model with observations have been carried out for the earth (cf. Fairfield, 1976), several detailed analyses have been done for the Venus magnetosheath (Spreiter and Stahara, 1980). The fact that the Venus ionospheric obstacle is much less compressible than the earth's magnetosphere, and is scaled much smaller, is an advantage for comparisons with the steady state model. The time scale for variations in the interplanetary field is typically short compared to the time (several hours) it takes a spacecraft to travel through the dayside magnetosheath at the earth. But the interplanetary field can be quite steady during the time interval of the Pioneer Venus orbiter traversal of the Venus magnetosheath (~.5 hr). The magnetosheath magnetic field model based on gasdynamics agrees quite well with the observed magnetic field at Venus. Although here the object of interest is the less well-behaved earth, it is considered that an idea of the magnetosheath field line geometries can be obtained from an examination of constant scale models with constant interplanetary fields. A sonic Mach number of 6 and a magnetopause shape derived from the Hedgecock and Thomas magnetosphere model (cf. Walker, 1976) were used in the gasdynamic calculation to produce the magnetosheath fields used here.

To determine the locations of magnetic merging on the magnetopause, the magnetospheric field at the magnetopause was presumed to be given by the Hedgecock and Thomas (cf. Walker, 1976) model. As described elsewhere (Luhmann et al., 1983) the

locations where this internal field was within  $\sim 10^\circ$  of antiparallel to the magnetosheath field were then defined as merging sites.

Routes for magnetospheric particle leakage are approximated by magnetosheath field lines which either drape against the dayside magnetopause, for the case of widespread leakage, or by field lines which originate at the magnetopause at the aforementioned merging sites.

Figures 1 and 2 illustrate the results of the modeling in the same format for the cases of widespread leakage and localized reconnection site leakage, respectively. These figures display projected views of the three-dimensional magnetosheath field line configuration for different interplanetary field orientations. The underlying magnetosheath draping is shown as fine lines. These field lines start at 49 points in interplanetary space on a square grid oriented perpendicular to the interplanetary field. The heavy lines in Figure 1 are projected views of field lines which pass within  $\sim 1$  earth radius of the magnetopause at the terminator plane at equispaced intervals of  $\sim 10^\circ$ . These produce a three-dimensional picture of the volume of flux tubes which would be populated by magnetospheric particles if the particles leak out over a large area of the dayside magnetopause. The shapes of the volumes are notably different for each interplanetary field configuration, appearing as sheets for interplanetary fields perpendicular to the flow, and as a cylindrical tube for radial magnetic field. Subsets of these volumes are connected to merging sites, as defined above, on the magnetopause. The heavy lines in Figure 2 identify groups of field lines which originate near those sites, which are shown on the magnetopause from the viewpoint of the sun in Figure 3. Figure 2 illustrates the importance of southward interplanetary field in obtaining large amounts of magnetospheric particle leakage if merging at the magnetopause is a necessary factor. Finally, Figure 4 shows the cross-sections of several of the volumes of flux tubes from Figures 1 and 2 at various planes in interplanetary space. This diagram gives

a feeling for the sizes of the volumes of magnetospheric particles that a spacecraft might traverse while located beyond the bow shock.

### Discussion and Conclusions

In the introductory section the effects of scattering of the particles by magnetic fluctuations and of drifts produced by the motional electric field ( $\bar{E} = \bar{V} \times \bar{B}$  where  $V$  = plasma velocity,  $B$  = magnetic field) were mentioned. Anderson (1981) has given a complete description of trajectory dispersion by the  $V \times B$  field in interplanetary space where  $V$  and  $B$  are uniform. However, the drift effects in the magnetosheath are not so simply described because of the complicated magnetosheath velocity field and the magnetic field, which varies with the interplanetary field orientation. Figure 5 shows several examples of particle trajectories originating near the subsolar magnetopause, drifting in the  $\bar{V} \times \bar{B}$  and  $\bar{B}$  fields from the gasdynamic magnetosheath model. As discussed by Anderson (1981) for the upstream region, the particle gyrocenter trajectories are dispersed antisunward from magnetic field lines according to their parallel (to  $\bar{B}$ ) velocities. Particles with small parallel velocities are swept into the flow, in the limit of zero parallel velocity their gyrocenters following streamlines. At the opposite extreme, particles with large parallel velocities have gyrocenter paths that lie practically along magnetic field lines. Most observations are of particles with intermediate behavior. Thus, some spatial dispersion of particles of different energies in the magnetosheath and upstream regions is to be expected. The anticipated spatial gradients, with low energies mostly antisunward, should be considered in interpreting delays in the onsets of fluxes at successively higher energies as observed from spacecraft moving from dawn toward noon. This spreading of the magnetospheric beam will distort the spatial distributions suggested by Figures 1-2 for particles with low parallel velocities. However, for energies  $>50$  keV and pitch angles  $>45^\circ$  field-aligned gyrocenter motion is probably a fair approximation.

On the subject of scattering, it has been established that magnetic fluctuations in the magnetosheath, <sup>apart</sup> from the turbulent boundary layer near the magnetopause (Hones, 1983), are confined to streamlines of magnetosheath plasma flow that are connected to the quasiparallel bow shock (Greenstadt et al., 1983, Russell and Luhmann, 1983). Figure 5 illustrates how sections of the trajectories of the magnetospheric particles intersect the regions (shaded) of fluctuating magnetic fields behind the quasiparallel bow shock on their way through the magnetosheath. The spectrum of the magnetosheath field fluctuations, which has been studied by Greenstadt et al. (1983) is similar in shape, and at least equivalent in power, to the spectrum of the waves upstream from the bow shock. The latter has been shown by Lee (1982) to often justify the use of the diffusion equation in describing the transport of upstream energetic particles. The upstream patterns for magnetospheric particle leakage shown in Figures 1 and 2 will under such circumstances be smeared out by the diffusing regions in the magnetosheath. However, some properties of the leakage patterns, such as the local time sector of the transmitted population, may be roughly preserved. An important point in connection with this geometry is that the upstream leakage frequently occurs through the region of the quasiparallel bow shock, where the so-called "diffuse" particle populations, consisting of nearly isotropic energetic ions, are observed (Ipavich et al., 1981, Paschmann et al., 1981, Bonifazi and Moreno, 1981). The present results suggest that caution should be exercised when interpreting these diffuse populations as ions locally accelerated in the upstream region. Other properties of the observed energetic diffuse ions that a magnetospheric source would explain are the apparent limiting fluxes, which are similar to the trapped flux near the magnetopause, the time constants for flux buildup after a sudden change in the interplanetary field, which may be the leakage and travel times to the upstream observing point, and the  $K_p$  dependence of the

energetic upstream population (West and Buck, 1976), since the trapped population at the magnetopause as well as the rate of leakage through reconnection sites (i.e., the areal extent of merging regions) will be greater under the conditions that produce high  $K_p$ . The observed frequent absence of energetic upstream electrons together with the diffuse ions can be attributed to leakage efficiencies and propagation differences for the two species, partly due to their very different gyroradii.

One obvious test that could be performed to determine the efficiency of upstream acceleration without contamination by the magnetospheric source is to measure energetic particles upstream of the bow shocks of planets with weak intrinsic fields like Venus and Mars. However, although magnetic field measurements are available for these planets, energetic particles were not measured on the spacecraft missions to them. In any case, the present study suggests that in interpreting observations of energetic particles near planetary bow shocks, one must consider not only whether the local magnetic field lines connect to the bow shock, but also whether they connect to the magnetopause.

#### Acknowledgments

One of the authors (JL) wishes to acknowledge, with thanks, discussions on the subject of upstream particles with N.A. Lee, F.M. Ipavich, D.D. Sentman, and W.I. Axford. This work was supported by NASA Grant

### Figure Captions

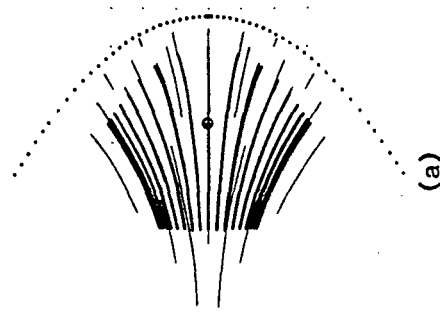
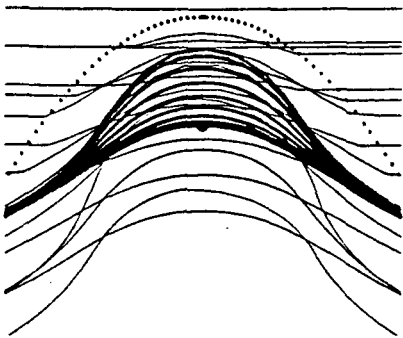
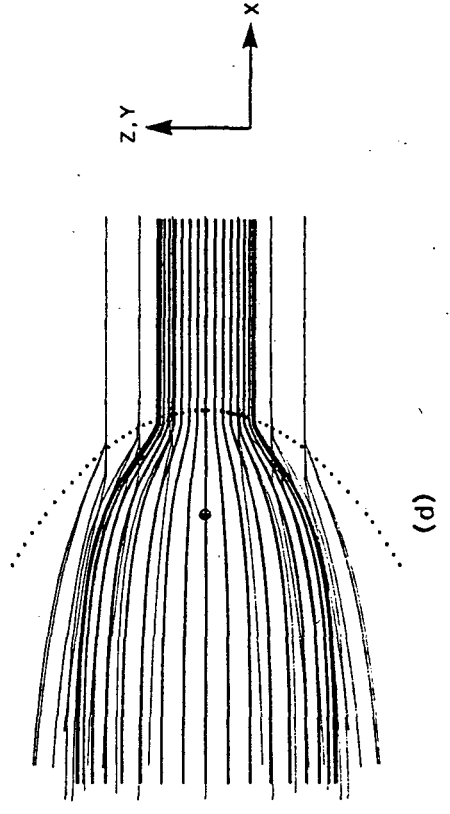
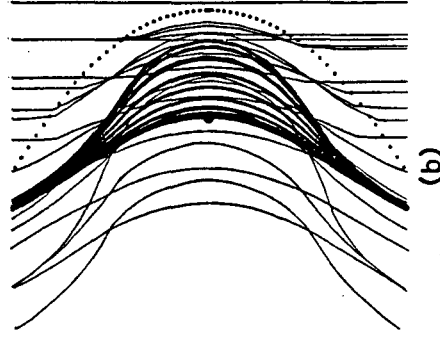
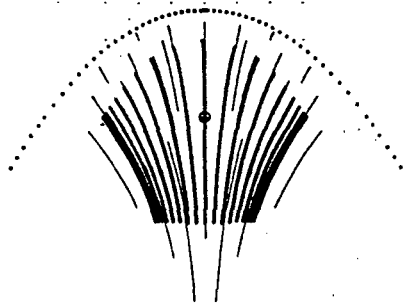
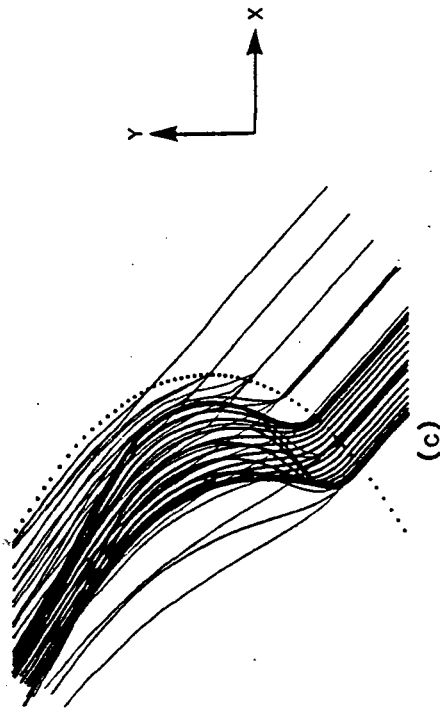
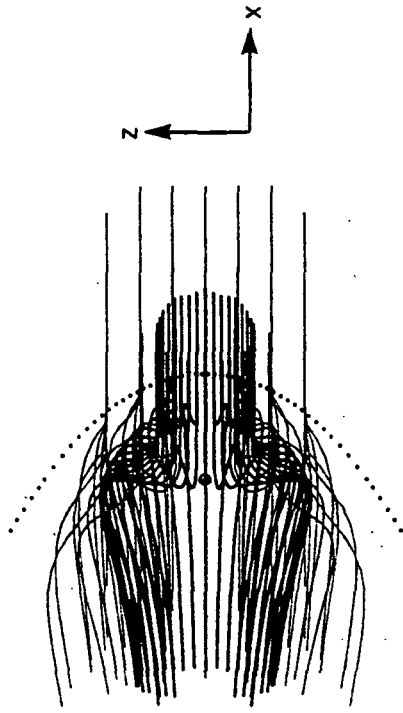
Figure 1. Projections (in the GSE coordinate system) of magnetosheath field lines (fine lines) and field lines passing within  $\sim 1 R_E$  of the magnetopause in the terminator plane (heavy lines) for various interplanetary field orientations: (a) northward or southward (Z-directed), (b) dawn or dusk (Y-directed), (c) Parker Spiral ( $45^\circ$  to X and Y axes, parallel to X-Y plane), (d) radial (X-directed). The gyrocenters of energetic particles which leak out of the magnetosphere over a large area of the magnetopause will follow paths roughly within the volumes defined by the heavy lines.

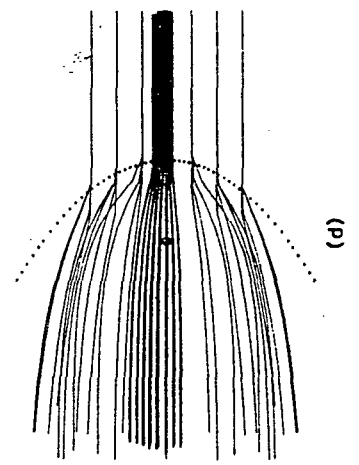
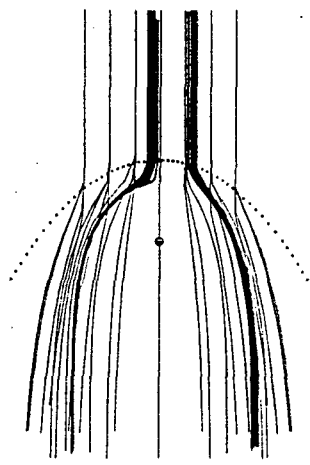
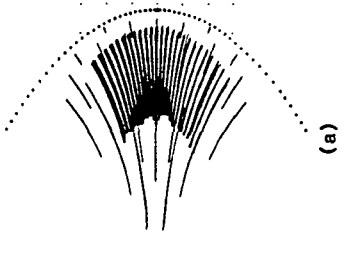
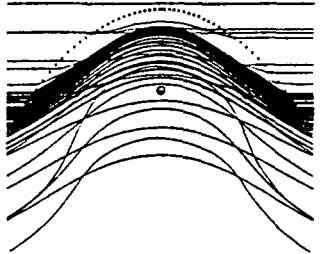
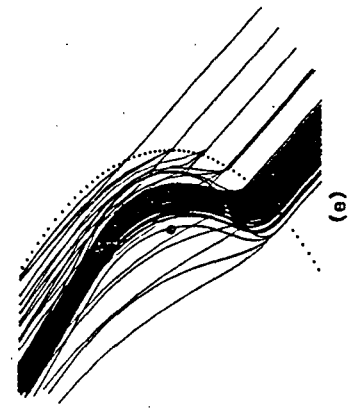
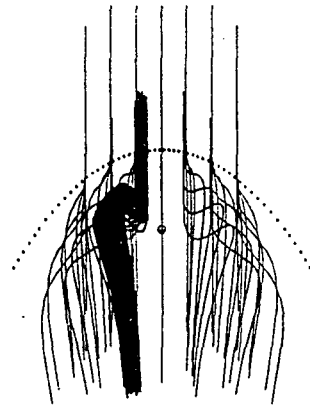
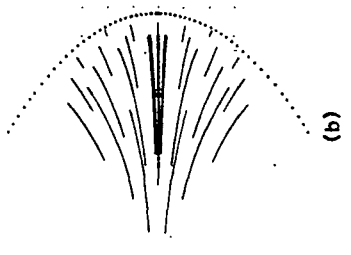
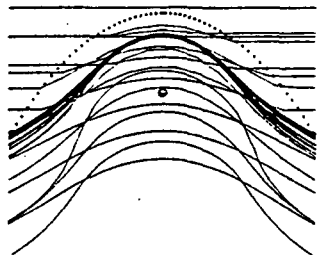
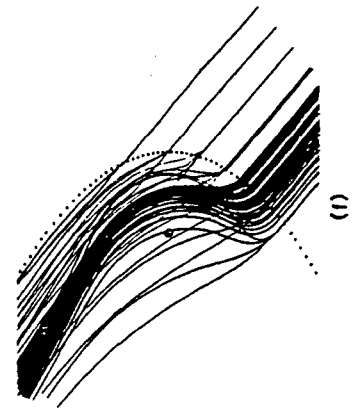
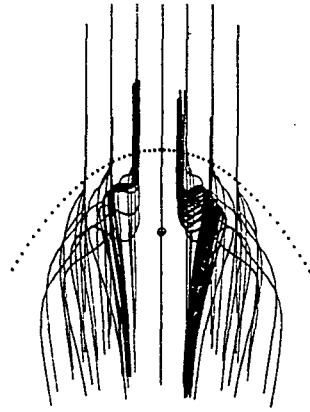
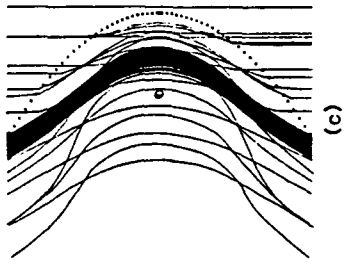
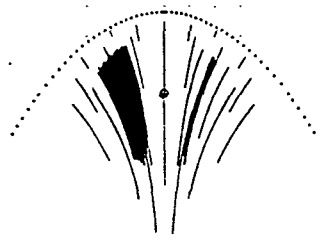
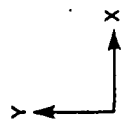
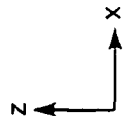
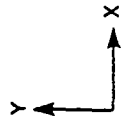
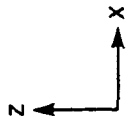
Figure 2. Same as Figure 1, but here the heavy lines originate near potential merging sites on the magnetopause (see Fig. 3), and the interplanetary field is: (a) southward, (b) northward, (c) Y-directed, (d) radial, (e) and (f) Parker Spiral toward and away, respectively.

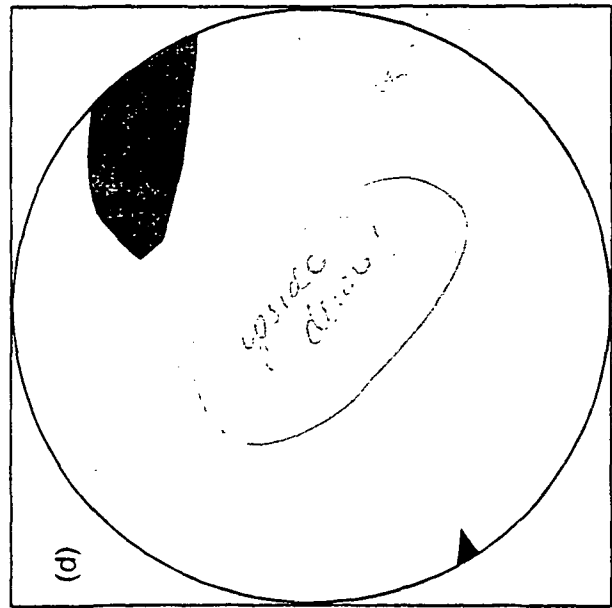
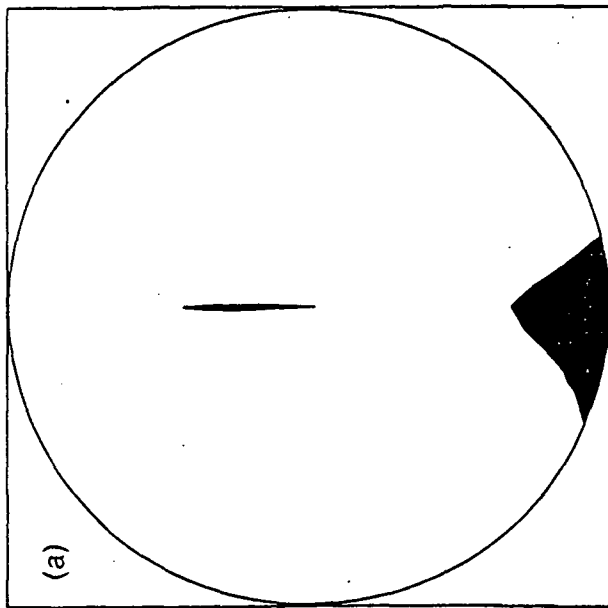
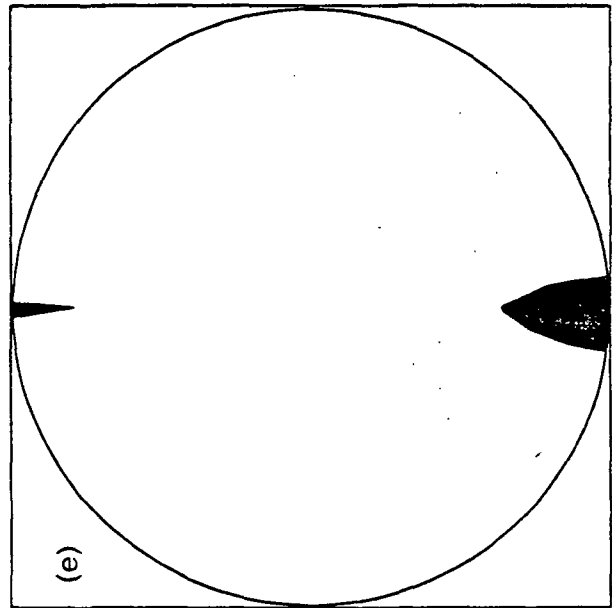
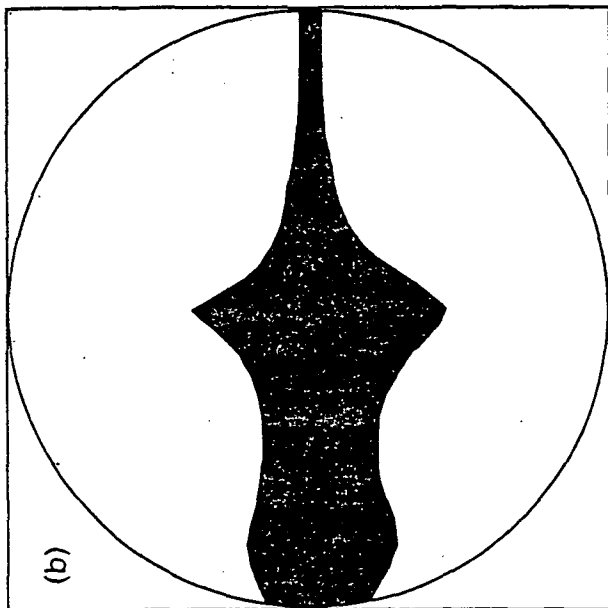
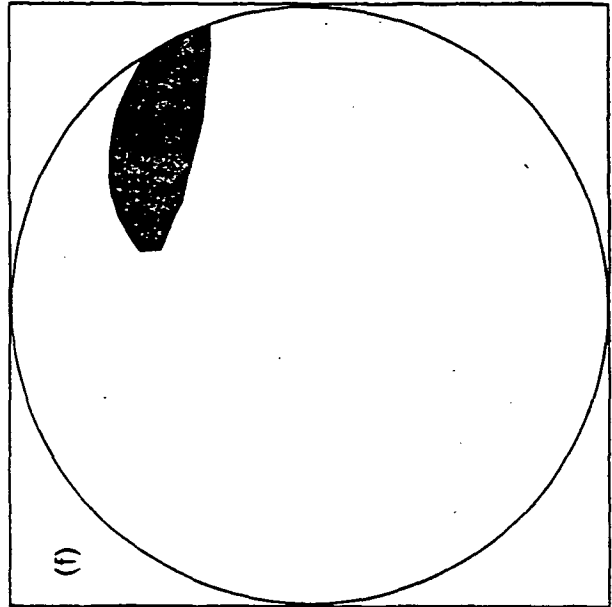
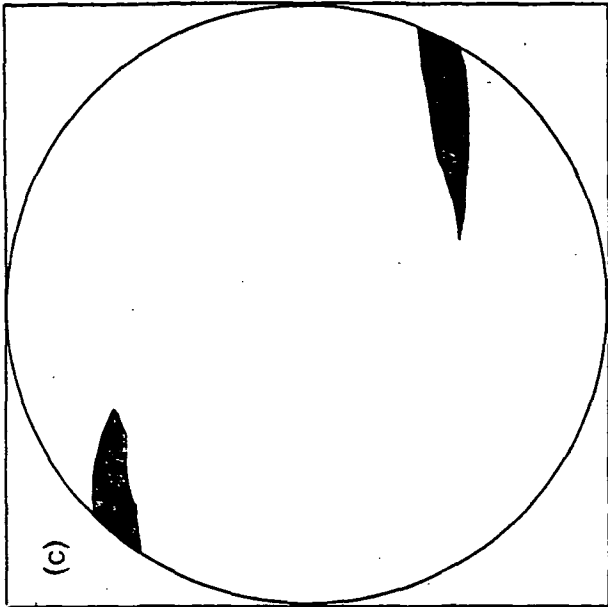
Figure 3. Projection of the magnetopause surface (in the GSE Y-Z plane) showing where the magnetospheric and magnetosheath model fields are within  $10^\circ$  of antiparallel at the magnetopause. Reconnection or merging is presumed to occur between the two fields at these sites. Merging produces normal components of the field on the boundary, allowing the adiabatic motion of particles from the magnetosphere to the magnetosheath. The field orientations are (a) radial, (b) southward, (c) Y-directed, (d) Parker Spiral away, (e) northward, (f) Parker spiral toward.

Figure 4. Cross-sections of some of the volumes defined by the heavy lines in Figures 1 and 2 at various planes parallel to the GSE coordinate axes. The light shading shows the areas within which widespread leakage (see Fig. 1) would be observed, while the dark shading shows these areas for localized, reconnection site leakage (see Fig. 2). The X, Y, or Z positions and interplanetary field orientations are indicated in the upper right.

Figure 5. Examples of particle trajectories in the model magnetosheath magnetic and electric (VXB) field. On the left, the interplanetary field is perpendicular to the flow. The light lines show the streamline and background field line geometry in the plane of symmetry. The particles launched near the subsolar magnetopause with  $45^\circ$  pitch angle, have energies of 1 keV, 5 keV and 50 keV from left to right. The shading shows where magnetosheath turbulence, which can scatter the particles, is expected behind the quasiparallel shock. On the right a similar diagram illustrates 1 keV and 5 keV particles for a Parker Spiral interplanetary field.



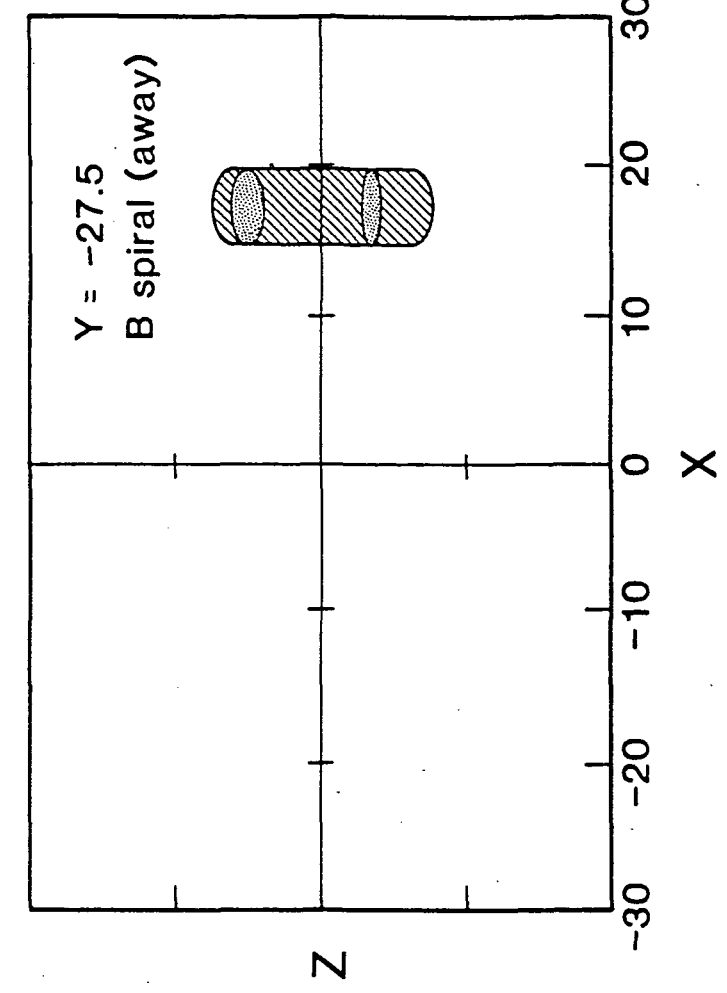
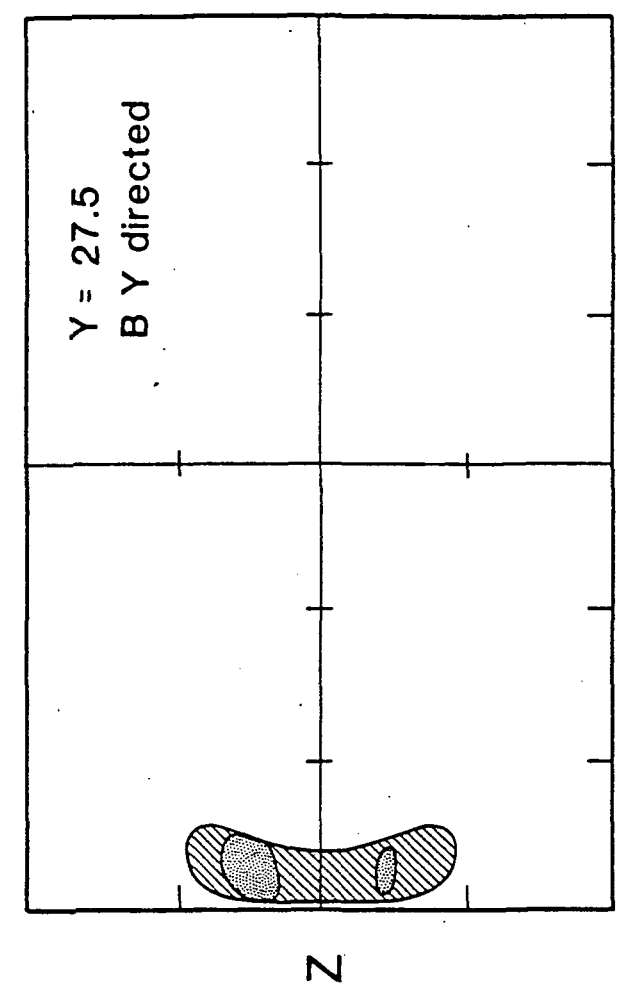
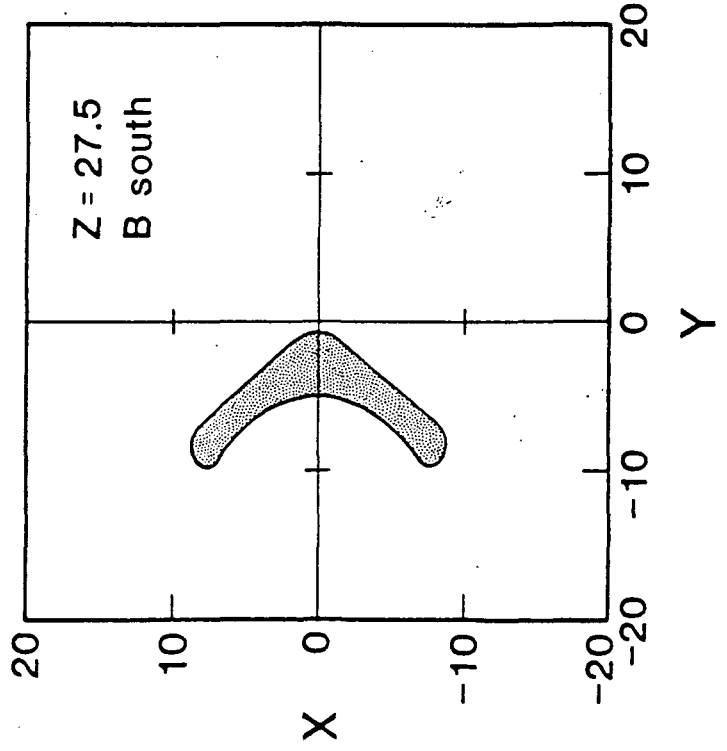
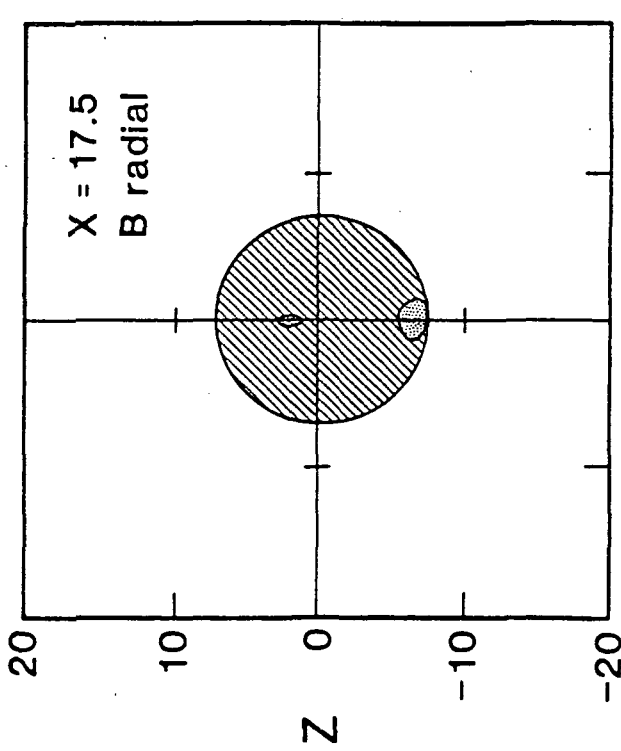


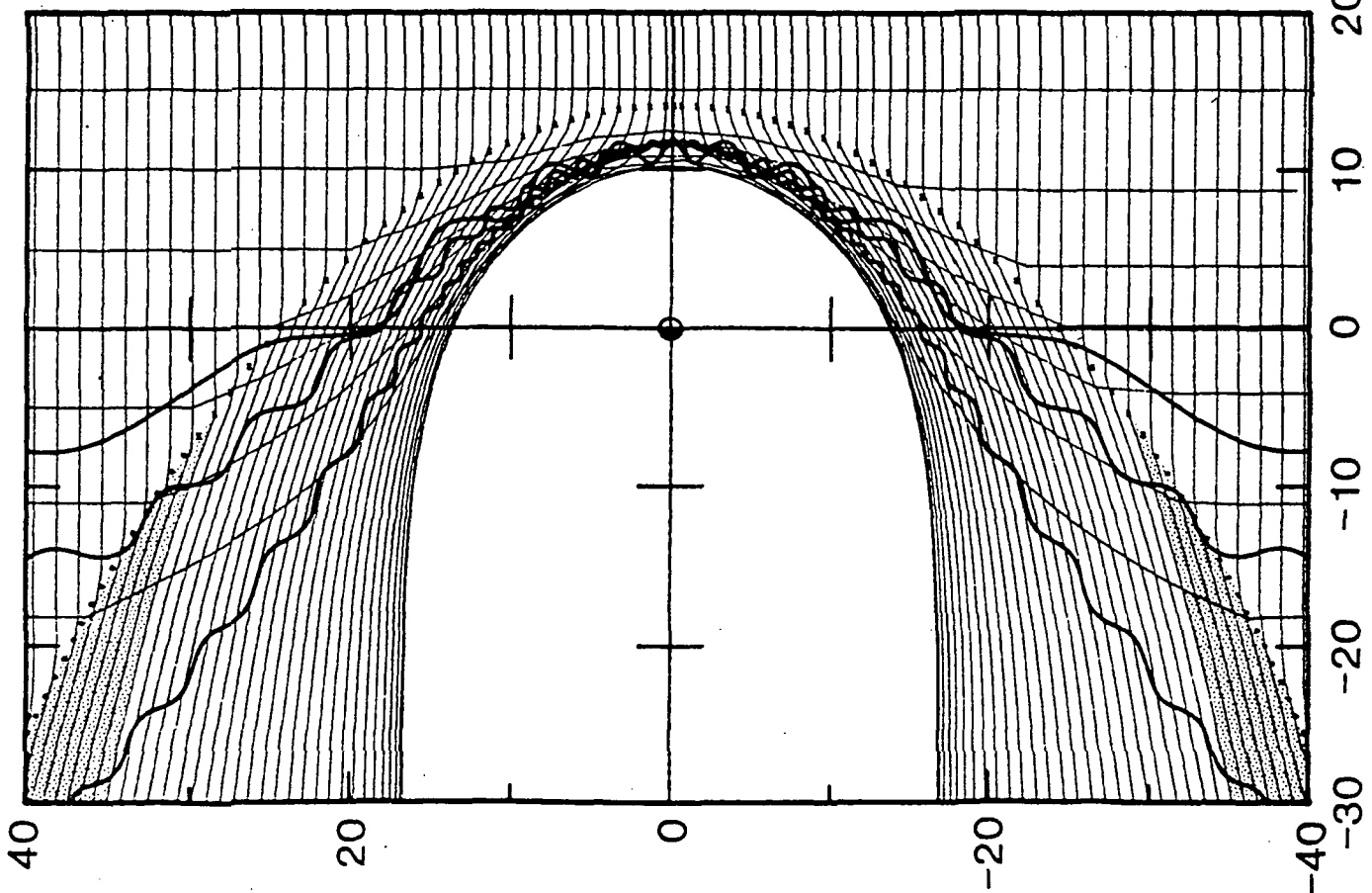
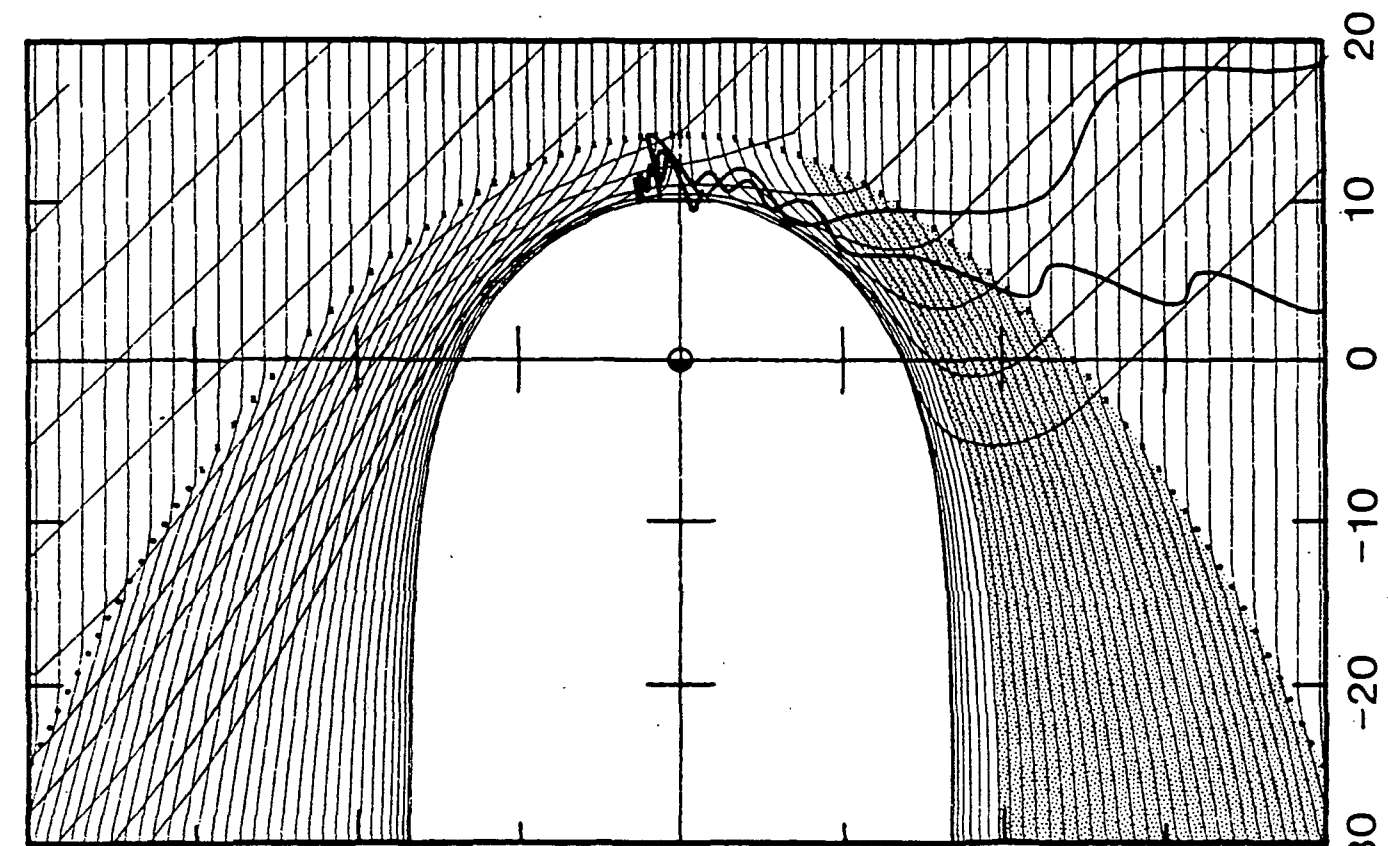


Z

Z

Y





MAGNETOPAUSE MERGING SITE ASYMMETRIES

N. U. Crooker

Department of Atmospheric Sciences

University of California

Los Angeles, California 90024

J. G. Luhmann

Institute of Geophysics and Planetary Physics

University of California

Los Angeles, California 90024

J. R. Spreiter

Department of Applied Mechanics

Stanford University

Stanford, California 94305

S. S. Stahara

R M Associates, Inc.

Lafayette, California 94549

March 1984

## Abstract

Regions where a draped model magnetosheath magnetic field is nearly antiparallel to a model geomagnetic field are shown to be asymmetric for an interplanetary magnetic field (IMF) at the garden hose angle, as suggested by Heelis. When the IMF has a southward component, the asymmetry favors the dawn region for both IMF polarities. The dusk region is favored when the IMF has a northward component. If the regions of antiparallel fields are assumed to be sites of maximum magnetic merging, then the asymmetry is consistent with observed seasonal variations of geomagnetic activity and with dawn-displaced magnetospheric phenomena. In the alternate merging geometry of a line passing through the subsolar region, the asymmetry is predominantly north-south rather than dawn-dusk. Merging line geometry is consistent with the seasonal variations but not with the dawn-displaced phenomena. However, in view of available direct observations of merging signatures in the subsolar region, it is suggested that merging sites may be determined by some combination of the antiparallel and merging line hypotheses.

## Introduction

In a series of papers, Aoki [1977], Hakamada et al. [1980], and Murayama et al. [1980] show that the level of substorm activity in the northern hemisphere depends upon the  $y$  component (GSM coordinates) of the interplanetary magnetic field (IMF) and the angle  $\chi$  between Earth's dipole axis and the  $z$  axis in a manner not predicted by theory. Similar effects also were demonstrated by Friis-Christensen and Wilhelm [1975] and Matsushita and Xu [1981 a,b]. Figure 1, reproduced from Murayama et al. [1980], shows the pattern for the westward auroral electrojet index AL, normalized by an adjusted product of the southward component of the IMF and the square of solar wind speed. When  $\chi$  is large and positive, during northern hemisphere summer, normalized AL is about twice as high for large negative  $B_y$  as for large positive  $B_y$ . As  $\chi$  decreases to negative values, the difference in normalized AL for negative and positive  $B_y$  decreases and then reverses. For large negative  $\chi$ , during northern hemisphere winter, normalized AL is about twice as high for large positive  $B_y$  as for large negative  $B_y$ . Also, there is an overall decrease in normalized AL from positive to negative  $\chi$ .

The variations in Figure 1 can be explained as a direct result of a dawnward displacement of the stagnation point in the magnetosheath flow pattern, under the assumption that energy transfer by magnetic merging is ordered in a coordinate system rotated from the GSM system so that its  $x$ -axis passes through the displaced stagnation point (Maezawa and Yoshizawa, unpublished manuscript, 1981). The required angular displacement is on the order of  $15^\circ$  (T. Murayama, private communication, 1981). Although magnetohydrodynamic effects can produce

a displacement of this size [Russell et al., 1981], and magnetosheath flow direction measurements support its occurrence for a single case [Crooker et al., 1984a], the condition under which it is predicted and observed is the infrequent condition of low Alfvén Mach number. It is clear from the statistical analysis of Crooker et al. that there is no average downward displacement of the stagnation point of the size required to cause the variations in Figure 1.

An alternative explanation was offered by Murayama et al. [1980]. The variations in Figure 1 also would follow if merging was favored on the dawn side of the dayside magnetopause. Under the assumption that the merging rate is highest where the magnetosheath and geomagnetic fields are antiparallel [Crooker, 1979], the merging rate will be highest on the dawn side when  $B_y$  is negative during northern hemisphere summer, when the dayside is dominated by the northern cusp region. These conditions correspond to the highest values of normalized AL at the top left in Figure 1. The remaining variations may be explained by the same line of argument, except for the overall decrease from top to bottom, which can be attributed to decreasing ionospheric conductivity. What the explanation lacks is mechanism for preferred dawnside merging.

Recently Heelis [1984] proposes just such a mechanism in order to interpret observations of high latitude ionospheric convection. The mechanism takes into account the effect of the x component of the IMF. Neglecting the draping of the IMF against the magnetopause, Heelis notes that an IMF with a southward component spiraling at the usual garden hose angle ( $B_y$  and  $B_x$  of opposite sign) is more nearly aligned with the magnetopause surface over the dawnside region of antiparallel fields as compared to the duskside region, both for IMF sectors pointing toward

and away from the sun. Similarly, the dusk side is favored for a southward IMF directed at the ortho-garden-hose angle. But since the garden hose spiral is the most common IMF orientation, it is the dawnside merging regions that are favored most often.

The purpose of the present paper is to test whether draping of the IMF against the magnetopause alters the effect described above, as might be expected, since draping is the process of forcing field lines to lie parallel to the magnetopause surface, regardless of the differential in the size of the component normal to the surface introduced by the presence of an x component far away from the surface. The problem is illustrated and analyzed in the next section. Also included is an analysis of the problem in terms of the alternative merging geometry in which only components of the IMF and geomagnetic field merge along a line passing through the subsolar region [Nishida and Maezawa, 1971; Sonnerup, 1974; Gonzalez and Mozer, 1974; Yeh, 1976]. In the third section, the degree to which the x component of the IMF is able to affect asymmetries is discussed, and the merits of the antiparallel region and merging line geometries are compared.

#### Analysis

Figure 2 is a schematic drawing of merging geometries for garden hose IMF orientations with southward components and x components pointing toward and away from the sun, as labeled. The views are from the sun looking toward the dayside magnetopause. The shaded areas in a and b extending from the cusps represent regions where the y and z components of the IMF, transverse to the Earth-sun line, are most

antiparallel to the y and z components of Earth's field at the magnetopause [Crooker 1979]. The solid vectors in each view indicate the projected direction of the magnetic field.

Figure 2a illustrates how the undistorted IMF projects against the magnetopause. If for simplicity the shape of the dayside magnetopause is assumed to be a hemisphere, then a linear IMF will be tangent to the surface along a great circle across the hemisphere, as indicated by the dashed lines in the figure. For a toward sector the dawnside shaded region is in the northern hemisphere, and the dashed line passes through most of its length. In the southern hemisphere the dashed line passes through a smaller portion of the duskside shaded region, far from the subsolar area. For an away sector, the dawn and dusk shaded regions reverse hemispheres, but the dashed line changes its orientation so that it still passes through most of the length of the dawnside region, in this case in the southern hemisphere. Since the IMF and Earth's field are nearest to being antiparallel where the dashed lines overlap the shaded regions, it follows that more merging will occur on the dawn side for both sector polarities, under the assumption that the merging rate is greatest where the fields are nearest being antiparallel.

However, if the IMF is draped against the magnetopause, it is tangent not only along the dashed lines in Figure 2a but across the entire surface, and the above argument is not applicable. Figure 2b illustrates how the dawn side remains the preferred site of merging even under conditions of draping. The parallel pairs of vectors represent IMF lines with no x-component. When they drape against the magnetopause, they acquire some curvature directed outward from the center; but the curvature is minimal [Crooker et al., 1984b] and is

symmetric with respect to the intersection of the lines with the shaded regions and is neglected here. The effect of adding an x component to the IMF is to cause the draped field lines to radiate from a point [Kartalev and Mastikov, 1982; Crooker et al., 1984b]. As the ratio of the x component to the transverse component increases from zero, the point from which the lines radiate moves radially inward from infinity, along the direction of the projected IMF. Thus, neglecting curvature, draped field lines change from being parallel for no IMF x component to being directed radially away from the subsolar point for no IMF transverse component [Spreiter et al., 1966]. The effect of adding an x component is to change the orientation of the magnetic field within the surface which lies tangent to the entire dayside magnetopause.

The sense of change is shown in Figure 2b for field lines which pass through the shaded regions. The pairs of field vectors radiating from points represent IMF lines with southward components at the garden hose orientation, draped against the magnetopause (neglecting curvature). Compared to the parallel vectors for an IMF with no x component, the radiating vectors are directed more southward in the dawnside shaded region and more northward in the duskside region for both toward and away polarities. The effect of this asymmetry is an enlargement and displacement toward the subsolar point of the dawnside region of antiparallel fields, and a corresponding shrinking and displacement away from the subsolar point of the duskside shaded regions.

The resulting asymmetry of the regions of antiparallel fields for the draped IMF in a garden-hose-spiraling toward sector is shown in Figure 3d. The pattern has been determined quantitatively by means of the computer model developed by Luhmann et al. [1984]. Results for the

away sector are not shown but are mirror symmetric about the equator. The shaded regions are areas where the Hedgecock-Thomas geomagnetic model field (R. J. Walker, unpublished manuscript, 1979) and the Spreiter-Stahara gasdynamic draped magnetosheath model field [Spreiter and Stahara, 1980] are within  $10^\circ$  of being antiparallel. The orientation of the transverse component of the IMF input to the magnetosheath model is indicated by the arrow at the center of the diagram. The x component of the IMF input is positive, as required for the garden hose orientation, and its magnitude is equal to the magnitude of the transverse component. The asymmetry predicted as a result of considering the geometry in Figure 2b is clearly shown in Figure 3d. The dawnside region of antiparallel fields is larger and nearer to the subsolar point than is the duskside region.

Figures 2 and 3 represent configurations for equinox. The seasonal variations in Figure 1 follow from the dawn preference demonstrated for equinox under the assumption that the summer hemisphere merging site dominates the winter hemisphere site, as the summer hemisphere cusp region tilts equatorward.

The regions of antiparallel fields for less southward orientations of the the transverse component of the IMF are shown in Figures 3a-c. In each case the magnitude of the x component of the IMF is equal to the magnitude of the transverse component and is directed toward the sun. As the z component shifts from southward to northward, the regions become smaller, as noted previously [Luhmann et al., 1984]. What is more relevant to the present discussion is that the asymmetry shifts from a dawnside to a duskside preference, although the duskside preference for a northward component in Figure 3a is not as pronounced

as the dawnside preference for a southward component in Figure 3d. The fact that the asymmetry switches from dawn to dusk as the IMF rotates from southward to northward does not affect the argument which requires a dawn preference to explain Figure 1, since most if not all of the energy transferred to the magnetosphere by merging occurs when the IMF has a southward component. On the other hand, the favored dusk merging for northward IMF may affect the pattern of polar cap convection and polar cap arcs (Chiu et al., paper in preparation).

To consider the effect of the x component of the IMF on the alternative geometry of a merging line, we return to Figure 2. In 2c the curves across the magnetopause represent projected separator lines in the magnetic configuration of a dipole field superposed upon a uniform field [e.g., Stern, 1973]. The separator has the form of a circle in this simple geometry, tilted with respect to the equatorial plane of the dipole. Two neutral points form when the uniform and dipole fields are antiparallel. They lie along the circle and are separated by  $180^\circ$ . The dayside neutral point is indicated by an encircled N in each view. Yeh [1976] identified the separator line with the merging line in an analysis of the dependence of its tilt on the orientation of the transverse component of the IMF, and Cowley [1981] noted that such a merging line would lie north of the dipole equator across most of the dayside for an IMF directed toward the sun and south of the equator for an IMF away from the sun. The separator merging lines in Figure 2c resemble the dashed lines in 2a. Both sets are projected circles, but the tilt angle of the separator lines is about half that of the dashed lines, and they illustrate completely different concepts. The separator merging line model was chosen for consideration

from among the several cited in the introduction because it is the only one which specifies the location of the line with respect to global features. Most other models simply assume, at least implicitly, that the merging line passes through the subsolar or stagnation point, in which case no asymmetries arise.

The obvious asymmetry in Figure 2c is the dawn preference for the location of the neutral point. However, this is exactly the location where the merging fields are antiparallel. If it is assumed that merging occurs preferentially near the neutral points [Stern, 1973], then the model becomes an antiparallel merging model, and the same reasoning given above for explaining the variations in Figure 1 applies. On the other hand, if the merging rate is assumed to be highest in the region nearest the subsolar point, then there is no dawn preference. But the seasonal variations in Figure 1 follow as a result of the north-south displacement of the merging line. During northern hemisphere summer, the subsolar point moves above the dipole equator, nearer to the merging line for the toward sector. Thus the merging rate and substorm activity should be highest for negative  $B_y$ , as observed. The opposite conditions hold during northern hemisphere winter.

#### Discussion

It has been argued that the x component of the IMF should have a negligible effect on the pattern of magnetic field orientation at the dayside magnetopause (V. M. Vasyliunas, discussion at the Chapman Conference on Reconnection, Los Alamos, 1983). Solar wind plasma that comes closest to the dayside magnetopause crosses the bow shock very

near the stagnation streamline in the gasdynamic model of magnetosheath flow [e.g., Spreiter et al., 1966]. In this region of the bow shock, only the transverse component of the IMF is amplified, by up to a factor of four, as the solar wind passes through the shock. Thus in any radial cross section of the dayside magnetosheath, the ratio of the x component to the transverse component decreases upon approach to the magnetopause.

The effect of the decreasing influence of the x component on the pattern in Figure 2b is that for a given ratio of IMF x to transverse components (or given cone angle), the point from which the field lines radiate moves outward upon approach to the magnetopause. In an example given by Kartalev and Mastikov [1982], for a cone angle of  $10^\circ$  the point moves from a radial distance of  $\sim 3 R_E$  to  $\sim 10 R_E$  as distance from the magnetopause decreases from about a third of the distance to the bow shock to essentially zero.

The magnetic field patterns used to generate the asymmetric merging site patterns in Figure 3 are on a magnetopause-shaped surface with a nose radius  $1 R_E$  larger than the model magnetopause. Examples of patterns on this surface for different IMF cone angles are given in Crooker et al. [1984b]. At this distance from the magnetopause the x component clearly is effective in producing asymmetric patterns, as Figure 3 illustrates. On a surface closer to the magnetopause, the asymmetries would be less pronounced.

At this stage no method exists for quantifying how large the asymmetry in the patterns in Figure 3 must be in order to produce the observed magnetospheric asymmetries. Thus the appropriate distance from the magnetopause in the model cannot be specified. However, observational evidence suggests that conditions at the magnetopause are

represented reasonably well by the gasdynamic model at distances of  $0.5 - 1 R_E$  outside the model magnetopause [Crooker et al., 1984b]. Also, flux transfer events, which are interpreted as signatures of magnetic merging, have a scale size on the order of  $1 R_E$  [Saunders et al., 1984]. Therefore it seems reasonable to assume that the x component of the IMF produces asymmetries as large as those shown in Figure 3.

With the above qualifications, it has been shown that the seasonal variations in Figure 1 can be explained by either of two hypotheses: The merging rate on the dayside magnetopause is highest either where the fields are most antiparallel or where a merging line passes closest to the subsolar point. A distinguishing feature between the two hypotheses is that the antiparallel hypothesis predicts a dawn preference for the merging site whereas the merging line hypothesis does not. A dawn preference seems to be required by Heelis [1984] to explain the dawn displacement of the throat region in the high latitude ionosphere where convection initiates, and thus his results favor the antiparallel hypothesis. Consistent with Heelis' observations is the pattern of Birkeland currents and electric fields in the high latitude ionosphere. Theory predicts that the pattern of currents should be rotated with respect to the pattern of electric fields in such a way that if the currents are aligned with the noon-midnight meridian, as observed, the electric fields should be rotated toward dawn [e.g., Harel et al., 1981]. Other magnetospheric phenomena which can be explained by a dawn preference for merging are discussed by Russell et al. [1981].

Direct observations at the magnetopause have not been definitive in distinguishing between the two hypotheses. Merging signatures of plasma acceleration [e.g., Sonnerup et al., 1981] and flux transfer events

[Rijnbeek et al., 1984; Berchem and Russell, 1984] have been observed to occur relatively uniformly across the dayside magnetopause by the ISEE 1 and 2 spacecraft, which were confined to latitudes equatorward of the cusps. This distribution favors the merging line hypothesis, since magnetosheath flow would carry flux tubes which have merged near the subsolar point uniformly away from the region. Furthermore, antiparallel merging predicts a minimum of merging at the subsolar point, which is not observed. On the other hand, flux transfer events display half-wave rectifier behavior: they occur for southward but not northward external field orientations [Rijnbeek et al., 1984; Berchem and Russell, 1984]. Half-wave rectifier behavior is a feature of the antiparallel hypothesis but not the merging line hypothesis [Crooker, 1980]: When the IMF is northward, no flux transfer occurs because no regions of antiparallel fields exist on closed field lines, equatorward of the cusps. Half-wave rectifier behavior is not a feature of the merging line hypothesis, since flux transfer occurs for nearly all IMF orientations because there is nearly always some component of the IMF that is antiparallel to the closed dayside field lines. Also, an estimate of the voltage associated with the observed flux transfer events yields a value which is at least a factor of ten lower than observed [Rijnbeek et al., 1984]. Although the estimate represents only a lower limit, it may be that more flux is transferred near the antiparallel regions in the vicinity of the cusps at latitudes not covered by the ISEE spacecraft.

Since both slow plasma speed characteristic of the subsolar region and antiparallel fields are conducive to high merging rates [e.g., Quest and Coroniti, 1978, 1981], it seems reasonable to expect that the

location of merging sites on the magnetopause are governed by some combination of both factors. Merging may occur more easily in the subsolar region than elsewhere for a given finite angle between the fields. The separator merging line in the simple dipole-plus-uniform-field geometry incorporates both factors if it is assumed that the merging rate varies along the line and peaks both at the neutral point and at the subsolar point. However, the magnetic field and flow distortions near the dayside magnetopause required by this simple model are unrealistic [Stern, 1973]. Observations [Crooker et al., 1984 a,b] show that flow and field more nearly follow the predictions of the hydrodynamic model incorporated in the antiparallel region diagrams in Figure 3. Perhaps a superposition of the contours in the diagrams with concentric circles centered on the subsolar point would produce a more accurate picture of merging sites. Further refinement may be achieved by taking into account the magnetic field strength and plasma density, which in classical merging theory control the merging rate [e.g., Sonnerup, 1974].

### Conclusions

Regions on the dayside magnetopause where the transverse component of the IMF is antiparallel to the geomagnetic field are located symmetrically about the subsolar point, one in each hemisphere in opposite quadrants. The addition of an x component to the IMF causes asymmetry in the pattern. For an IMF with a southward component and x and y components of opposite sign giving the usual garden hose orientation, the sense of the asymmetry favors the dawnside region both

for toward and away sectors. This asymmetry was noted by Heelis [1984] to result from contact between undistorted IMF lines and the magnetopause. It has been shown here that the same asymmetry develops for draped field lines but for different reasons. In the case of undistorted IMF lines, the addition of an x component causes asymmetry in the component normal to the magnetopause; in the case of draped field lines, the IMF x component causes asymmetric changes in the orientation of the component tangent to the magnetopause. A dawn preference for flux transfer through magnetic merging can account for a wide range of observations. For northward IMF at the garden hose angle, when no flux transfer occurs in the antiparallel merging model, it has been shown that the asymmetry favors the dusk side.

Asymmetries which develop as a consequence of the x component of the IMF in the alternate geometry of a merging line passing through the subsolar region also are considered. No dawn preference emerges, but direct observations of merging signatures at the magnetopause suggest that the location of merging sites is determined by some combination of the slow flow speed characteristic of the subsolar region and the degree to which the merging fields are antiparallel.

Acknowledgments. The authors thank C. T. Russell and G. L. Siscoe for helpful comments. This work was supported by the National Aeronautics and Space Administration under grants NSG5351 and NASW-3791 and by the National Science Foundation under grant ATM-82-10691.

## References

- Aoki, T., Influence of the dipole tilt angle on the development of auroral electrojets, J. Geomag. Geoelectr., 29, 441-453, 1977.
- Berchem, J., and C. T. Russell, Flux transfer events on the magnetopause: Spatial distribution and controlling factors, J. Geophys. Res., submitted, 1984.
- Cowley, S. W. H., Asymmetry effects associated with the X component of the IMF in a magnetically open magnetosphere, Planet. Space Sci., 29, 809-818, 1981.
- Crooker, N. U., Dayside merging and cusp geometry, J. Geophys. Res., 84, 951-959, 1979.
- Crooker, N. U., The half-wave rectifier response of the magnetosphere and antiparallel merging, J. Geophys. Res., 85, 575-578, 1980.
- Crooker, N. U., G. L. Siscoe, T. E. Eastman, L. A. Frank, and R. D. Zwickl, Large scale flow in the dayside magnetosheath, J. Geophys. Res., submitted, 1984a.
- Crooker, N. U., J. G. Luhmann, C. T. Russell, E. J. Smith, J. R. Spreiter, and S. S. Stahara, Magnetic field draping against the dayside magnetopause, J. Geophys. Res., submitted, 1984b.
- Friis-Christensen, E., and J. Wilhjelm, Polar cap currents for different directions of the interplanetary magnetic field in the Y-Z plane, J. Geophys. Res., 80, 1248-1260, 1975.
- Gonzalez, W. D., and F. S. Mozer, A quantitative model for the potential resulting from reconnection with an arbitrary interplanetary magnetic field, J. Geophys. Res., 79, 4186-4194, 1974.
- Hakamada, K., T. Aoki, and T. Murayama, Influence of the east-west

component of the interplanetary magnetic field on the intensity of the auroral electrojet, Planet. Space Sci., 28, 29-39, 1980.

Harel, M., R. A. Wolf, R. W. Spiro, P. H. Reiff, and C.-K. Chen, Quantitative simulation of a magnetospheric substorm, 2. Comparison with observations, J. Geophys. Res., 86, 2242-2260, 1981.

Heelis, R. A., The effects of the interplanetary magnetic field on dayside high latitude ionospheric convection, J. Geophys. Res., in press, 1984.

Kartalev, M. D., and I. P. Mastikov, Steady-state magnetic field in the magnetosheath, Planet. Space Sci., 30, 473-481, 1982.

Luhmann, J. G., R. J. Walker, C. T. Russell, N. U. Crooker, J. R. Spreiter, and S. S. Stahara, Patterns of magnetic field merging sites on the magnetopause, J. Geophys. Res., 89, 1739-1742, 1984.

Matsushita, S., and W.-Y. Xu, IMF sector behavior estimated from geomagnetic data at South Pole, J. Geophys. Res., 86, 3628-3634, 1981a.

Matsushita, S., and W.-Y. Xu, IMF sector effects on the polar geomagnetic field in winter, J. Geophys. Res., 86, 7733-7743, 1981b.

Murayama, T., T. Aoki, H. Nakai, and K. Hakamada, Empirical formula to relate the auroral electrojet intensity with interplanetary parameters, Planet. Space Sci., 28, 803-813, 1980.

Nishida, A., and K. Maezawa, Two basic modes of interaction between the solar wind and the magnetosphere, J. Geophys. Res., 76, 2254-2264, 1971.

Quest, K., and F. V. Coroniti, Linear theory of tearing for the day-side magnetosphere (abstract), EOS Trans. AGU, 59, 351, 1978.

- Quest, K. B., and F. V. Coroniti, Tearing at the dayside magnetopause, J. Geophys. Res., 86, 3289-3298, 1981.
- Rijnbeek, R. P., S. W. H. Cowley, D. J. Southwood, and C. T. Russell, A survey of dayside flux transfer events observed by ISEE 1 and 2 magnetometers, J. Geophys. Res., 89, 786-800, 1984.
- Russell, C. T., H.-C. Zhuang, R. J. Walker, and N. U. Crooker, A note on the location of the stagnation point in the magnetosheath flow, Geophys. Res. Lett., 8, 984-986, 1981.
- Saunders, M. A., C. T. Russell, and N. Sckopke, Flux transfer events: Scale size and interior structure, Geophys. Res. Lett., 11, 131-134, 1984.
- Sonnerup, B. U. O., Magnetopause reconnection rate, J. Geophys. Res., 79, 1546-1549, 1974.
- Sonnerup, B. U. O., G. Paschmann, I. Papamastorakis, N. Sckopke, G. Haerendel, S. J. Bame, J. R. Asbridge, J. T. Gosling, and C. T. Russell, Evidence for magnetic field reconnection at the Earth's magnetopause, J. Geophys. Res., 86, 10049-10067, 1981.
- Spreiter, J. R., A. L. Summers, and A. Y. Alksne, Hydromagnetic flow around the magnetosphere, Planet. Space Sci., 14, 223-253, 1966.
- Spreiter, J. R., and S. S. Stahara, A new predictive model for determining solar wind - terrestrial planet interactions, J. Geophys. Res., 85, 6769-6777, 1980.
- Stern, D. P., A study of the electric field in an open magnetospheric model, J. Geophys. Res., 78, 7292-7305, 1973.
- Yeh, T., Day side reconnection between a dipolar geomagnetic field and a uniform interplanetary field, J. Geophys. Res., 81, 2140-2144, 1976.

## List of Figures

Figure 1. Dependence of the AL index of substorm activity on the dipole tilt angle  $\chi$  and on the y component of the IMF. The AL index is normalized by an adjusted product of the southward component  $B_s$  of the IMF and the solar wind speed  $V$  [from Murayama et al., 1980].

Figure 2. Views from the sun of the dayside magnetopause, for IMF orientations at the garden hose angle pointing toward and away from the sun, as indicated. The plus sign marks the subsolar point for equinox, and the minus signs mark the positions of the cusps. The shaded areas in (a) and (b) indicate regions where the transverse components of the IMF (solid vectors) are most nearly antiparallel to the geomagnetic field. The schematic drawings demonstrate how asymmetries develop for a.) antiparallel regions and undistorted IMF lines, b.) antiparallel regions and draped IMF lines, and c.) subsolar merging lines which are separator lines in the dipole-plus-uniform field superposition model. The encircled N along each merging line marks the location of a neutral point.

Figure 3. Views of a model dayside magnetopause showing contours of the degree to which the geomagnetic field and the draped magnetosheath field are antiparallel, after Luhmann et al. [1984]. The shaded areas indicate regions where the fields are within  $10^\circ$  of being antiparallel. The blank areas cover regions where no component of the two fields are antiparallel. The orientation of the transverse component of the IMF input to the model is shown in the center of each diagram. The

orthogonal x component is equal in magnitude to the transverse component and points toward the sun, such that the IMF spirals at its normal garden hose angle.

$AL/(B_S + 0.5)V^2$

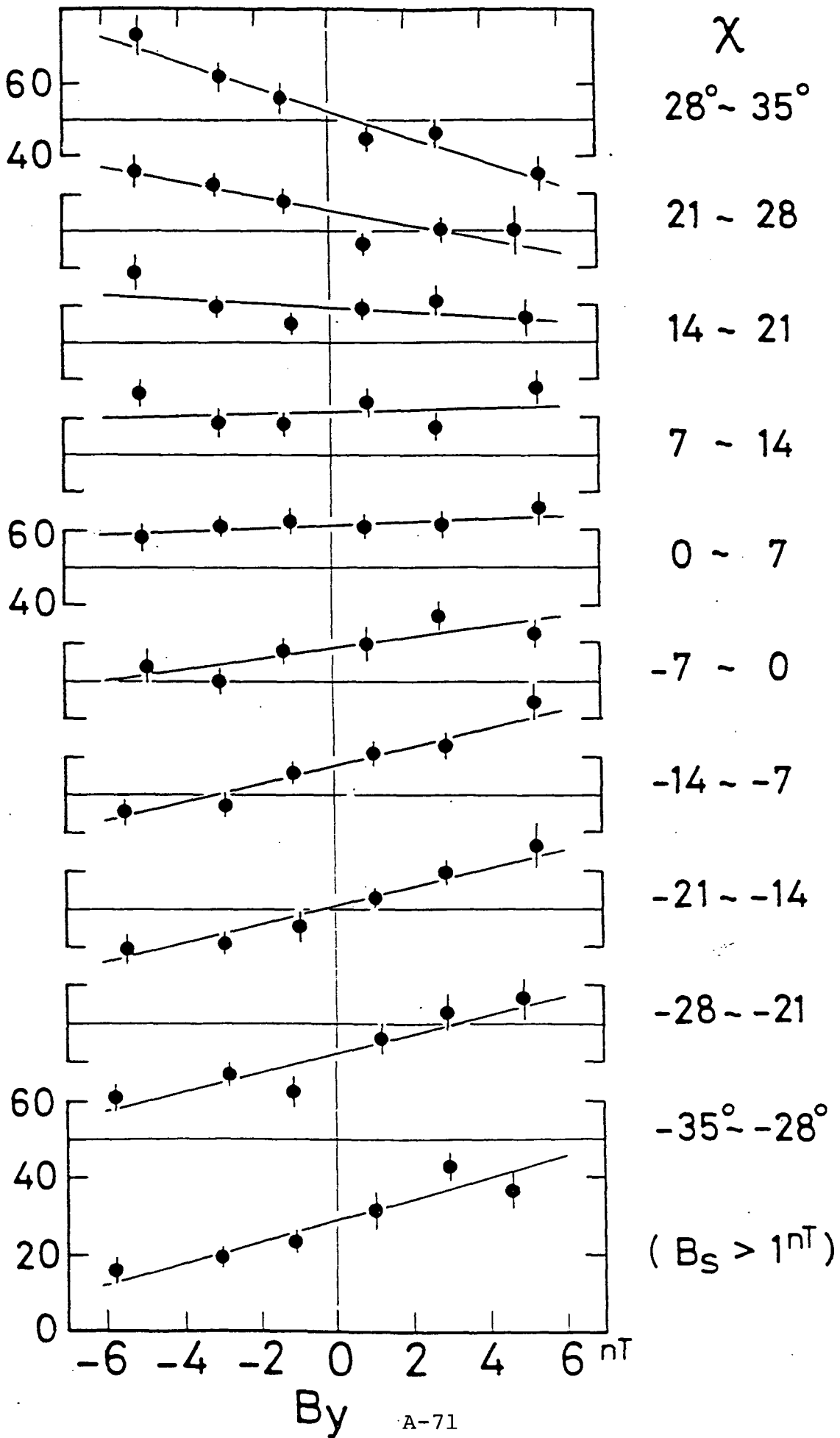
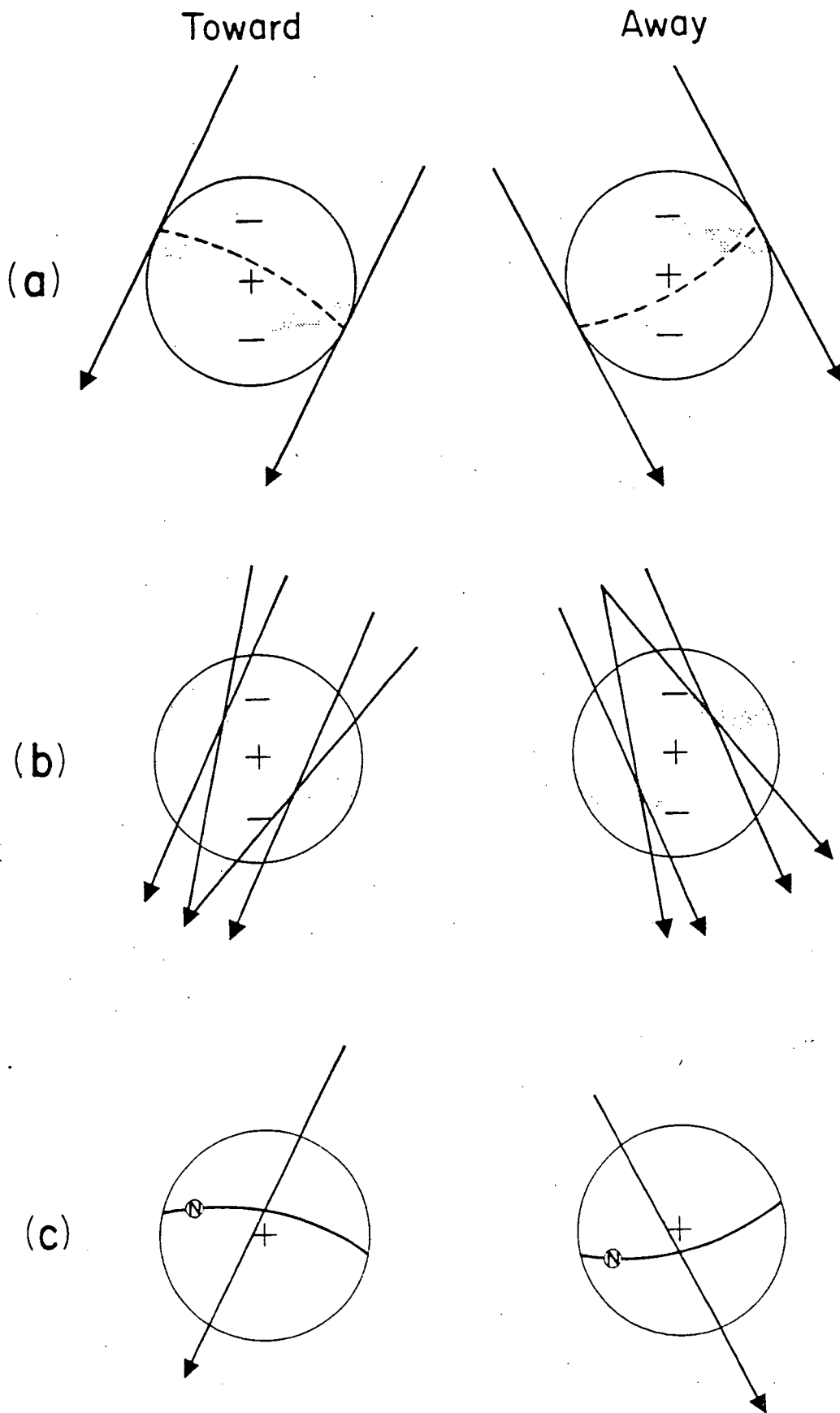
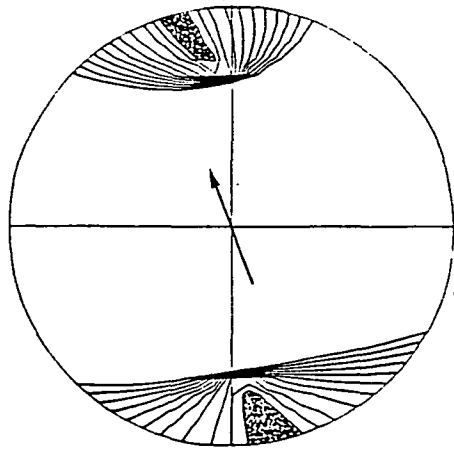


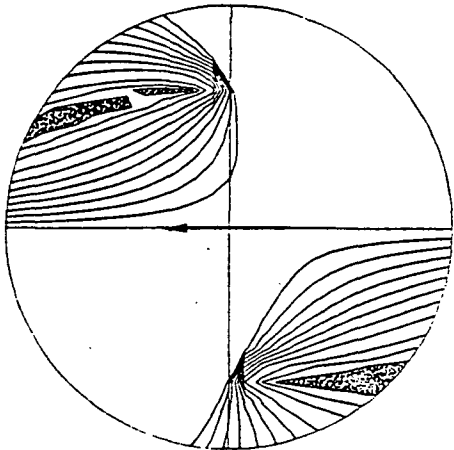
Fig. 1



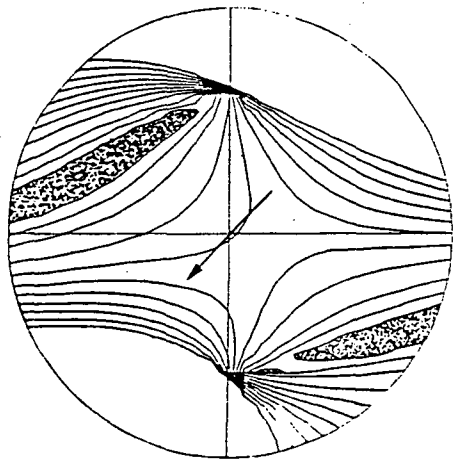
**a**



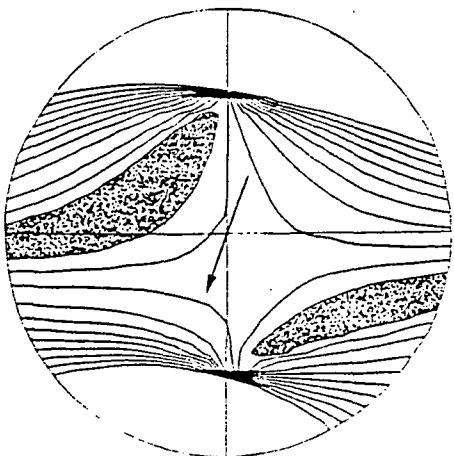
**b**



**c**



**d**



MAGNETIC FIELD DRAPING AGAINST THE DAYSIDE MAGNETOPAUSE

N. U. Crooker

Department of Atmospheric Sciences

University of California

Los Angeles, California 90024

J. G. Luhmann and C. T. Russell

Institute of Geophysics and Planetary Physics

University of California

Los Angeles, California 90024

E. J. Smith

Jet Propulsion Laboratory

California Institute of Technology

Pasadena, CA 91109

J. R. Spreiter

Department of Applied Mechanics

Stanford University

Stanford, California 94305

S. S. Stahara

R M Associates

Lafayette, California 94549

March 1984

## Abstract

Interplanetary magnetic fields observed upstream of Earth's magnetosphere at ISEE 3 form input for a gasdynamic model of magnetic field draping in the dayside magnetosheath. Model results near the magnetopause are compared with appropriately lagged observations at ISEE 1. In 16 of 24 cases, the angle between the transverse component of the model and observed fields is less than  $20^\circ$ . The agreement is surprisingly good in view of the uncertainty introduced by the large distances between ISEE 1 and ISEE 3. The results indicate that magnetohydrodynamic and energy transfer processes at the magnetopause do not cause large distortions of the magnetosheath magnetic field. In addition, a comparison between observed and model field magnitudes indicates that immediately outside the magnetopause the observed field behaves like the model field at a distance of  $\sim 0.5 R_E$  from the magnetopause, outside the region where magnetohydrodynamic effects make the gasdynamic model inapplicable. Patterns of model magnetic field orientation at the magnetopause are presented for practical application.

## Introduction

Knowledge of the orientation of the magnetic field in the magnetosheath near the magnetopause relative to its orientation in the solar wind is important not only for understanding the dynamics of magnetosheath flow but also for understanding the process of energy transfer across the magnetopause. Theoretical progress in this area has been reviewed briefly by Crooker et al. [1984a]. Here we compare observations to the predictions of the simplest magnetosheath model in which the magnetic field is convected to the magnetopause by gasdynamic flow [Spreiter et al., 1966; Alksne, 1967]. Forces produced by the magnetic field on the flow are not taken into account.

Similar but qualitative comparisons have been made by Fairfield [1967] and Behannon and Fairfield [1969]. They show that there is large scale distortion of the magnetic field throughout the magnetosheath. The pattern of distortion is a draping of the field lines over the dayside magnetosphere, as predicted by the hydrodynamic models. The field lines become nearly tangent to the magnetopause surface as they convect along it.

Recent improvements in the gasdynamic model allow direct comparisons with data to be made relatively easily [Spreiter and Stahara, 1980a,b; Russell et al., 1984]. In this paper, magnetic field orientations are compared for the twenty-four cases of ISEE 1 data just outside the dayside magnetopause, which have been studied previously for magnetic field compression [Crooker et al., 1982] and plasma flow deflection [Crooker et al., 1984a], with the aid of data from ISEE 3 in the role of solar wind monitor. Also, as a supplement to the compression study, the

observed and model magnetic field magnitudes are compared. In addition to the data comparison, patterns of model field orientation at the magnetopause are presented for various orientations of the interplanetary magnetic field (IMF).

#### Data Analysis and Results

The times and ISEE 1 spacecraft coordinates at the magnetopause for the twenty-four cases are listed in Table 1 of Crooker et al. [1982]. Also listed are the geocentric solar ecliptic (GSE) components of the appropriately lagged IMF values measured at ISEE 3. The latter were used to rotate the observed ISEE 1 GSE magnetic field components, the ISEE 1 GSE spacecraft coordinates, and the IMF components themselves into geocentric interplanetary medium (GIPM) coordinates [Bieber and Stone, 1979]. In this system the IMF lies parallel to the x-y plane.

The GIPM y-z components of the magnetic field observed at ISEE 1 are shown as solid vectors in Figure 1. They are grouped according to the IMF azimuth angle  $A = \tan^{-1}(-B_y/|B_x|)$ , where  $B_x$  and  $B_y$  are the GIPM x and y components of the IMF. The use of GIPM coordinates insures that the IMF points toward or away from Earth in the +x,-y quadrant, in the "normal" spiral configuration, and A is defined to be the angle between the x axis and the IMF in that quadrant, regardless of the polarity of the field. The base of each vector is plotted at scaled y-z coordinates of the spacecraft location at the time of the magnetopause crossing. The scaling is to a common magnetopause surface, specified by the gasdynamic model, with a nose radius  $R_M = 10 R_E$ .

The dashed vectors emanating from the same spacecraft coordinates in

Figure 1 are the y-z components of the model field. The GIPM IMF components for each case were used as input to a model flow field with average solar wind parameters of Mach number eight and polytropic index two. Although solar wind parameters measured at ISEE 3 were available for each case, the flow field was not changed accordingly because of the orders of magnitude more computer time which would be required. This constraint has a negligible effect on the resultant magnetic field orientations but does affect the field magnitude, as discussed later. The model vectors in Figure 1 represent the magnetic field a small distance away from the magnetopause, on a magnetopause-shaped surface with  $R_M = 10.5 R_E$ . Values close to the boundary were not used in order to avoid the region of rapidly increasing magnetic field magnitude upon approach to the magnetopause which is unrealistic but inherent in the gasdynamic model [e.g., Alksne, 1967].

Figures 2 and 3 summarize the results. The angular separations between the observed and model vectors in the y-z plane in Figure 1 are presented in histogram form in Figure 2. The angles range from  $0^\circ$  to  $180^\circ$ , but two-thirds of the cases have angular separations of less than  $20^\circ$ .

The observed and model field magnitudes,  $B_O$  and  $B_M$ , respectively, are plotted against each other in Figure 3. The model values have been adjusted by a factor of  $(10/R_M)^{3/2}$  in order to match the size of the magnetosphere for each observed case, following the results of Crooker et al. [1982], where  $R_M$  is given by equation (5) in that paper. The dashed line is not a fit to the points. It is included simply to indicate where the points would fall if the model were a perfect predictor. The correlation coefficient between the  $B_M$  and  $B_O$  values is 0.84.

## Model Magnetic Field Patterns

In order to better understand the expected variation of magnetic field vector pattern with angle  $A$  between the IMF and the  $x$  axis in Figure 1, model patterns across the face of the magnetopause have been constructed. They are shown in Figure 4 in order of increasing  $A$  from top to bottom. The order is the same as in Figure 1 except that the increments of increase are somewhat different. The patterns show the  $y$ - $z$  components of the draped field on a surface with  $R_M = 11 R_E$ , outside the model magnetopause with  $R_M = 10 R_E$ . The radial extent of the patterns in the  $y$ - $z$  plane is  $15 R_E$ . The lengths of the short lines forming the patterns are proportional to field strength within each pattern, but the proportionality factor changes from pattern to pattern. For example, a line of a given length in the  $90^\circ$ -diagram is 4.4 times stronger in field magnitude than a line of the same length in the  $0^\circ$ -diagram. This difference reflects the greater degree of compression for an IMF oriented perpendicular to the Earth-sun line.

The main feature of the patterns which changes with  $A$  is the location of the point from which the short lines radiate. For  $A = 0^\circ$ , this point is at the center of the diagram, on the stagnation streamline. Projected to the magnetopause, at the stagnation point, it is the point where the magnetic field vanishes. As  $A$  becomes finite, the point moves rapidly away from the dayside, to the left in the figure, for the usual garden hose spiral angle. For  $A = 15^\circ$  the point is just at the edge of the pattern, a distance of  $15 R_E$  from the center. The

projection of the point to where the field vanishes at the magnetopause is even further from the center of the figure. [See Kartalev and Mastikov, 1982, for a more detailed analysis of the behavior of this point.] For  $A = 90^\circ$ , the point is at infinity, and the pattern becomes symmetric across the noon meridian.

### Discussion

The comparison between the observed and model field orientations in Figures 1 and 2 tests not only the ability of the model to predict the observations but also the ability of IMF measurements made considerably upstream of the magnetosphere to be representative of conditions in its immediate vicinity. Statistical results indicate that 75% of the time the IMF orientation at the sunward-libration-point orbit of ISEE 3 is within  $30^\circ$  of its orientation measured near Earth after a lag time equal to the solar wind advection time (T. J. Kelly et al., paper in preparation, 1984). In the present analysis extra care was taken to determine the best lag time between ISEE 1 and ISEE 3 by matching magnetic features in the two data sets, at least within a few hours of the ISEE 1 magnetopause crossing. Still it is likely that a substantial fraction of the spread in the histogram in Figure 2 is the result of changing field orientation between ISEE 3 and the near-Earth environment. In the case of the largest value in the histogram, it is clear that a solar wind discontinuity which occurred very near the chosen time interval was responsible for most of the angular difference. In view of the uncertainty introduced by using ISEE 3 IMF input to the model, the results in Figures 1 and 2 are remarkably good. They suggest

that conditions at the magnetopause are well-represented by the gasdynamic model slightly away from the magnetopause.

A similar conclusion may be drawn from the comparison of magnetic field magnitudes in Figure 3. Although the dashed line is not a good fit to the points, at least there is a clear correlation between the values. Perhaps a better fit would be obtained if the flow field were adjusted according to the solar wind Mach number for each case. But even without improving the fit, again it seems that the model values outside the region where the field increases unrealistically are not unreasonably far from the values observed directly outside the magnetopause.

On the other hand, for practical purposes, the empirical formula for magnetic field strength outside the magnetopause determined by Crooker et al. [1982] gives more accuracy than the gasdynamic model, at least for the average solar wind Mach number flow field used here. A plot of the empirical formula values against the model values (not shown) is similar to Figure 3 except that the scatter is somewhat less and the slope of a line fit to the points is clearly steeper than the dashed line. Since the empirical formula values represent smoothed observed values, it appears that a systematic difference exists between the model and observations. It is apparent even in Figure 3 that the model predicts values that are too low when the observed values are low and too high when the observed values are high. This systematic difference could be the effect of not taking the solar wind Mach number into account in the model flow fields if the sonic Mach number, used in the model, varies in phase with the Alfvén Mach number in the solar wind.

The model patterns in Figure 4 differ from previously published

patterns such as those of Alksne [1967] and Luhmann et al. [1984] in that they give the vector orientation of the portions of field lines which come nearest to the magnetopause rather than distortions along the entire length of field lines passing through the magnetosheath. The field line distortions tend to give the false impression that the draped pattern against the magnetopause has more curvature than shown in Figure 4. The lack of substantial curvature in the y-z plane is consistent with the fact that models which do not take field line draping into account nevertheless are reasonably successful in predicting the magnetospheric response to IMF-orientation dependent energy transfer [e.g., Gonzalez and Mozer, 1974; Crooker, 1979].

The patterns in Figure 4 are similar to the vector plots of Kartalev and Mastikov [1982] for a comparable gasdynamic model except that their plots are on bow-shock-shaped surfaces in the magnetosheath rather than on a magnetopause surface. The Figure 4 plots should be useful for magnetopause studies which require knowledge of magnetosheath field orientation at the dayside magnetopause, except for  $A < 15^\circ$ , when the location of the point from which the field lines radiate is highly variable with distance from the magnetopause as well as with  $A$  [Kartalev and Mastikov, 1982]. Since all field directions are present within a small distance of this point, comparison with observations in its vicinity can result in large uncertainties. Part of the success of the field orientation comparisons in Figures 1 and 2 is that  $A > 15^\circ$  for all cases.

Because  $A$  is large for the cases studied here and also because the curvature of the model draped field pattern is small, the y-z component of the IMF could be substituted for the model field in the orientation

comparison and the results would not be significantly different. The  $20^\circ - 30^\circ$  width of the peak of the histogram in Figure 2 is comparable to or larger than the angular differences between the IMF and draped field orientations. On the other hand, angular deviations of this size, directed opposite from each other in opposite hemispheres, are large enough to account for some pronounced magnetospheric asymmetries [Crooker et al., 1984b].

### Conclusions

1. The magnetic field in the magnetosheath measured within a few minutes of a spacecraft crossing of the magnetopause does not appear to be significantly distorted by boundary processes. Its observed orientation is relatively consistent with the predictions of simple gasdynamic theory. This conclusion does not imply that magnetohydrodynamic and energy transfer processes do not occur at the magnetopause [see, for example, Crooker et al., 1984a], but only that they do not cause large magnetic field distortions.

2. The magnetic field strength as well as its orientation immediately outside the magnetopause is predicted within a factor of two or better by the gasdynamic model parameters for an average flow field at a distance of  $\sim 0.5 R_E$  from the model magnetopause, outside of the region where the model field strength increases rapidly and clearly is not applicable. More accuracy may be achieved by adjusting the flow field according to solar wind Mach number.

3. The pattern of magnetic field draping against the magnetopause in the plane perpendicular to the Earth-sun line has little curvature.

The main variation in pattern occurs for decreasing cone angle  $A$  (increasing ratio of  $x$  to transverse component). The variation is gradual except for  $A$  decreasing from  $\sim 15^\circ$  to  $0^\circ$ . In this range the pattern shifts from a nearly uniformly directed field in the subsolar region to a pattern in which all field directions are present [see, also, Kartalev and Mastikov, 1982; Crooker et al., 1984b].

Acknowledgments. This work was supported by the National Aeronautics and Space Administration under grants NSG 5351 and NASW 3791 and by the National Science Foundation under grant ATM-82-10691.

## List of Figures

Fig. 1. Comparison between observed (solid) and model (dashed) magnetic field vectors in the plane perpendicular to the Earth-sun line, grouped according to the cone angle  $A$  between the observed IMF input to the model and the Earth-sun line. The views are from the sun in GIPM coordinates, in which the IMF lies parallel to the  $x$ - $y$  plane and  $A$  is its azimuth angle, which always lies in the  $+x, -y$  quadrant.

Fig. 2. Histograms of angular separations between observed and model vectors in Figure 1.

Fig. 3. Observed magnetic field magnitudes  $B_o$  plotted against model magnitudes  $B_m$ , which have been adjusted according to the size of the magnetosphere for each case. The dashed line indicates where the points would lie if the model were a perfect predictor.

Fig. 4. Model magnetic field patterns against the dayside magnetopause in the plane perpendicular to the Earth-sun line, covering a circle of radius  $15 R_E$  centered on the subsolar point, for a range of IMF cone angles  $A$  indicated in the left margin. The views and coordinates are the same as in Figure 1.

## References

- Alksne, A. Y., The steady-state magnetic field in the transition region between the magnetosphere and the bow shock, Planet. Space Sci., 15, 239-245, 1967.
- Behannon, K. W., and D. H. Fairfield, Spatial variations of the magnetosheath magnetic field, Planet. Space Sci., 17, 1803-1816, 1969.
- Bieber, J. W., and E. C. Stone, Energetic electron bursts in the magnetopause electron layer and in interplanetary space, in Magnetospheric Boundary Layers, edited by B. Battrock, pp. 131-135, ESA SP-148, Paris 1979.
- Crooker, N. U., Dayside merging and cusp geometry, J. Geophys. Res., 84, 951-959, 1979.
- Crooker, N. U., G. L. Siscoe, C. T. Russell, and E. J. Smith, Magnetic field compression at the dayside magnetopause, J. Geophys. Res., 87, 10,407-10,412, 1982.
- Crooker, N. U., G. L. Siscoe, T. E. Eastman, L. A. Frank, and R. D. Zwickl, Large scale flow in the dayside magnetosheath, J. Geophys. Res., submitted, 1984a.
- Crooker, N. U., J. G. Luhmann, J. R. Spreiter, and S. S. Stahara, Magnetopause merging site asymmetries, J. Geophys. Res., submitted, 1984b.
- Fairfield, D. H., The ordered magnetic field of the magnetosheath, J. Geophys. Res., 72, 5865-5877, 1967.
- Gonzalez, W. D., and F. S. Mozer, A quantitative model for the potential resulting from reconnection with an arbitrary interplanetary magnetic field, J. Geophys. Res., 79, 4186-4194, 1974.
- Kartalev, M. D., and I. P. Mastikov, Steady-state magnetic field in the magnetosheath, Planet. Space Sci., 30, 473-481, 1982.

- Luhmann, J. G., R. J. Walker, C. T. Russell, N. U. Crooker, J. R. Spreiter, S. S. Stahara, and D. J. Williams, Characteristics of the magnetospheric source of interplanetary energetic particles, J. Geophys. Res., in press, 1984.
- Russell, C. T., J. G. Luhmann, J. R. Spreiter, and S. S. Stahara, The magnetic field of Mars: Implications from gasdynamic modeling, J. Geophys. Res., in press, 1984.
- Spreiter, J. R., A. L. Summers, and A. Y. Alksne, Hydromagnetic flow around the magnetosphere, Planet. Space Sci., 14, 223-253, 1966.
- Spreiter, J. R., and S. S. Stahara, A new predictive model for determining solar wind - terrestrial planet interactions, J. Geophys. Res., 85, 6769-6777, 1980a.
- Spreiter, J. R., and S. S. Stahara, Solar wind flow past Venus: Theory and comparisons, J. Geophys. Res., 85, 7715-7738, 1980b.

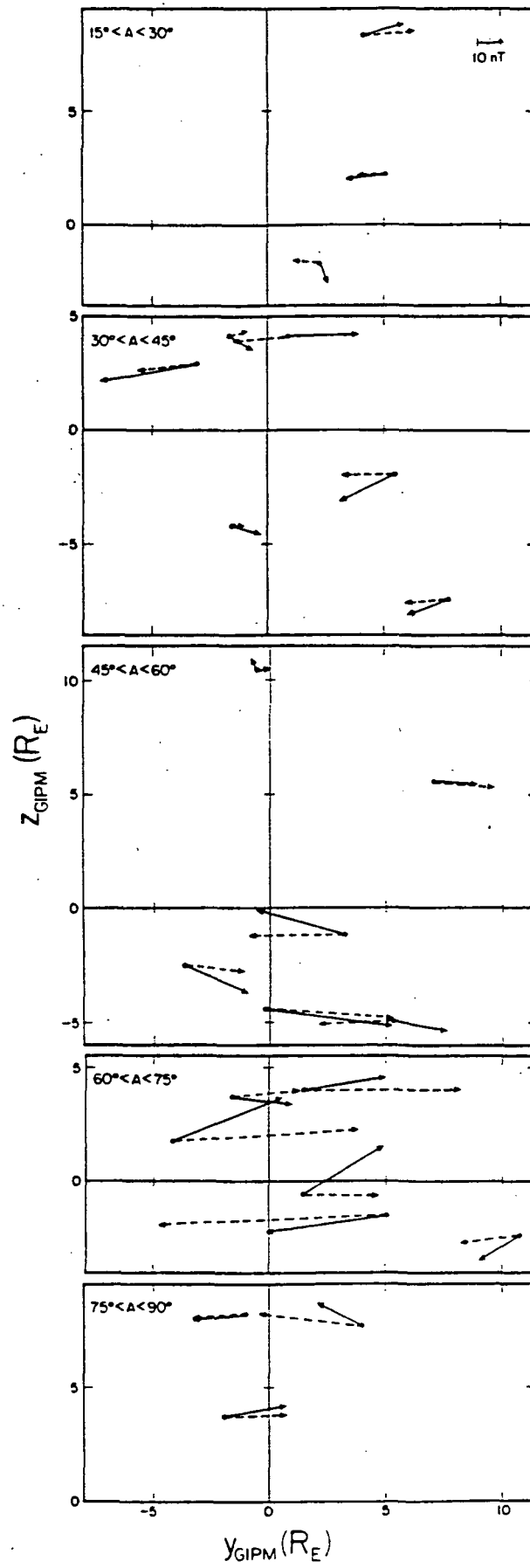


Figure 1

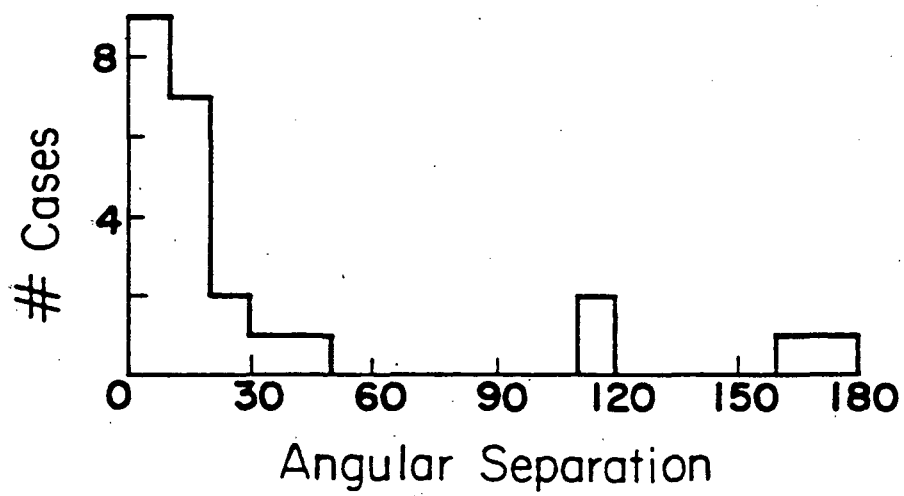


Figure 2

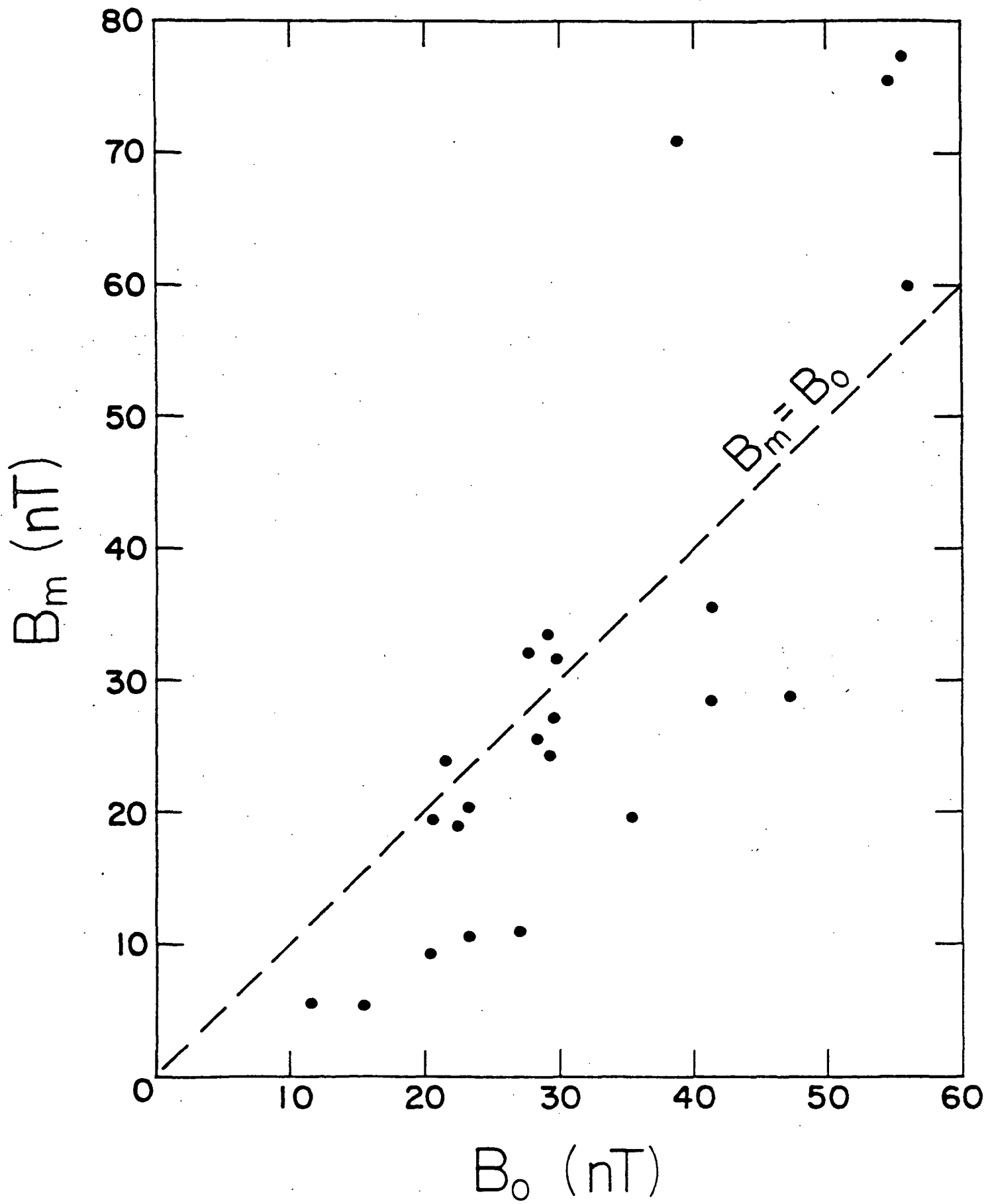


Figure 3

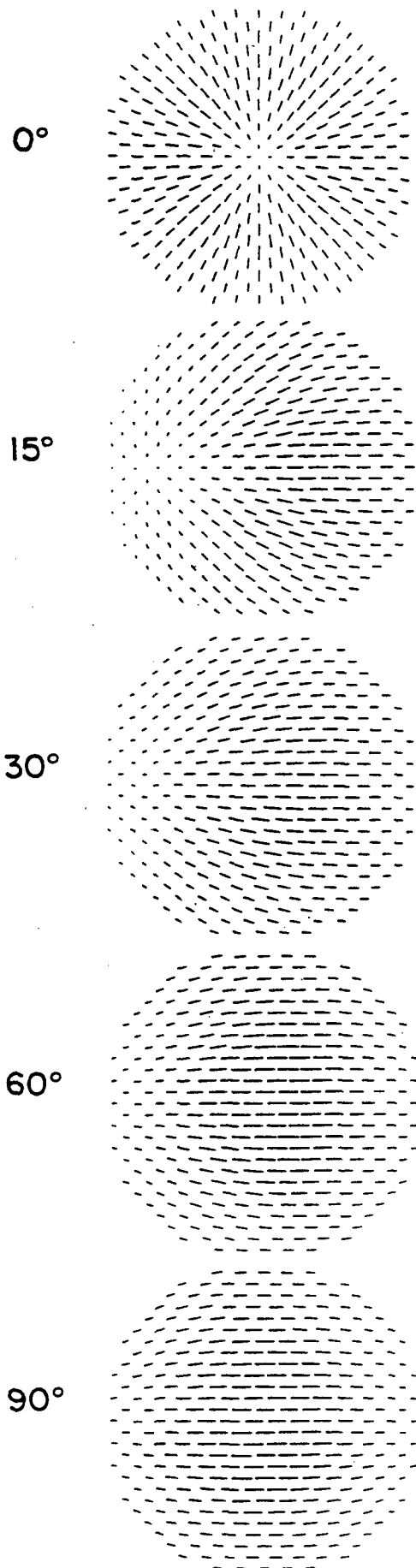


Figure 4

THE MAGNETIC FIELD OF MARS:  
IMPLICATIONS FROM GASDYNAMIC MODELING

C.T. Russell<sup>1</sup> and J.G. Luhmann  
Institute of Geophysics and Planetary Physics  
University of California, Los Angeles  
Los Angeles, California 90024

J.R. Spreiter  
Division of Applied Mechanics  
Stanford University  
Stanford, California 94305

S.S. Stahara  
RMA Associates  
3738 Mount Diablo Boulevard, Suite 200  
Lafayette, California 94549

IGPP Publication No. 2468

Revised January 1984

<sup>1</sup>Also Department of Earth and Space Science, UCLA

## ABSTRACT

On January 21, 1972 the Mars-3 spacecraft observed a variation in the magnetic field during its periapsis passage over the dayside of Mars that was suggestive of entry into a Martian magnetosphere. We have obtained the original data and trajectory (Sh. Sh. Dolginov, personal communication, 1983), and have attempted to simulate the observed variation of the magnetic field using a gasdynamic simulation. In the gasdynamic model we first generate a flow field and then use this flow field to carry the interplanetary magnetic field through the Martian magnetosheath. The independence of the flow field and magnetic field calculation allows us to converge rapidly on an IMF orientation which would result in a magnetic variation similar to that observed by Mars-3. There appears to be no need to invoke an entry into a Martian magnetosphere to explain these observations.

Of the magnetic fields of the four terrestrial planets, the magnetic field of Mars is least understood, even though Mars has been visited by many spacecraft. The reason for this gap in our understanding is that of the many U.S. spacecraft to Mars, only the first, Mariner 4, in 1965, carried a magnetometer, and on this mission the flyby distance was so great that only brief encounters with the planetary bow shock and magnetosheath were observed (Smith, 1969). At least three Soviet Martian orbiters have carried magnetometers, but none of these spacecraft have provided low altitude (<1000 km) data or measurements directly behind the planet. Nevertheless, some of these measurements have been interpreted as indicative of the existence of an intrinsic planetary magnetic field. The Mars 5 measurements behind, but not directly behind, the planet have been interpreted as indicating a tail (Dolginov et al., 1976). The Mars 2 measurements have been interpreted as indicating a dipole moment with its axis in the equatorial plane (Smirnov et al., 1978). The Mars 3 measurements have been interpreted to indicate, on one occasion, an entry into a Martian magnetosphere (Dolginov et al., 1973; Gringauz et al., 1974). However, for this interpretation to be correct, the dipole moment would have to be aligned with the spin axis. Finally, the Soviet measurements have recently been re-interpreted in terms of an eroded magnetosphere in which the dipole axis is antiparallel to the Martian spin axis (T. K. Breus, personal communication, 1983).

These interpretations have been criticized on several counts. The size of the magnetic moment consistent with the reported Mars 5 tail encounters is smaller than that reported from the dayside Mars 3 entry (Russell, 1978a). Further, the putative tail entries are suspect because of the direction of the field in the region inferred to be "tail". The Mars 2 inferences are

inconsistent with the Mars 3 inferences, but are consistent with the magnetotail being due to draped interplanetary magnetic field lines (Russell, 1981). We note that Venus has no discernible intrinsic field, yet still has a magnetotail formed from the interplanetary magnetic field (Russell et al., 1981a). Finally, the Mars 3 measurements have been interpreted as passage through a magnetosheath, rather than a magnetosphere (Wallis, 1975; Russell, 1978b). Wallis (1975) suggested that the region that Dolginov et al. (1973) had identified as magnetosheath could equally well be interpreted as the foreshock region. Russell (1978b) suggested that the putative magnetospheric field had the draping pattern of magnetosheath field lines. At that time there was no convenient means to test the hypothesis. However, code development since that time now permits a relatively simple test of this hypothesis, and it is the purpose of this note to perform such a test.

We note that the subject of Martian magnetism is controversial. A synopsis of the various arguments has been presented by Slavin and Holzer (1982). It is not the purpose of this paper to address all the points raised in that paper. Herein we address only the question of whether the claimed entry of Mars 3 into a Martian magnetosphere has another equally plausible explanation. Similar fields may have been observed on Mars 2 but the lack of orientation information about the solar direction has precluded the interpretation of these fields in terms of an intrinsic Martian magnetic moment (Dolginov, 1978a).

#### GASDYNAMIC MODELING

Numerical models of the solar wind interaction with planetary obstacles have now been in use for nearly two decades (cf. Spreiter et al., 1966). Code developments and technological change since that time have decreased the cost and increased the speed and flexibility of the models (Spreiter

and Stahara, 1980a, b), and provided the capability of intercomparing observations and models along actual spacecraft trajectories. A feature of the gasdynamic model makes the model easy to use for the task at hand. Because of the assumption of high Alfvénic Mach number inherent in the model, the determination of the magnetic field is decoupled from that of the flow field. Once the flow solution is calculated, the magnetic field can then be subsequently determined by solving the remaining equations involving the magnetic field, employing the same values for density and velocity, previously determined from the flow solution. The magnetic field thus determined does not interact back on the flow. The flow solution depends upon oncoming Mach number, the ratio of specific heats,  $\gamma$  and obstacle shape but is independent of the IMF.

We use this magnetic field independence in our investigations below in the following manner. First, we calculated the flow field around the obstacle for a given Mach number,  $\gamma$ , and shape. We choose a magnetosonic Mach number of 7.7 as being appropriate for average solar wind conditions at Mars (Russell et al., 1982b), and use this value as the analogous Mach number in the gasdynamic code. For an obstacle shape we use a Venus shape with an ionospheric scale height of 0.025. The solution is quite insensitive to this latter quantity as long as it is smaller than about 0.1. The choice of  $\gamma$ , the ratio of specific heats is not a simple matter. Fairfield (1971) and Zhuang and Russell (1981) both deduced that a value  $\gamma = 2$  gives the best fit to the terrestrial magnetosheath thickness. Slavin et al. (1983) have found good agreement for the Mars shock location using  $\gamma = 2$ . Tatrallyay et al. (1983) have found that  $\gamma = 1.85$  provides the best fit for shock jumps at Venus. However, Tatrallyay et al. (1983) also find an Alfvénic Mach number dependence

for the value of  $\gamma$  and that the best fit value of  $\gamma$  is 1.6 above an Alfvénic Mach number of 7. One explanation for these differences is that the most appropriate value for  $\gamma$  in the Rankine-Hugoniot MHD equations and the most appropriate  $\gamma$  for the gasdynamic code for simulation of bow shock location are different. Thus, it may not be possible to simultaneously simulate the proper shock jump and shock location. We have chosen to optimize our parameters to reproduce the shock location and not to reproduce precisely the jump. Thus we have used a Mach number of 7.7 and a  $\gamma$ -value of 2.

After the flow field solution is obtained, we can calculate the magnetic field along the trajectory of the spacecraft as if the magnetic field lines were dye lines in a fluid flow. This calculation is rapid and can be repeated at small cost in computing time. Thus, it is feasible to hunt for a suitable IMF direction, flow observation angle, or obstacle size.

Previous work has used the gasdynamic simulation to determine whether the bow shock location of Mars implies an obstacle of the size of the planet plus ionosphere or somewhat larger (Russell, 1977; 1970; Slavin et al., 1983). Once that obstacle size is determined, one has the further problem of whether the ionosphere is strong enough to stand-off the solar wind (Intriligator and Smith, 1979; Slavin and Holzer, 1982). In this study, we use the gasdynamic simulation in a different way. We wish to examine whether we can replicate the Mars 3 magnetic field observations, which were claimed to indicate a magnetospheric entry, with a trajectory passing solely through the magnetosheath. This argument has been made in the past (Russell, 1978b), but not as quantitatively as is now possible.

## CALCULATIONS

The magnetic field observations that we are attempting to model are shown in Figure 1. Panel (a) shows the time series and panel (b) shows the field vectors and trajectories projected into the Y-Z plane. The field values and the trajectory have been supplied in tabular form by Sh. Sh. Dolginov (personal communication, 1983) to whom we are very grateful. The trajectory is very similar to that originally derived by Russell (1978b; 1979). However, use of investigator-supplied values removes the uncertainty associated with the original interpolation process and a possible source of error. Table 1 lists the position of Mars-3 at selected times. The magnetic field values also closely resembled those published by Gringauz et al. (1974) and Russell (1978b; 1979) as well as those in the early publications by Dolginov and coworkers. However, there is ambiguity and inconsistency in the various descriptions of the coordinate system used to display the Mars-3 magnetic field data. We use herein the latest definition (Dolginov, 1978) in which the direction of the Y-component is in the direction of planetary motion. As we show below this definition of coordinates provides internal consistency in the behavior of the data. We emphasize that we must judge consistency in terms of the variations in the data, since the zero levels of the Mars-3 magnetometer are not known. Our modeling provides an estimate of these uncertainties and they prove to be large.

If we assume that the Mars-3 magnetometer's zero levels remained unchanged during its periapsis passage on 1/21/72, we can use the field variations to initialize our simulation effort. It is both our hypothesis and Wallis' (1975) that an inbound shock crossing occurred at  $1829 \pm 2$  (across an unfortunately timed data gap of 4 minutes duration) and an outbound crossing occurred at 1959.

The latter time was also given as the outbound shock crossing by Dolginov et al. (1975). However, there is little change in the vector field direction there. This fact suggests that the outbound shock is a quasi-parallel shock, i.e., the IMF is parallel to the shock normal at this point. The inbound shock has a more rapid increase, as if it were a quasi-perpendicular shock.

Table 2 lists the median magnetic field vectors from 1815 to 1845 Universal Time across the feature we interpret to be the inbound shock crossing. The Mars 3 magnetometer returned 8 values of the magnetic field in rapid succession every 2 minutes only some of which were successfully recovered. The right-hand column labeled N lists the number of values available at each recording interval. Assuming that the noise on the measurements, both due to the ambient medium and due to the spacecraft, were randomly positive and negative, we used the median values in each telemetry interval as our best estimate. Medians have been used because mean values are sensitive to occasional very inaccurate values whereas medians are not.

For our first estimate of the IMF field, we take the jump in field across the inbound shock divided by three and assume this to be the IMF value. As shown in Table 2, the upstream values are "noisy". However, since we are merely attempting to determine a starting value we will simply use the value at 1827 as the upstream value and the value at 1831 as the downstream value. One-third of this difference is  $(-1.5, -4.5, 0.9)$  which provides our first estimate of the upstream field corrected for zero level errors. Figure 2 panel (a) shows the time series derived using this vector as input and an ionopause altitude of 430 km. The altitude of 430 km was chosen so that the shock occurred at the correct location after aberration was included. This

is consistent with the estimate of Wallis (1975) of the altitude of significant atmospheric interaction. While the shock location is in fact quite sensitive to the chosen altitude of the ionopause, the actual solar wind conditions for 1/21/72 are unknown and possible MHD effects on magnetosheath thickness are also unknown. The important point is that the required altitude of the ionopause to fit the data is at a plausible altitude for the ionopause.

The inbound shock crossing occurs about 8 minutes early and the outbound shock about 22 minutes early. If we rotate the flow  $9^\circ$  in the direction of aberration expected from planetary motion, we obtain the time series shown in Figure 2 panel (b). A  $9^\circ$  aberration angle is only about  $5^\circ$  larger than that expected due to Mars' orbital motion transverse to the solar wind flow and well within the known amplitude of solar wind directional variations. We note that other flow directions will also reproduce the observed shock locations for example a total aberration angle of  $7^\circ$  and a flow from the south of  $4^\circ$  will do as well.

The model time series of Figure 2 resemble the variations seen in Figure 1. However, the model variations are smaller than the observations, especially in the  $B_z$  component. Further, the jump in the magnetic field at the outbound shock seems larger in the models than in the data. Hence we need to make the IMF larger, more negative along the Z-direction and more aligned with the outbound shock normal. Figure 3 shows the results of using an input value of  $(-4, -4.5, -3)$  nT and an aberration of 7 degrees with the flow coming from  $4^\circ$  below the ecliptic plane. The panel on the right shows the model and on the left the observations with the baselines corrected so that the average IMF readings agree. The qualitative behavior of each of the corresponding traces agrees. The magnitude of the variations are equal but the traces differ in the exact timing of the peaks and the rapid variations

in direction. There are many possible reasons for such differences. There are questions of the appropriate choice of  $\gamma$  and  $M_{MS}$  for this day and of the accuracy of the gasdynamic simulation of an MHD problem. We may not have made the best choice of the IMF orientation. Further, it is certain that the IMF did not remain steady during the Mars flyby, as assumed in the simulation.

In order to determine whether our solution is, in fact, a reasonable one, Figures 4, 5 and 6 compare individual vectors from the observations and model. Figure 4 shows the solar ecliptic plane projection. The field vectors to the right and left of Mars agree quite well. Only during the subsolar passage is there a major disagreement. There is certainly no hint in these data that a magnetosphere has been entered. Figure 5 shows the vectors projected in the dawn-dusk plane. There is very good agreement in this projection except near the inbound shock crossing, where there is some apparent temporal variation. Finally, in Figure 6, we show the two solar-cylindrical projections. Again, the agreement is very good, except for obvious temporal fluctuations and in a region near closest approach. This latter distortion is a pulling of the field toward the antisolar direction as if there were some drag on the flow in this region. Such a drag could be provided by mass-loading such as proposed originally by Wallis (1975). However, calculations suggest that mass-loading is weak at Mars (Russell et al., 1983). If, indeed, mass-loading is responsible for this distortion, then our present atmospheric model requires revision.

Earlier, we speculated that the inbound shock was a quasi-perpendicular shock and the outbound shock was quasi-parallel. This is, of course, implicit in the solutions we have derived, but it is of some interest to check this assumption. We can use the coplanarity assumption to derive the shock normal

from the model field values. These normals are (.144, -.624, -.442) and (.618, .705, .347). Since the IMF value input to the model was (-4, -4.5, -3), these correspond to  $\theta_{BN}$  values of  $77^\circ$  and  $12^\circ$ , respectively, for the inbound and outbound shocks. These values are those of a quasi-perpendicular shock and a quasi-parallel shock, as we originally assumed.

#### DISCUSSION AND CONCLUSIONS

The model values do not perfectly replicate the data. Part of the differences are certainly due to temporal variations in the interplanetary magnetic field. Some of the difference may be attributable to non-gasdynamic effects, such as magnetic forces and mass-loading. In view of the existence of so many reasons why there should be differences, the observed agreement is heartening. We have found a magnetosheath magnetic field along the Mars 3 trajectory which resembles the Mars 3 observations. Thus, the Mars 3 data do not provide unambiguously evidence for an intrinsic Martian magnetic field. Our best fit obstacle size is also quite consistent with an ionospheric obstacle. Not only is the solar wind much weaker at Venus than at Mars, but also the Mars gravitational field is weaker. Hence, the upper atmosphere and ionosphere of Mars will have much greater scale heights than at Venus, all else being equal. On the other hand, in situ measurements of both the field and plasma of the Martian ionosphere will be necessary before the exact nature of the ionopause is determined. This study says only that any planetary field did not extend much above 400 km on 1/21/72, and certainly not to 1,200 km, the location of Mars-3. We note that these conclusions agree with Dubinin et al. (1983) based on analogy with laboratory data. However, they feel there may be evidence for an intrinsic field in the tail data of Mars 5.

Finally, we have shown that the gasdynamic simulation provides a powerful tool for interpreting magnetic measurements obtained in planetary magnetosheaths. In the past this important capability has not been fully exploited.

#### Acknowledgments

We gratefully acknowledge the receipt of the Mars 3 trajectory and magnetic field values from Sh. Sh. Dolginov in a very timely manner. This work was supported at UCLA by the National Science Foundation under Grant NSF ATM-82-10691, at Stanford by the National Aeronautics and Space Administration under grant NAGW 278, and at Neilsen Engineering under NASA Contract NASW-3791.

## REFERENCES

- Dolginov, Sh. Sh., On the magnetic field of Mars: Mars -2 and -3 evidence, Geophys. Res. Lett., 5, 89, 1978a.
- Dolginov, Sh. Sh., The magnetic field of Mars, Kosmich. Issled., 16, 257-268, 1978b.
- Dolginov, Sh. Sh., Ye. G. Yeroshenko and L. N. Zhuzgov, Magnetic field in the very close neighborhood of Mars according to data from the Mars -2 and -3 spacecraft, J. Geophys. Res., 78, 4779, 1973.
- Dolginov, Sh. Sh., Ye. G. Yeroshenko and L. N. Zhuzgov, The magnetic field of Mars from Mars-3 and Mars-5 data, Kosmich. Issled., 13, 108-122, 1975.
- Dolginov, Sh. Sh., Ye. G. Yeroshenko, L. N. Zhuzgov, V. A. Sharova, K. I. Gringauz, V. V. Bezrukikh, T. K. Breus, M. I. Verigin and A. P. Remizov, Magnetic field and plasma inside and outside of the Martian magnetosphere, in Solar-Wind Interaction with the Planets Mercury, Venus and Mars, pp. 1-18, NASA SP 397, Washington, D.C., 1976.
- Dubinin, E. M., P. L. Israelovich, I. M. Podgorny and S. I. Shkol'nikova, Nature of the magnetic fields near Mars, Kosmich. Issled., 21, 111, 1983.
- Fairfield, D. H., Average and unusual locations of the Earth's magnetopause and bow shock, J. Geophys. Res., 76, 6700, 1971.
- Gringauz, K. I., V. V. Bezrukikh, T. K. Breus, M. I. Verigin, G. I. Volkov and A. V. Dyachkov, Study of solar plasma near Mars and on Earth-Mars route using charged particle traps on a Soviet spacecraft in 1971-1973  
II. Characteristics of electrons along orbits of artificial Mars satellites Mars-2 and Mars-3, Kosmich. Issled., 12, 585-599, 1974.
- Intriligator, D. S. and E. J. Smith, Mars in the solar wind, J. Geophys. Res., 84, 8427, 1979.

- Russell, C. T., On the relative locations of the bow shocks of the terrestrial planets, Geophys. Res. Lett., 4, 387-390, 1977.
- Russell, C. T., The magnetic field of Mars: Mars-5 evidence re-examined, Geophys. Res. Lett., 5, 85-88, 1978a.
- Russell, C. T., The magnetic field of Mars: Mars-3 evidence re-examined, Geophys. Res. Lett., 5, 81-84, 1978b.
- Russell, C. T., The Martian magnetic field, Phys. Earth Planet. Inter., 20, 237-246, 1979.
- Russell, C. T., The magnetic fields of Mercury, Venus and Mars, Adv. Space Res., 1, 3-20, 1981.
- Russell, C. T., J. G. Luhmann, R. C. Elphic and F. L. Scarf, The distant bow shock and magnetotail of Venus: Magnetic field and plasma wave observations, Geophys. Res. Lett., 8, 843-846, 1981.
- Russell, C. T., M. M. Hoppe and W. A. Livesey, Overshoots in planetary bow shocks, Nature, 296, 45-48, 1982.
- Russell, C. T., T. I. Gombosi, M. Horanyi, T. E. Cravens and A. F. Nagy, Charge-exchange in the magnetosheaths of Venus and Mars: A comparison, Geophys. Res. Lett., 10, 163-164, 1983.
- Slavin, J. A. and R. E. Holzer, The solar wind interaction with Mars revisited, J. Geophys. Res., 87, 10285, 1982.
- Slavin, J. A., R. E. Holzer, J. R. Spreiter, S. S. Stahara and D. S. Chausee, Solar wind flow about the terrestrial planets, 2. Comparison with gas-dynamic theory and implications for solar-planetary interactions, J. Geophys. Res., 88, 19-35, 1983.
- Smirnov, V. N., A. N. Omel'chenko and O. L. Vaisberg, Possible discovery of cusp near Mars, Kosmich. Issled., 16, 864-869, 1978.

- Smith, E. J., Planetary magnetic field experiments, in Advanced Space Environments, (edited by O. L. Tiffany and E. M. Zaitzoff), American Astronautical Society, Tarzana, CA, 1969.
- Spreiter, J. R. and S. S. Stahara, A new predictive model for determining solar wind-terrestrial planet interactions, J. Geophys. Res., 85, 6769, 1980a.
- Spreiter, J. R. and S. S. Stahara, Solar wind flow past Venus: Theory and comparisons, J. Geophys. Res., 85, 7715, 1980b.
- Spreiter, J. R., A. L. Summers and A. Y. Alksne, Hydromagnetic flow around the magnetosphere, Planet. Space Sci., 14, 223, 1966.
- Tatrallyay, M., C. T. Russell and J. G. Luhmann, On the proper Mach number ratio of specific heats for modelling the Venus bow shock, J. Geophys. Res., submitted, 1983.
- Wallis, M. K., Does Mars have a magnetosphere?, Geophys. J.R. Astron. Soc., 41, 349, 1975.
- Zhuang, H-C. and C. T. Russell, An analytic treatment of the structure of the bow shock and magnetosheath, J. Geophys. Res., 86, 2191-2205, 1981.

Table 1. Mars-3 Trajectory

<u>Universal Time</u>	<u>XSE</u>	<u>YSE</u>	<u>ZSE</u>
1801	-0.177 $R_M$	-2.788 $R_M$	-0.747 $R_M$
1831	0.659	-1.313	-1.042
1901	0.956	0.758	-0.639
1931	0.240	2.198	0.499
2001	-0.641	2.927	1.557

Table 2. Median Magnetic Field Vectors

<u>Universal Time</u>	<u>BX SE<sup>+</sup></u>	<u>BY SE<sup>+</sup></u>	<u>BZ SE<sup>+</sup></u>	<u>N</u>
1815	-0.6	3.3	-6.2	6
1817	-2.4	3.9	-7.8	8
1819	-2.3	3.9	-5.5	8
1821	-2.0	4.5	-6.2	8
1823	-2.6	5.5	-5.2	3
1825	-3.9	7.8	-7.8	5
1827	-3.9	5.2	-7.8	1
1829	—	—	—	0
1831	-8.4	-8.4	-5.2	3
1833	-9.1	-10.4	-7.8	2
1835	-11.0	-13.0	-9.1	8
1837	-10.4	-13.0	-13.6	3
1839	-10.4	-12.6	-16.9	8
1841	-10.4	-12.3	-20.2	5
1843	-10.4	-8.4	-23.4	5
1845	-8.1	-5.2	-22.1	4

<sup>+</sup>Zero levels unknown

Figure 1. Magnetic field observed by the Mars 3 spacecraft on 01/21/72.  
(a) Time series in solar ecliptic coordinates.  
(b) Vectors along the trajectory projected into the Y-Z solar ecliptic plane. No zero level corrections have been applied.

Figure 2. Magnetic field calculated along Mars 3 trajectory using a ratio of specific heats,  $\gamma$ , of 2 a magnetosonic Mach number of 7.7, and an ionopause altitude of 430 km, with an IMF of  $(-1.5, -4.5, 0.90)$  nT.  
(a) Model A with no aberration of the solar wind.  
(b) Model B with a  $9^\circ$  aberration of the solar wind in the direction of the average expected solar wind observation.

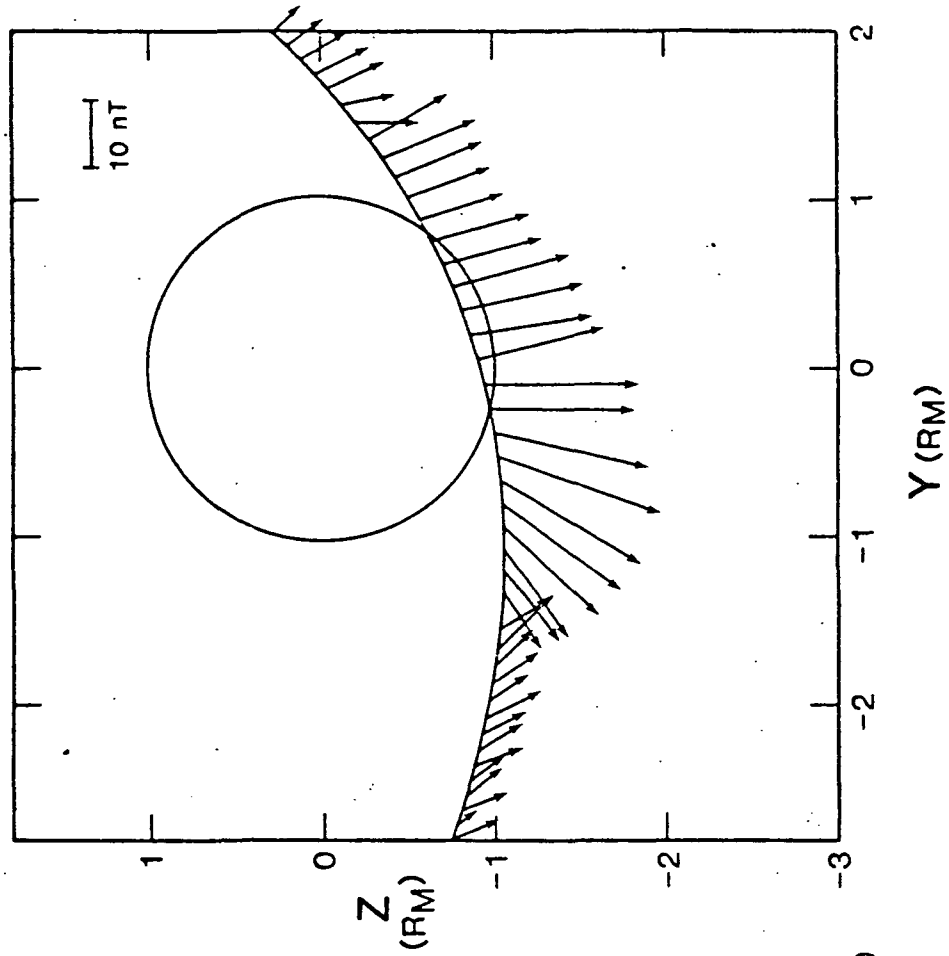
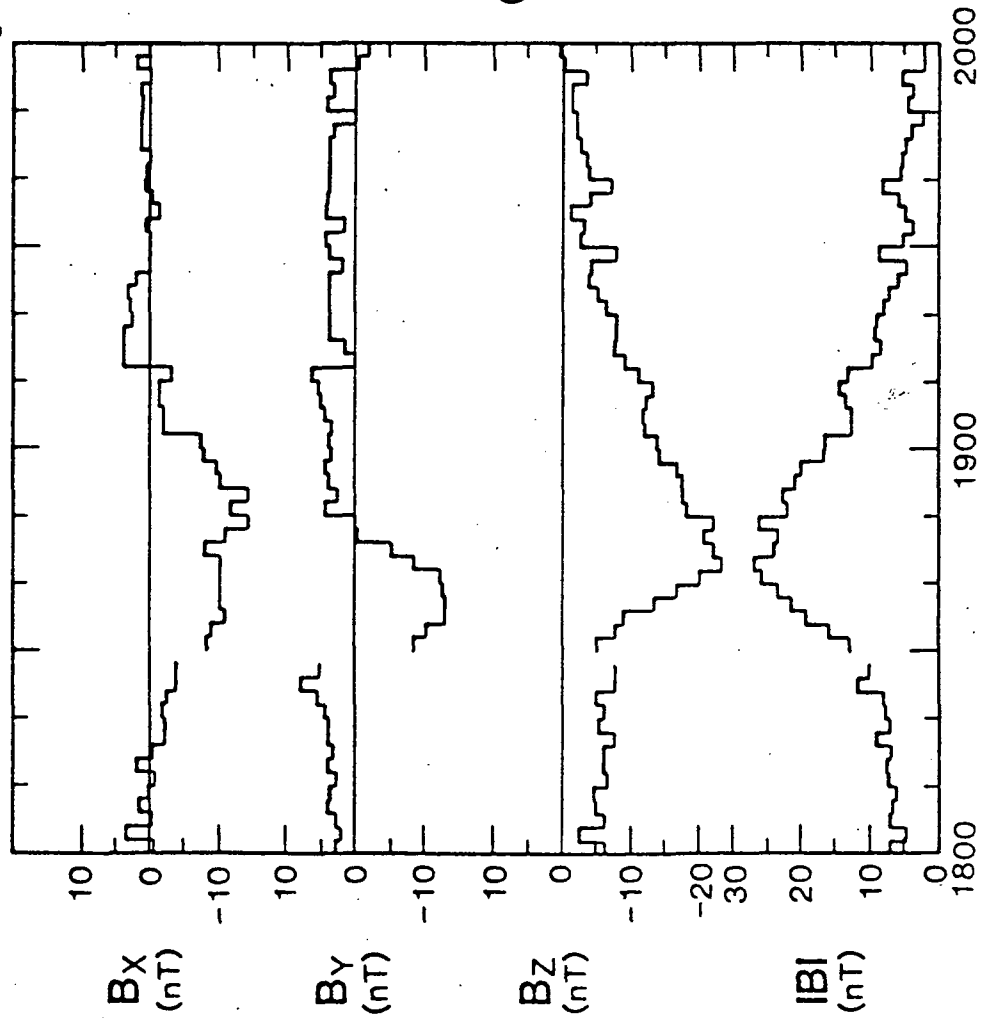
Figure 3. Magnetic field along the Mars 3 trajectory  
(a) Panel on left shows observations corrected so that average IMF is same as IMF in model C.  
(b) Panel on right shows model C. All parameters are the same as in models B, except IMF has been changed to  $(-4, -4.5, -3)$ , and flow is aberrated  $7^\circ$  in ecliptic plane and  $4^\circ$  from the South.

Figure 4. Ecliptic plane projection of magnetic field along Mars 3 trajectory.  
(a) Corrected observations.  
(b) Model C.

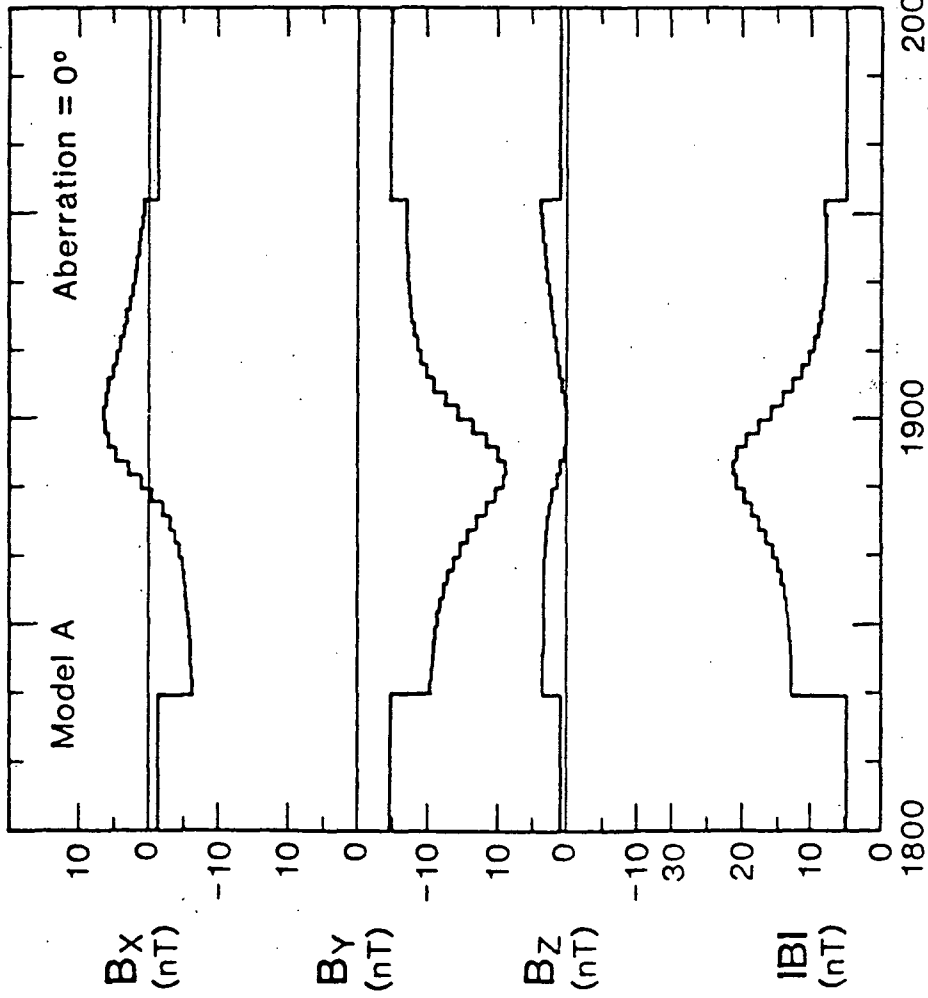
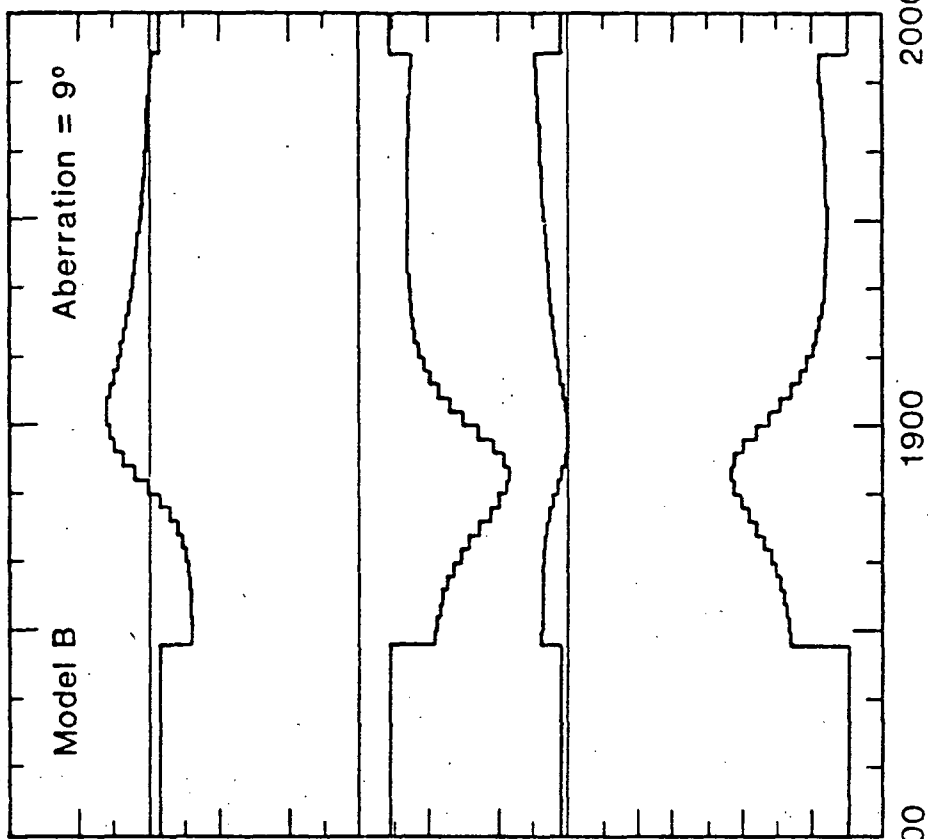
Figure 5. Dawn-dusk plane projection of magnetic field along Mars 3 trajectory.  
(a) Corrected observations.  
(b) Model C

Figure 6. Solar-cylindrical projection of magnetic field along Mars 3 trajectory.  
(a) Corrected observations.  
(b) Model C.

Original Data



$M_{MS} = 7.7$      $B_{IMF} = (-1.5, -4.5, 0.9) \text{ nT}$   
 $\gamma = 2.0$     Ionopause Altitude = 430 km



Universal Time

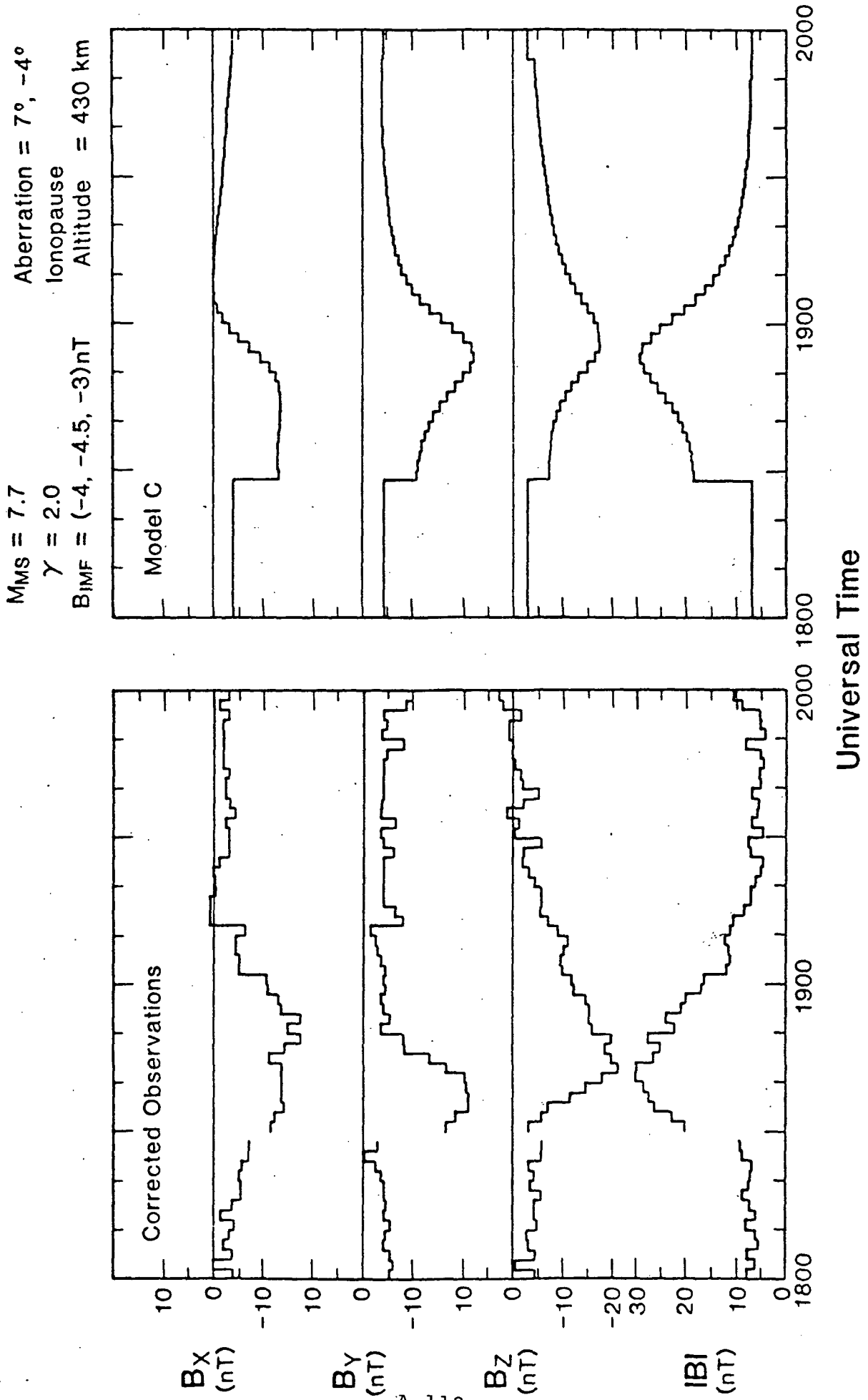
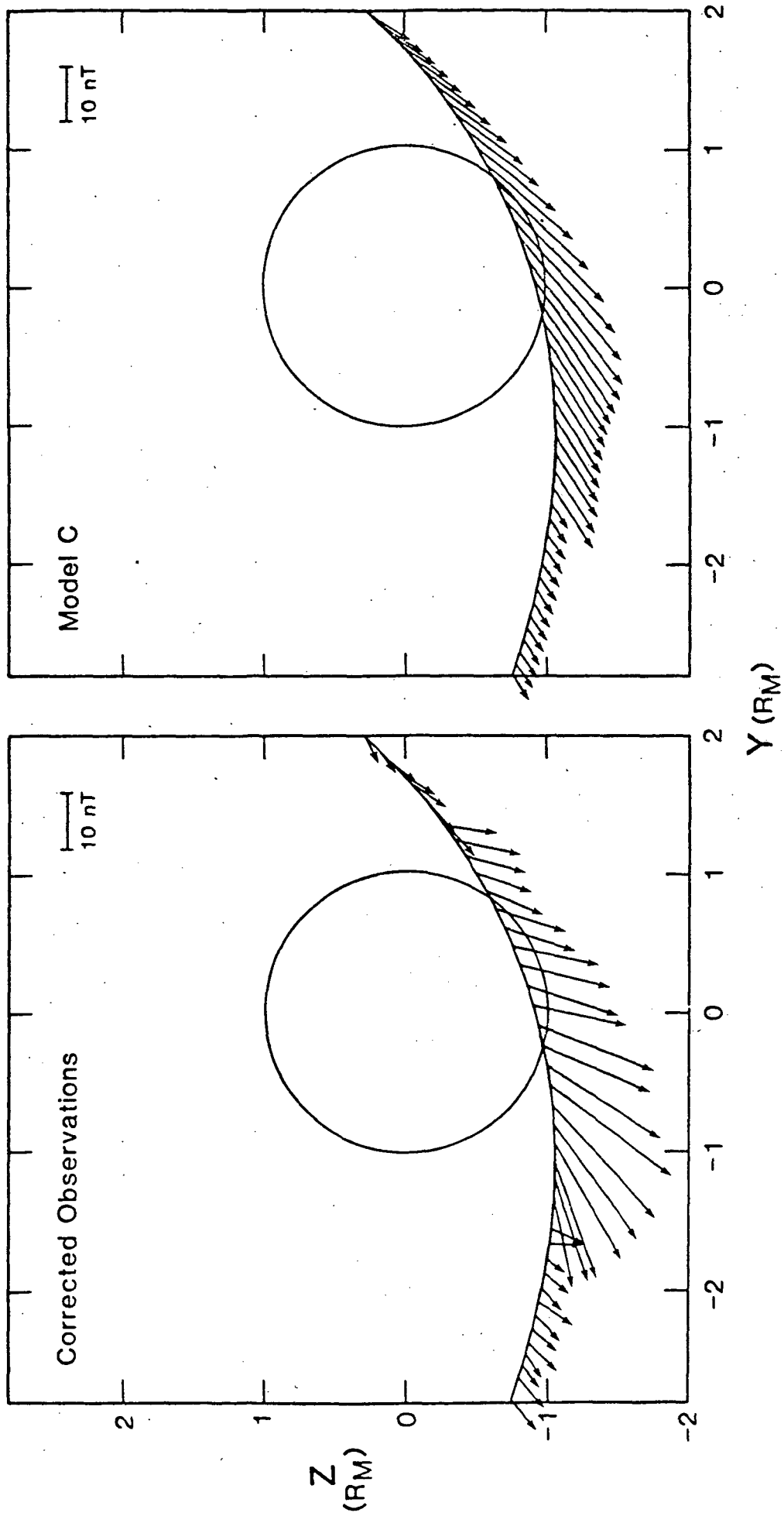
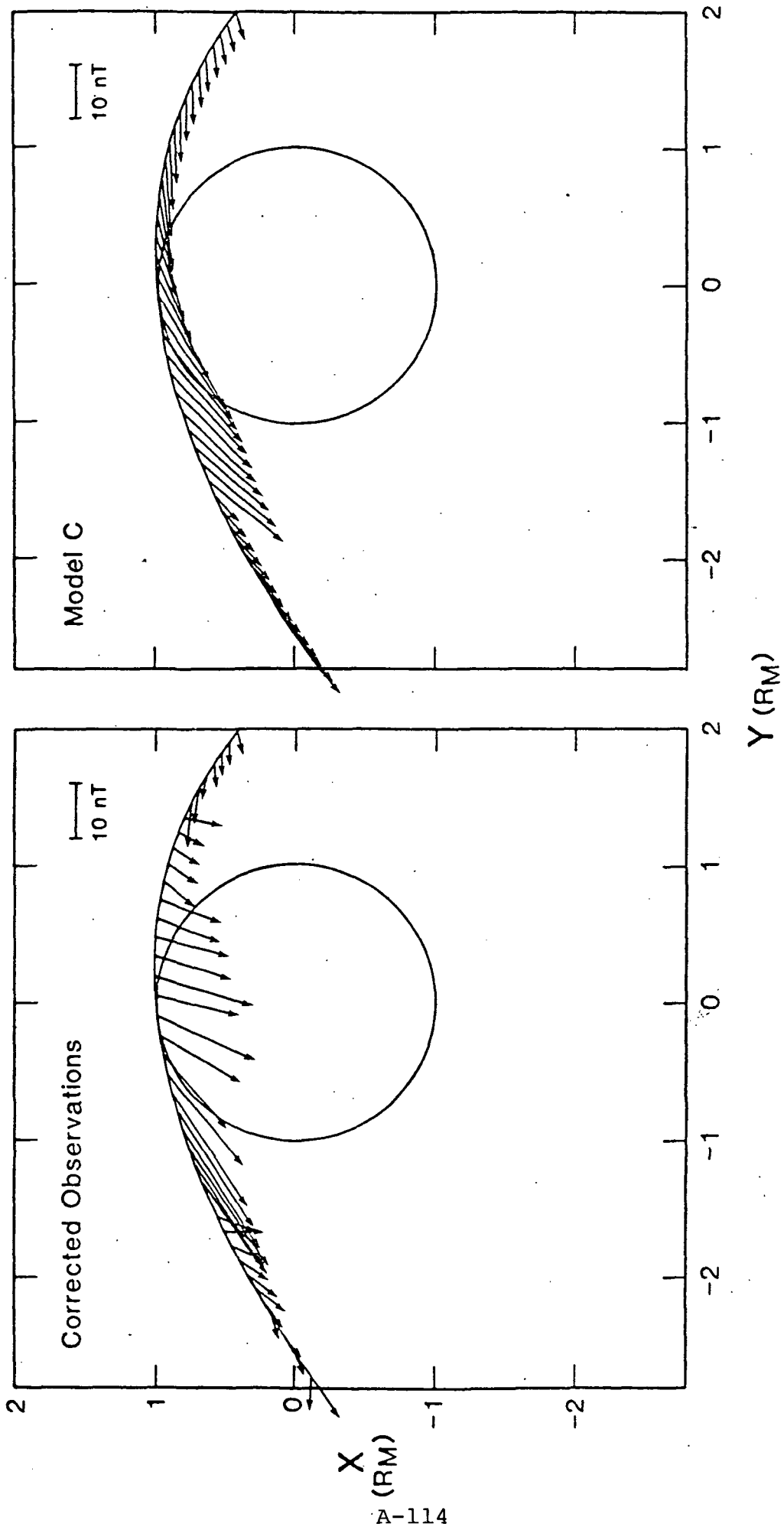
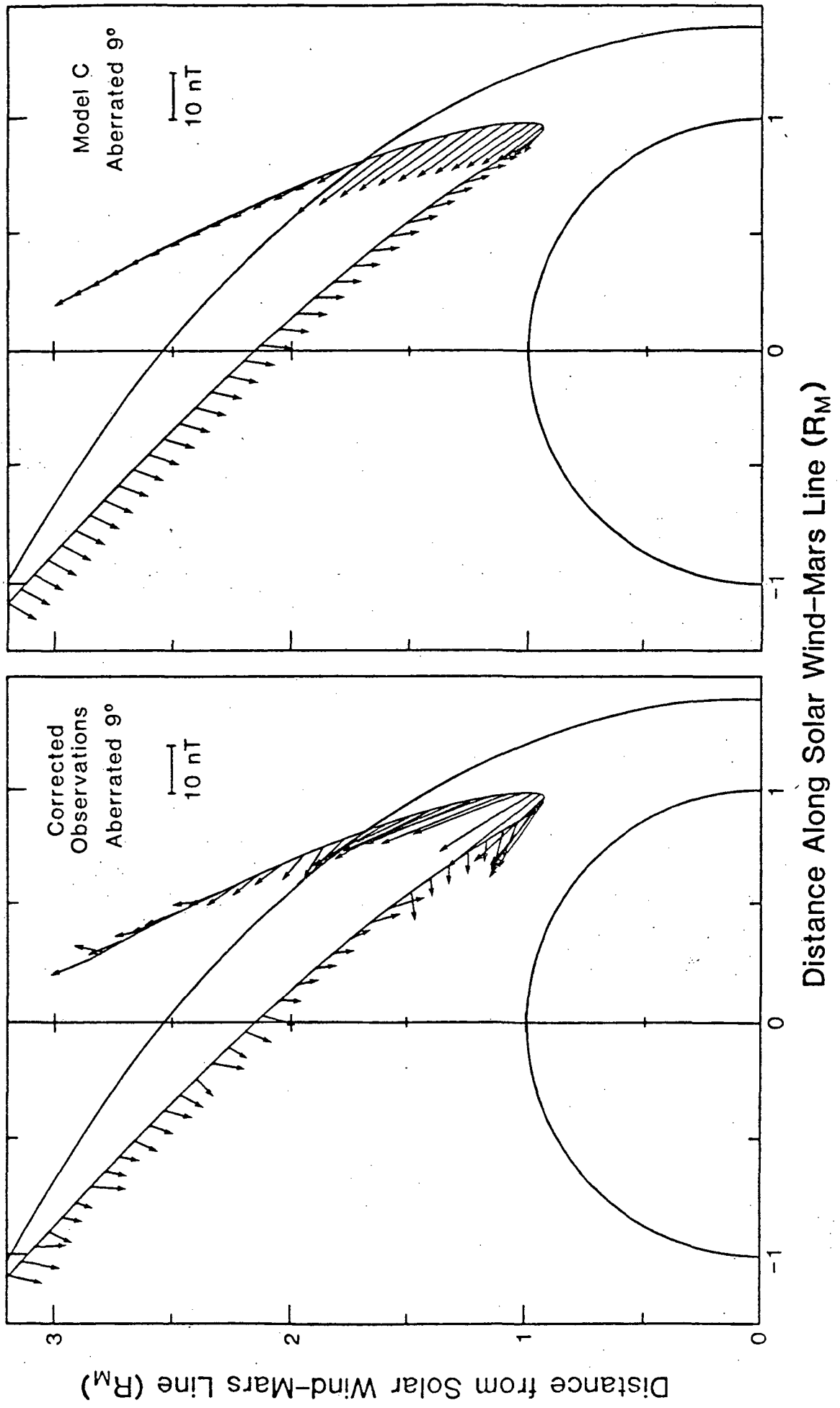


Figure 3







Gasdynamic Modeling of the Jupiter and Saturn Bow Shocks:

Solar Wind Flow About the Outer Planets

J.A. Slavin and E.J. Smith  
Jet Propulsion Laboratory, California Institute of Technology  
Pasadena, CA 91109

J.R. Spreiter  
Stanford University  
Stanford, CA 94035

S.S. Stahara  
Nielson Engineering and Research, Inc.  
Mountain View, CA 94305

Submitted to J. Geophys. Res.

April, 1983

## ABSTRACT

Pioneer 10,11 and Voyager 1,2 observations are used to study global aspects of the solar wind interaction with Jupiter and Saturn. Upstream solar wind measurements and scaling laws are used to characterize the relevant flow parameters,  $P_{sw}$ ,  $P_o/P_{sw}$ ,  $M_s$ ,  $M_A$ , and IMF spiral angle near the orbits of these two planets. Bow shock and magnetopause position are found to vary as the fourth root of dynamic pressure at Jupiter and the sixth root at Saturn with average solar wind stand-off distances of  $68 R_j$  and  $19 R_s$ , respectively. In shape, the Jovian bow shock and magnetopause surfaces are similar to their terrestrial counterparts, but with a magnetosheath that is about 45% thinner than predicted by axisymmetric gasdynamic theory. This result is interpreted as further evidence for strong polar flattening at Jupiter relative to the other known magnetospheres. The Saturnian magnetopause and bow shock boundaries are significantly more flared than at the earth with a subsolar magnetosheath that is 20% thinner than predicted by axisymmetric gasdynamic theory. The very blunt magnetopause may be due in part to the decrease in  $P_o/P_{sw}$  with increasing distance from the sun and its effect on flaring and tail diameter. Comparison with gasdynamic theory at Saturn produces better agreement than at Jupiter and suggests that the amount of polar flattening at Saturn is intermediate between Earth and Jupiter. Finally, a gasdynamic model of solar wind flow past Titan during the 1% of the time when it's orbit is upstream of the Saturn bow shock is presented.

## Introduction

The flow of solar wind about the planets is determined by upstream parameters and the nature of the interaction which deflects the incident plasma. Being a fundamental problem in solar-planetary physics, the subject has received considerable attention in the literature (Spreiter, 1984; Russell, 1984). Due to the many successful U.S. and U.S.S.R. missions to Mercury, Venus, Earth, and Mars during the 1960's and 1970's, the emphasis of these studies has been on the inner planets (Breus, 1979; Russell, 1979; Siscoe and Slavin, 1979; Fairfield, 1979; Gringauz, 1981; Slavin and Holzer, 1982). The interaction with each planet is somewhat different and that difference is manifested in the pattern of solar wind flow about the body. The near total absorption of the incoming solar wind by the Moon results in no upstream bow shock and a wake containing little plasma (Siscoe et al., 1969). At Venus the electrically conducting ionosphere diverts most of the solar wind and gives rise to a relatively strong bow shock (Slavin et al., 1980), but neutral atmosphere interactions and ionospheric dissipation result in 1-10% absorption, a thinner than expected magnetosheath, and the pick-up of  $O^+$  (Slavin et al., 1980; Intriligator, 1982; Cloutier, 1984). Fewer observations are available at Mercury and Mars, but their small dipole moments are expected to make surface/interior conductivity at Mercury and ionosphere/atmosphere characteristics at Mars important factors in their response to various solar wind conditions (Siscoe et al., 1975; Slavin and Holzer, 1979; Suess and Goldstein, 1979; Intriligator and Smith, 1979; Slavin and Holzer, 1982).

The purpose of this study is to extend certain aspects of the work that has been done on the terrestrial planets to Jupiter and Saturn. In particular, the Pioneer 10,11 and Voyager 1,2 observations near Jupiter and Saturn are used to characterize the relevant upstream flow parameters at 5 and 9 AU, model bow shock/magnetopause position as a function of dynamic pressure, and compare the overall results with the predictions of gasdynamic theory. The results are found to have significant implications for both solar wind interaction modeling and our picture of the Jovian and Saturnian magnetospheres.

### Solar Wind Parameters

The radial gradients in the solar wind (Smith and Wolfe, 1979; Burlaga et al., 1982; Gazis, 1984; Slavin et al., 1984a) result in major variations of the mean flow parameters across the orbits of the planets. Tables 1 and 2 display average interplanetary conditions and derived parameters based upon the scaling laws and 1 AU values adopted by Slavin and Holzer (1981). Over the 30 AU distance separating Mercury and Neptune the total changes in  $V_{sw}$ ,  $T_e$ ,  $T_p$ ,  $B$ , and  $N$  are factors of 1, 5,  $2 \times 10^1$ ,  $3 \times 10^2$ , and  $10^4$ , respectively. In Table 2 these values have been used to calculate the flow parameters that are most relevant to our study. For gasdynamic descriptions, the flow is completely determined by the obstacle boundary conditions and sonic Mach number with an appropriate adiabatic exponent (Spreiter et al., 1966; Dryer and Heckman, 1967). The full MHD treatment yields the flow field for a given set of obstacle boundary conditions, sonic Mach number, Alfvénic Mach Number, and the upstream magnetic field orientation (Spreiter and Rizzi, 1974). Two additional parameters, solar wind dynamic pressure,  $P_{sw} = \rho V^2$ , and the ratio of static to dynamic pressure,  $[B^2/8\pi + nk(T_i + T_e)]/V^2$ , have been included because they determine magnetopause radius and shape respectively (Coroniti and Kennel, 1972).

The greatest changes are in the dynamic pressure and static to dynamic pressure ratios which change by factors of  $10^4$  and  $10^1$  over 30 AU. For a given planetary magnetic moment, the results are larger, more flared magnetopauses with increasing distance from the sun as a result of the usual pressure balance arguments (Coroniti and Kennel, 1972). Both sonic and Alfvénic Mach numbers increase by about a factor of 3 over the orbits of the planets. The expected results will be more strong, supercritical bow shocks with slightly thinner magnetosheaths and smaller Mach cones as distance from the sun increases (Spreiter et al., 1966; Slavin et al., 1984b). In addition, the increased  $M_A$  values should result in improved agreement between MHD and gasdynamic theory with increasing distance from the sun as the IMF weakens and the magnetic terms tend toward zero (Spreiter and Rizzi, 1974). Finally, the IMF shifts from being nearly aligned with the solar wind flow at Mercury to perpendicular by the orbit of Jupiter. The main effect of the spiral angle variation will be in the planetary foreshocks and regions of the shock surfaces which are quasi-parallel and quasi-perpendicular (Greenstadt et al., 1984).

In order to validate these models, hourly averaged merged plasma and magnetic field data sets for Pioneer 10 and 11 near Jupiter and Saturn, respectively, were assembled. Histograms of  $M_S$  and  $M_A$  for intervals when the spacecraft were outside of the shock and within 0.1 AU of the orbits of each planet were calculated. As shown, the time each spacecraft spent near the planet corresponded to several solar rotations and probably provided a good measure of conditions around those points in the solar cycle. The mean sonic Mach numbers were  $M_S=9.9$  at Jupiter and 11.1 at Saturn. The Alfvénic Mach numbers were 16.9 and 18.1, respectively. Hence, it appears that at least during the Pioneer epoch the sonic Mach numbers were well predicted, but the absolute values of the Alfvénic Mach numbers and their gradient may be underestimated.

### Bow Shock and Magnetopause Models

Jupiter and Saturn have now be visited by a total of 4 and 3 spacecraft, respectively. Thus, we have more boundary crossings than at Mercury where there were just the two rapid Mariner 10 fly-bys, but fewer than at Venus, Earth, or Mars. Figure 3 displays the Pioneer and Voyager trajectories in planet centered cylindrical coordinates. A single average shock and magnetopause crossing per inbound or outbound leg based upon encounters confirmed by both the plasma and magnetic field groups (Wolfe et al., 1974; Mihalov et al., 1975; Wolfe et al., 1980; Smith et al., 1974; 1975; 1980a,b; Bridge et al., 1979a,b; 1981; 1982; Ness et al., 1979a,b; 1981; 1982) is plotted for comparison. At both planets the scatter without solar wind pressure corrections is considerable. In particular, the Voyager 1 and 2 Saturn outbound encounters stand out as examples of compression and rarefaction events to be discussed later.

The trajectories in Figure 3 indicate that we have boundary crossings clustered in the subsolar, terminator, and downstream regions. When fitting these measurements, our intention is to study the dayside solar wind interaction. For this reason the downstream passes, Voyager 1,2 at Jupiter and Voyager 1 at Saturn, will not be considered. Inclusion of downstream boundary crossings would force the model fits to be hyperbolas for the bow shocks and blunted cylinders for the magnetopauses independent of the actual shape of the dayside boundaries (Slavin et al., 1984b). This data selection decisions also make it possible to directly compare the Jupiter and Saturn results to those obtained previously for the inner planets using similar criteria (Slavin and Holzer, 1981).

For modeling the Jupiter and Saturn boundary surfaces the three parameter second order method which Slavin and Holzer (1981) have applied to the inner planets will be used. The shock and magnetopause surfaces are assumed to be symmetric about

the aberrated planetocentric orbital x axis (i.e.  $V_{sw}/|V_{sw}|=-\hat{x}'$ ) over the low latitude band sampled by these spacecraft. The equation for the model surface is

$$r = L/(1 + \epsilon \cos \theta) \quad (1)$$

where  $r$  is radial distance from the conic focus at  $x'=x_0$ ,  $\epsilon$  is the surface eccentricity, and  $L$  is the semi-latus rectum. As discussed in the papers by Slavin and co-workers, linear least squares techniques may be applied to (1) for determining the best  $x_0$ ,  $\epsilon$ , and  $L$  values.

In Figures 4, 5, 7, and 8 the bow shock and magnetopause crossings at Jupiter and Saturn are modeled in aberrated coordinates both with and without corrections for upstream pressure. The many multiple crossings recorded per pass due to boundary motion were averaged together when not separated by intervals of about 10 hours or more. This procedure eliminates weighting of the fits toward passes with large numbers of crossings due to boundary waves (Slavin and Holzer, 1981). Actual upstream solar wind speeds were used in aberrating the points, when it was available, and 430 km/s was assumed when it was not.

The top panels of Figures 4, 5, 7, and 8 display the crossings and best fits in the absence of any corrections for upstream dynamic pressure. The fits are all reasonably good, but the rms deviations normal to the curves is large. Using these shapes, the individual crossings were extrapolated down to the stagnation line,  $\theta=0^\circ$ , and plotted against the observed upstream dynamic pressure in Figures 6 and 9. In the case of the magnetopause crossings, the external pressure was inferred from the state of compression of the magnetic field just inside of the magnetopause using the method of Slavin et al. (1983). As noted in the figures, a simple Newtonian pressure balance is assumed using minimum variance magnetopause normals determined by previous studies (Sonnerup et al.; Smith et al., 1980b; Ness et al., 1979a,b; 1981; 1982). The resulting measure of dynamic pressure,  $P_{sw}^*$ , is equal to the actual dynamic pressure only if the plasma pressure just inside the magnetopause is small, as will be discussed later.

The Jovian shock position in Figure 6 varies as the  $-1/4.0$  power of dynamic pressure while the magnetopause responds as  $-1/4.4$  power of the inferred dynamic pressure. Since the two surfaces must on average move together, this result suggests effect of magnetospheric plasma on magnetopause pressure balance must not have changed greatly over the temporal and spatial intervals covered by these crossing. Assuming a  $-1/4$  exponential dependence, the bow shock and magnetopause crossings at Jupiter have been scaled to their average pressures and modeled in the bottom panels of Figures 4 and 5. The result is a 25-55% decrease in the rms deviations with only slightly altered shapes.

Figure 9 shows the results when the same procedure is applied to Saturn. Again, the pressure dependences for the two different methods and surfaces are similar with exponents of  $-1/5.1$  and  $-1/6.1$ . Assuming the  $-1/6$  power pressure dependence, the bottom panels of Figures 7 and 8 display the pressure corrected Saturn bow shock and magnetopause surfaces. The model surface shapes show a large change due to the

corrections associated with the low external pressures during the outbound Pioneer 11 and Voyager 2 passes. The pressure corrections produce 30-40% reductions in the normal rms deviations.

In Figure 3 it pointed out that the Voyager 1 downstream boundary crossings, which were excluded from our study, occurred much closer to the  $x'$  axis than would be expected from the general location of the Pioneer 11 and Voyager 2 encounters. Some studies (e.g. Behannon et al., 1983) have gone so far as to suggest that the Voyager 2 crossings included in our study were at unusually great distances due to the immersion of Saturn in Jupiter's tail. Fortunately, the pressure corrections in Figures 7 and 8 have taken into account these low external pressures, regardless of the cause. An equally important question that does not appear to have been addressed in the past is whether or not the downstream Voyager 1 crossings corresponded to high solar wind pressures. Due to the downstream nature of the crossings either high dynamic or static pressure could depress the magnetopause location. While the complete plasma and magnetic field data sets and minimum variance analyses for these boundary encounters have not been published, Slavin et al. (1983a) did note unexpectedly high tail magnetic fields, based upon typical 9 AU solar wind conditions such as in Table 2, just inside the Voyager 1 outbound magnetopause crossing. Without a minimum variance analysis it is not possible to determine the relative effects of dynamic and static pressure and make a rigorous pressure correction. However, an upper limit has been set in Figure 10 by assuming that the balance only involved static solar wind pressure and lobe magnetic fields. Under this situation the diameter of the tail varies as the square root of the tail field,  $B_t$ , relative to the terminal field derived from the static pressure in Table 2,  $B_{te}$  (e.g. Coroniti and Kennel, 1972). Based upon ISEE-3 experience at the Earth (Slavin et al., 1983c), the downstream distance at which this is strictly true at Saturn may be on the order of 10 to 12 solar wind stand-off distances, or 200-240  $R_s$ . For this reason the triangle in Figure 10 marking the pressure corrected Voyager 1 magnetopause crossing is only an upper limit. However, comparison with the extrapolated Saturn dayside magnetopause model indicates that the actual pressure correction might produce good agreement. This is particularly true when it is remembered that while we only modeled the forward magnetopause, the surface must eventually turn over and become cylindrical. In terms of modeling the entire magnetopause, a 2nd order fit is generally used up to an obstacle radius or so downstream and then straight lines are assumed as in Fairfield (1971). The alternatives are less flexible asymptotic functions (e.g. Howe and Binsack, 1972) or awkward, less physical higher order polynomial expansions.

The pressure normalized dayside boundary models for Jupiter and Saturn produced by this study are compared with the results from other planets in Figure 11. The bottom panel plots magnetopause location in units of the distance to the subsolar point (i.e. obstacle radii,  $R_{OB}$ ). As discussed earlier, the Saturn and Jupiter models are based upon low latitude observations of a three dimensional surface which may exhibit significant polar flattening. For Earth, the observations extend over a greater range of latitude on a surface which possesses only a small amount of flattening. As shown, the Jupiter magnetopause is slightly blunter than that of the Earth, but much less than at Saturn.

The top panel of Figure 11 displays bow shock location at Venus, Mars, Earth, Jupiter, and Saturn in units of planetocentric distance to the nose of the shock,  $R_{SN}$ . The models for the inner planets come from the work of Slavin and Holzer (1981) which used the same modeling techniques and data selection criteria as were applied to Jupiter and Saturn in this study. As shown, the Jupiter and Earth surfaces are again quite similar in shape, but with the Jupiter shock the less blunt, perhaps due to the higher Mach numbers at 5 AU. Saturn again possesses the most flared surface shape. This ordering is in reasonable agreement with that of the magnetopause surfaces in the lower panel. Hence, there is general consistency between the two sets of boundaries. As discussed by Slavin et al. (1983b), the bow shocks at Venus and Mars are less blunt than at Earth due to their lack of strong intrinsic magnetic fields and limited solar wind-natural atmosphere interactions. Under these conditions the obstacle tends to follow the circular shape of the planet with little flaring.

Finally, in Figure 10 the Jupiter and Saturn magnetosheath boundaries are compared with the Earth results of Slavin and Holzer (1981). For this purpose it is necessary to scale the bow shock and magnetopause models to a common dynamic pressure and hence make a reasonable assumption concerning the relationship of  $P_{sw}$  to  $P_{sw}^*$ . In the case of Jupiter, a beta of 1 inside the magnetopause appears consistent with the Voyager particle measurements (Krimigis et al., 1981). The actual dynamic pressure would then be twice the  $P_{sw}^*$  value inferred from the magnetic field alone. This assumption also appears reasonable in that it makes the average dynamic pressure during the shock crossings in Figure 4 nearly equal to that during the magnetopause encounters in Figure 5. At Saturn plasma was also detected within the magnetosphere, but beta appears to have been generally of order  $10^{-1}$ , or less, near the magnetopause (Lanzerotti et al., 1983). Due to both the Voyager results and the near sixth root pressure dependence in Figure 9, we have assumed  $P_{sw} = P_{sw}^*$  for the purposes of this study. Finally, the bow shock and magnetopause surfaces for all three planets have been plotted in units of magnetopause nose distance from the center of the planet termed the obstacle radius,  $R_{OB}$ .

The surfaces in Figure 12 display two interesting results. At Jupiter, the subsolar magnetosheath appears to be much thinner than the earth despite the similar shapes for their low latitude magnetopause magnetospheric boundaries. The ratios of subsolar shock to magnetopause radius are 1.41, 1.25, and 1.53 at Earth, Jupiter, and Saturn, respectively. In the case of Saturn the magnetopause appears to be more flared than at the earth or Jupiter, but with a magnetosheath that is only little thicker than its terrestrial counterpart. While the limited amount of coverage provided by the Pioneer and Voyager Missions may have had some influence on these results, both findings appear to be experimentally significant and potentially important. In later sections these effects are investigated with gasdynamic flow calculations and contrasted with other observations on the solar wind interaction with these planets.

## Solar Wind Stand-Off Distance

Using the magnetopause models and Pioneer data sets described earlier, we have examined the distribution of solar wind dynamic pressure and its effect on the distance to the nose of the magnetosphere,  $R_N$ . As shown in Figure 13, the range in solar wind stand-off distance at Jupiter appears to vary from about  $40 R_J$  to  $110 R_J$  with a mean near  $R_N = 68 R_J$ . A larger solar wind data set covering more of the solar cycle would increase these overall limits, but the predicted distribution appears to agree well with the observed magnetopause locations. In the case of Saturn, Figure 14 indicates that the range is less than at Jupiter due to its earth-like compressibility. The bounds are about 12 and  $24 R_S$  with a mean of  $18.8 R_S$ . Again, the observed Pioneer and Voyager magnetopause crossings agree well with the predicted distribution.

As would be expected due to its immense size, the variability in magnetospheric diameter size at Jupiter will almost never extend down to the major satellites and expose them to the solar wind. The situation at Saturn is quite different as has been recognized by many other studies (e.g. Wolf and Neubauer, 1982). In particular, Titan's  $20.3 R_S$  orbit places it just beyond the average  $18.8 R_S$  subsolar diameter of the Saturnian magnetosphere. Hence, Titan usually spends a portion of its orbit in the magnetosheath. About 1% of time, when  $R_N < 14 R_S$ , part of Titan's orbit will take it out into the solar wind upstream of Saturn's bow shock. While not common, this situation is similar in probability to the terrestrial magnetopause being pushed down to geosynchronous orbit; an infrequent, but well observed phenomenon. Finally, it is noted that the E-ring is near the limits of how far the Saturn magnetopause might be depressed. Under intervals of extreme solar wind pressure, the electromagnetic environment of the outermost ring particles might be influenced by the solar wind.

## Gasdynamic Modeling

Single fluid axially symmetric gasdynamic calculations have proved quite useful in the study of solar wind flow past the inner planets. For our best observed case, the Earth, gasdynamic theory is able to do a very good job of predicting bow shock position and other global characteristics of the flow (Fairfield, 1971; 1979; Slavin et al., 1983). At Venus, where the atmosphere forms a distributed source interacting with the solar wind, comparison of the observations with simple gasdynamic calculations of flow about a thin tangential discontinuity has made it possible to identify perturbations due to the charge exchange and photoion pickup (Slavin et al., 1980; 1983b).

The gasdynamic approximation states that the MHD equations reduce to the simpler gasdynamic equations for weak magnetic fields in the sense of large  $M_A^2 = \frac{1}{2} \rho V^2 / (B^2 / 8\pi)$  (Spreiter et al., 1966). Inspection of Table 2 and Figures 1,2 shows that gasdynamic theory should be least applicable at Mercury and most useful at Jupiter and beyond. Given the good agreement at 1 AU, the expectation would be that gasdynamic theory should yield a very accurate description of the flow about Jupiter and Saturn.

Figures 15 and 16 compare the predictions of the Spreiter and Stahara (1980; Stahara et al., 1980) gasdynamic code with our observational models at Jupiter and Saturn. The tangential discontinuity obstacle in their code is axially symmetric with shape given by the parameter,  $H/R_0$ . As shown by dashed lines in the two figures, we have selected  $H/R_0$  values which give excellent agreement with the forward magnetopause surfaces at both planets. The differences between the observed and assumed obstacle surfaces behind the terminator only influence the very distant downstream flow (Slavin et al., 1984b). Based upon Table 2 and Figures 1 and 2, sonic Mach numbers of 10 and 12 were used to represent average conditions at Jupiter and Saturn. The final parameter needed for the gasdynamic model is the adiabatic exponent,  $\gamma$ . On the basis of previous studies (Slavin et al., 1983b), the value of 2 was used. It provided the best agreement between theory and observation with regard to shock position and average flow characteristics at 1 AU.

In Figure 15 the observed location of the Jovian bow shock is much lower than predicted. The actual thickness of the Jovian magnetosheath is only 45% of the value predicted by the gasdynamic model. This result is well outside the fitting error bars and much larger than the expected sampling uncertainty based upon the 5 passes through the subsolar region shown in Figure 3. For Saturn, Figure 16 displays better agreement between the gasdynamic model and observation, but with the predicted subsolar magnetosheath about 20% too thin. The poorer sampling at Saturn may have contributed to the discrepancy through the observational model, but the overestimate of magnetosheath width for both cases suggests a common cause peculiar to the Jovian and Saturnian magnetospheres.

In Figure 17 we suggest that the poor agreement between observation and the gasdynamic code, relative to past terrestrial experience, stems from its assumption of axial symmetry. At the Earth, both theory and observation indicate that the eccentricity of the magnetospheric cross section in the terminator plane is small,  $\epsilon < 0.2$  (Holzer and Slavin, 1978). While the higher latitudes at Jupiter and Saturn have not been examined in situ, theoretical models of the Jovian field (e.g. Engle and Beard, 1980) suggest considerable polar flattening,  $\epsilon \sim 0.8$ , ultimately due to the large amount of plasma within the magnetosphere and its rapid rotation rate. Saturn is presumably intermediate with a high rotation rate and more magnetospheric plasma than at Earth, but less than at Jupiter (Krimigis et al., 1983; MacLennan et al., 1983; Lanzerotti et al., 1983).

In terms of our comparison, the Pioneer and Voyager observational models are based upon moderate to low latitude observations. For flow about a non-axially symmetric body, streamlines cease to be axially symmetric with mass flux being channelled from longer paths about the broader body sections toward the shorter paths—about the less blunt sections. The result is a net transfer of mass flux from the low latitude magnetosheath, thereby reducing its width, to the high latitude magnetosheath which grows in width relative to the axisymmetric case. Hence, the application of an axially symmetric model to only polar measurements would produce a theoretical magnetosheath that was thicker

than observed, while the opposite is true for the equatorial study in Figures 15 and 16. The magnitude of the discrepancy caused by the assumption of axial symmetry increases as the amount of polar flattening increases. Hence, the smaller disagreement at Saturn supports the idea that Saturn's magnetosphere exhibits properties which are intermediate between the earth and Jupiter in terms of the importance of rotation rate and internal plasma sources.

As was reported in the preceding section, Titan's orbit will lie upstream of the Saturn bow shock about 1% of time. During these occasions Titan will sometimes find itself interacting directly with the solar wind. If it is sufficiently magnetized, then a small intrinsic field magnetosphere will form. Alternatively, the solar wind may impinge directly upon the ionosphere/atmosphere as at Venus. In either event, the interaction may be unique due to Titan's thick atmosphere, low gravity, and large neutral atmosphere scale heights resulting in cometary amounts of photoionization and charge exchange (Hartle et al., 1982).

Figure 17 presents a qualitative picture of the Titan interaction just upstream of Saturn's bow shock during an interval of high solar wind pressure. The flow about Titan is represented by a  $M_s=12$ ,  $\gamma=2$ ,  $H/R_0=0.8$  gasdynamic model with the nose of the obstacle being  $1.5 R_T$  from the center of the body (i.e. near the exobase). The gasdynamic model does not explicitly take into account the neutral atmosphere interaction, but the conceptual picture should be correct unless the mass loading is sufficient to do away with the bow shock by gradually slowing and absorption of the flow (Wallis, 1973). Depending upon upstream IMF orientation, an interesting mutual foreshock region might be created with seed particles from Titan's bow shock influencing the much larger Saturnian foreshock. Otherwise, the Saturnian bow shock should be relatively unaffected by the Titan interaction. Even on streamlines adjacent to the Titan tail may reach solar wind speeds a few obstacle radii downstream depending upon the strength of mass loading effects. The portion of Saturn's bow shock which stands in the Titan magnetosheath is termed a secondary bow shock. Small transverse gradients in the Titan magnetosheath may slightly alter its shape, as shown, but unless strong mass loading occurs over a large region the strength of the secondary bow shock will be almost that of the rest of Saturn's shock. Finally, Titan's tail is depicted as an analogue of the Venus tail (Russell et al., 1982). For the Titan location relative to the Saturn magnetopause chosen in Figure 17, Titan's tail will fail to form a tight bundle downstream of the Saturn bow shock due to the slow flow speeds near the stagnation region. If the solar wind pressure were ever strong enough to place Titan upstream of the flanks of Saturn bow shock, then a much longer tail could form in the super-sonic, super-Alfvenic Saturn magnetosheath away from the stagnation region.

#### Discussion and Summary

In this study we have used to the Pioneer and Voyager observations to characterize the solar wind conditions near the orbits of Jupiter and Saturn, create pressure corrected models of their bow shock and magnetopause surfaces, and compared the results with the predictions of

gasdynamic theory. Previously, some examinations of boundary location and response to pressure have been conducted for individual missions (e.g. Smith et al., 1980; Smith et al., 1981; Bridge et al., 1982; Ness et al., 1981; 1982), but none performed a comprehensive study using both the Pioneer and Voyager data sets.

Our study of the boundary surface pressure dependences produced reasonable agreement between the magnetopause and bow shock observations at each planet. This finding supports the general validity of the method and assumptions used to infer solar wind dynamic pressure from the magnetopause measurements. More importantly, the overall results confirm the approximate fourth root and sixth root dependences of boundary position on dynamic pressure that have been determined for Jupiter and Saturn, respectively, by earlier studies (e.g. Siscoe et al., 1980; Smith et al., 1981; Bridge et al., 1982).

Magnetopause flaring at the earth has been well studied both theoretically and experimentally (e.g. Coroniti and Kennel, 1972; Slavin et al., 1983c). The flaring angle,  $\psi$ , is determined everywhere by the pressure balance condition

$$(\rho_{sw} v_{sw}^2 \sin^2 \psi + P_o)_{sw} = (B^2/8\pi + nk(T_e + T_i))_{msp} \quad (2)$$

where  $\rho_{sw} v_{sw}^2 \sin^2 \psi$  is the normal component of the dynamic pressure and  $P_o$  is the static pressure in the solar wind. The right hand side describes the internal pressure just inside the magnetopause. The presence of the bow shock may be ignored here because it does not change the total pressure on the left hand side and the ratio of static to dynamic pressure in the magnetosheath rapidly moves toward solar wind values with increasing distance from the stagnation region (Spreiter et al., 1966). In the subsolar region the flaring angle is large and the dynamic pressure dominates the external pressure. However, at large distances downstream the flaring angle decreases to zero and the tail reaches its terminal configuration where solar wind static pressure alone balances internal pressure.

Based upon this pressure balance model, two ways of increasing the magnetopause flaring angle have been suggested which may explain the bluntness of the Jovian and Saturnian magnetopause surfaces. When equation (2) is solved iteratively to arrive at an actual obstacle surface (Spretier and Stahara, 1980), the shape of the surface is moderately sensitive to the internal pressure dependence upon radius (i.e. its compressibility). The weaker the pressure dependence (e.g. fourth root at Jupiter versus sixth root at Earth and Saturn), the greater the outward displacement and flaring along the flanks as decreases. This effect could produce the slightly increased flaring at Jupiter relative to the Earth, but it would not apply to Saturn. The second possible cause of enhanced flare angles was suggested in reference to Saturn by Slavin et al. (1983a). As the flaring angle decreases toward zero, the external pressure in (2) becomes simply the static pressure. The terminal diameter of the tail, which ultimately determines the total bluntness of the magnetopause and its overall flaring, is therefore only a function of the external static pressure and the internal magnetic flux content of the tail lobes (Coroniti and

Kennel, 1972). As the ratio of  $P_0$  to  $P_{sw}$  decreases with increasing distance from the sun, there is a trend toward larger diameter tails and therefore blunter dayside magnetopause surfaces. In the case of Jupiter the effect will be offset by the small size of the Jovian polar cap (Behannon et al., 1981) compared to those of Earth and Saturn (Ness et al., 1982). Hence, while further study is needed on this subject, there does exist a mechanism for producing the strong flaring at Saturn and weak flaring at Jupiter appear in our boundary models.

Finally, comparison of our observational results with gasdynamic calculations based upon typical Mach numbers for the outer solar system determined that the subsolar Jovian and Saturnian magnetosheaths are 45% and 20% thinner than expected. We have suggested that the most plausible cause for this result is polar flattening of these magnetospheres not included in the axially symmetric gasdynamic code. Previously, polar flattening at Jupiter has not only been predicted theoretically, but it has also been invoked to explain some aspects of the Jovian magnetosheath by other studies (Lepping et al., 1980). Our findings support the results of these previous investigations and present evidence that Saturn may be intermediate between Jupiter and Earth with respect to polar flattening.

Acknowledgements. Plasma measurements at Jupiter and Saturn were provided by the Ames Research Center (P.I., A. Barnes) and MIT (P.I., H.S. Bridge) experimenter groups. The authors also wish to acknowledge useful discussions with Z.K. Smith on the Jupiter solar wind interaction. One of the authors (JAS) thanks the NASA/NRC research associate program for financial support. The research described in this report at the Jet Propulsion Laboratory, California Institute of Technology was carried out under contract with the National Aeronautics and Space Administration. Support for this effort at Stanford University and Nielsen Engineering came from NASA contracts NAGW-278 and NASW-3791.

## References

- Behannon, K.W., R.P. Lepping, and N.F. Ness, Structure and dynamics of Saturn's outer magnetosphere and boundary regions, *J. Geophys. Res.*, 88, 8791, 1983.
- Burlaga, L.F., R.P. Lepping, K.W. Behannon, L.W. Klein, and F.M. Neubauer, Large scale variations in the IMF: Voyager 1 and 2 observations between 1-5 AU., *J. Geophys. Res.*, 87, 4345, 1982.
- Breus, T.K., Venus: Review of present understanding of solar wind interaction, *Space Sci. Rev.*, 23, 253, 1979.
- Bridge, H.S., J.W. Belcher, A.J. Lazarus, J.D. Sullivan, R.L. McNutt, F. Bagenal, J.D. Scudder, E.C. Sittler, G.L. Siscoe, V.M. Vasyliunas, C.K. Goertz, and C.M. Yeates, Plasma observations near Jupiter: Initial results from Voyager 1, *Science*, 204, 987, 1979a.
- Bridge, H.S., J.W. Belcher, A.J. Lazarus, J.D. Sullivan, F. Bagenal, R.L. McNutt, K.W. Ogilvie, J.D. Scudder, E.C. Sittler, V.M. Vasyliunas, and C.K. Goertz, Plasma observations near Jupiter: Initial results from Voyager 2, *Science*, 206, 972, 1979b.
- Bridge, H.S., J.W. Belcher, A.J. Lazarus, S. Olbert, J.D. Sullivan, F. Bagenal, P.R. Gazis, R.E. Hartle, K.W. Ogilvie, J.D. Scudder, E.C. Sittler, A. Eviatar, G.L. Siscoe, C.K. Goertz, and V.M. Vasyliunas, Plasma results near Saturn: Initial results from Saturn, *Science*, 212, 217, 1981.
- Bridge, H.S., F. Bagenal, J.W. Belcher, A.J. Lazarus, R.L. McNutt, J.D. Sullivan, P.R. Gazis, R.E. Hartle, K.W. Ogilvie, J.D. Scudder, E.C. Sittler, A. Eviatar, G.L. Siscoe, C.K. Goertz, and V.M. Vasyliunas, Plasma observations near Saturn: Initial results from Voyager 2, *Science*, 215, 563, 1982.
- Cloutier, P.A., Formation and dynamics of large-scale magnetic structures in the ionosphere of Venus, *J. Geophys. Res.*, 89, 2401, 1984.
- Coroniti, F.V., and C.F. Kennel, Changes in magnetospheric configuration during substorm growth phase, *J. Geophys. Res.*, 77, 3361, 1972.
- Dryer, M., and G.R. Heckman, On the hypersonic analogue as applied to planetary interactions with the solar plasma, *Planet. Space Sci.*, 15, 515, 1967.
- Engle, I.M., and D.B. Beard, Idealized Jovian magnetosphere shape and field, *J. Geophys. Res.*, 85, 579, 1980.
- Fairfield, D.H., Average and unusual locations of the earth's bow shock and magnetopause, *J. Geophys. Res.*, 76, 6700, 1971.
- Fairfield, D.H., Global aspects of the Earth's magnetopause, *Magnetospheric Boundary Layers*, Ed. B. Battrock, ESA SP-148, The Netherlands, 1979.
- Gazis, P.R., Observations of plasma bulk parameters and the energy balance of the solar wind between 1 and 10 AU, *J. Geophys. Res.*, 89, 775, 1984.
- Greenstadt, E., V. Formisano, C. Goodrich, J. Gosling, M. Lee, M. Leroy, M. Mellott, K. Quest, A.E. Robson, P. Rodriguez, J. Scudder, J. Slavin, M. Thomsen, D. Winske, and C.S. Wu, Proceedings of the Solar Terrestrial Physics Workshop, Coolfont, West Virginia, 1984.
- Gringauz, K.I., A comparison of the magnetospheres of Mars, Venus, and Earth, *Adv. Space Sci.*, 1, 5, 1981.
- Hartle, R.E., E.C. Sittler, Jr., K.W. Ogilvie, J.D. Scudder, A.J.

- Lazarus, and S.K. Atreya, Titan's ion exosphere observed from Voyager 1, *J. Geophys. Res.*, 87, 1383, 1982.
- Holzer, R.E., and J.A. Slavin, Magnetic flux transfer associated with expansions and contractions of the dayside magnetosphere, *J. Geophys. Res.*, 83, 1978.
- Intriligator, D.S., and E.J. Smith, Mars in the solar wind, *J. Geophys. Res.*, 84, 8427, 1979.
- Intriligator, D.S., Observations of mass addition to the shocked solar wind of the Venusian ionosheath, *Geophys. Res. Lett.*, 9, 727, 1982.
- Krimigis, S.M., J.F. Carbary, E.P. Keath, C.O. Bostrom, W.I. Axford, G. Gloeckler, L.J. Lanzerotti, and T.P. Armstrong, Characteristics of hot plasma in the Jovian magnetosphere: Results from the Voyager spacecraft, *J. Geophys. Res.*, 86, 8227, 1981.
- Krimigis, S.M., J.F. Carbary, E.P. Keath, T.P. Armstrong, L.J. Lanzerotti, and G. Gloeckler, General characteristics of hot plasma and energetic particles in the Saturnian magnetosphere: Results from the Voyager spacecraft, *J. Geophys. Res.*, 88, 8871, 1983.
- Lanzerotti, L.J., C.G. MacLennan, R.P. Lepping, and S.M. Krimigis, On the plasma conditions at the dayside magnetopause of Saturn, *Geophys. Res. Lett.*, 10, 1200, 1983.
- Lepping, R.P., L.F. Burlaga, L.W. Klein, J.M. Jessen, and C.C. Goodrich, Observations of the magnetic field and plasma flow in Jupiter's magnetosheath, *J. Geophys. Res.*, 86, 8141, 1981.
- MacLennan, C.G., L.J. Lanzerotti, S.M. Krimigis, and R.P. Lepping, Low-energy particles at the bow shock, magnetopause, and outer magnetosphere of Saturn, *J. Geophys. Res.*, 88, 8817, 1983.
- Mihalov, J.D., H.R. Collard, D.D. McKibbin, J.H. Wolfe, and D.S. Intriligator, Pioneer 11 encounter: Preliminary results from the Ames Research Center plasma analyzer experiment, *Science*, 188, 448, 1975.
- Ness, N.F., M.H. Acuna, R.P. Lepping, L.F. Burlaga, K.W. Behannon, and F.M. Neubauer, Magnetic field studies at Jupiter by Voyager 1: Preliminary results, *Science*, 204, 982, 1979a.
- Ness, N.F., M.H. Acuna, R.P. Lepping, L.F. Burlaga, K.W. Behannon, and F.M. Neubauer, Magnetic field studies at Jupiter by Voyager 2: Preliminary results, *Science*, 206, 966, 1979b.
- Ness, N.F., M.H. Acuna, R.P. Lepping, J.E.P. Connerney, K.W. Behannon, L.F. Burlaga, and F.M. Neubauer, Magnetic field studies by Voyager 1: Preliminary results at Saturn, *Science*, 212, 211, 1981.
- Ness, N.F., M.H. Acuna, K.W. Behannon, L.F. Burlaga, J.E.P. Connerney, R.P. Lepping, and F.M. Neubauer, Magnetic field studies by Voyager 2: Preliminary results at Saturn, *Science*, 215, 558, 1982.
- Russell, C.T., J.G. Luhmann, R.C. Elphic, and F.L. Scarf, The distant bow shock and magnetotail of Venus: Magnetic field and plasma wave observations, *Geophys. Res. Lett.*, 8, 843, 1981.
- Russell, C.T., The interaction of the solar wind with Mars, Venus, and Mercury, *Solar Wind Plasma Physics*, eds. C.F. Kennel, L.J. Lanzerotti, and E.N. Parker, pp. 208-252, North-Holland Pub., Amsterdam, 1979.
- Russell, C.T., Napa Conference Review, 1984.
- Siscoe, G.L., E.F. Lyon, J.H. Binsack, and H.S. Bridge, Experimental evidence for a detached lunar compression wave, *J. Geophys. Res.*,

- 74, 59, 1969.
- Siscoe, G.L., N.F. Ness, and C.M. Yeates, Substorms on Mercury?, J. Geophys. Res., 80, 4359, 1975.
- Siscoe, G.L., and J.A. Slavin, Planetary magnetospheres, Rev. Geophys. Space Phys., 17, 1677, 1979.
- Siscoe, G.L., N.U. Crooker, and J.W. Belcher, Sunward flow in Jupiter's magnetosheath, Geophys. Res. Lett., 7, 25, 1980.
- Slavin, J.A., and R.E. Holzer, The effect of erosion on the solar wind stand-off distance at Mercury, J. Geophys. Res., 84, 2076, 1979.
- Slavin, J.A., R.C. Elphic, C.T. Russell, F.L. Scarf, J.H. Wolfe, J.D. Mihalov, D.S. Intriligator, L.H. Brace, H.A. Taylor, Jr., and R.E. Daniell, Jr., The solar wind interaction with Venus: Pioneer Venus observations of bow shock location and structure, J. Geophys. Res., 85, 7625, 1980.
- Slavin, J.A., and R.E. Holzer, Solar wind flow about the terrestrial planets, 1. Modeling bow shock position and shape, J. Geophys. Res., 86, 11,401, 1981.
- Slavin, J.A., and R.E. Holzer, The solar wind interaction with Mars re-visited, J. Geophys. Res., 87, 10,285, 1982.
- Slavin, J.A., E.J. Smith, P.R. Gazis, and J.D. Mihalov, A Pioneer - Voyager study of the solar wind interactions with Saturn, Geophys. Res. Lett., 10, 9, 1983a.
- Slavin, J.A., R.E. Holzer, J.R. Spreiter, S.S. Stahara, and D.S. with gas dynamic theory and implications for solar-planetary interactions, J. Geophys. Res., 88, 19, 1983b. Slavin, J.A., E.J. Smith, and B.T. Thomas, Large scale gradients in the IMF: Helios 1,2, ISEE-3, and Pioneer 10,11, Geophys. Res. Lett., 11, 279, 1984a.
- Slavin, J.A., R.E. Holzer, J.R. Spreiter, and S.S. Stahara, Planetary Mach cones: Theory and observation, in press, J. Geophys. Res., 1984b.
- Smith, E.J., L. Davis, Jr., D.E. Jones, P.J. Coleman, Jr., D.S. Colburn, P. Dyal, C.P. Sonett, and A.M.A. Frandsen, The planetary magnetic field and magnetosphere of Jupiter: Pioneer 10, J. Geophys. Res., 79, 3501, 1974.
- Smith, E.J., L. Davis, Jr., D.E. Jones, P.J. Coleman, Jr., D.S. Colburn, P. Dyal, and C.P. Sonett, Jupiter's magnetic field, magnetosphere, and interaction with the solar wind: Pioneer 11, Science, 188, 451, 1975.
- Smith, E.J., and J.H. Wolfe, Fields and plasmas in the outer solar system, Space Sci. Rev., 23, 217, 1979.
- Smith, E.J., L. Davis, Jr., D.E. Jones, P.J. Coleman, Jr., D.S. Colburn, P. Dyal, and C.P. Sonett, Saturn's magnetic field and magnetosphere, Science, 207, 407, 1980a.
- Smith, E.J., L. Davis, Jr., D.E. Jones, P.J. Coleman, Jr., D.S. Colburn, P. Dyal, and C.P. Sonett, Saturn's magnetosphere and its interaction with the solar wind, 85, 5655, 1980b.
- Smith, Z.K., M. Dryer, R.W. Fillius, E.J. Smith, and J.H. Wolfe, -013 Compression of Jupiter's magnetosphere by the solar wind: Reexamination via MHD simulation of evolving corotating interaction regions, J. Geophys. Res., 86, 6773, 1981.
- Sonnerup, B.U.O., E.J. Smith, B.T. Tsurutani, and J.H. Wolfe, Structure of Jupiter's magnetopause: Pioneer 10 and 11 observations, J. Geophys. Res., 86, 3321, 1981.

- Spreiter, J.R., A.L. Summers, and A.Y. Alksne, Hydromagnetic flow around the magnetosphere, Planet. Space Sci., 14, 223, 1966.
- Spreiter, J.R., and A.W. Rizzi, Aligned MHD solution for solar wind flow past the earth's magnetosphere, Acta Astronautica, 1, 15, 1974.
- Spreiter, J.R., and S.S. Stahara, A new predictive model for determining solar wind-terrestrial planet interactions, J. Geophys. Res., 85, 6769, 1980.
- Spreiter, J.R., and S.S. Stahara, Napa Conference Review, 1984.
- Stahara, S.S., D. Klenke, B.C. Trudinger, and J.R. Spreiter, Application of advanced computational procedures for modeling the solar wind interaction with Venus - Theory and computer code, NASA CR-3267, 1980.
- Suess, S.T., and B.E. Goldstein, Compression of the Hermaean magnetosphere by the solar wind, J. Geophys. Res., 84, 3306, 1979.
- Wallis, M.K., Weakly shocked flows of the solar wind plasma through the atmospheres of comets and planets, Planet. Space Sci., 21, 1647, 1973.
- Wolf, D.A., and F.M. Neubauer, Titan's highly variable plasma environment, J. Geophys. Res., 87, 881, 1982.
- Wolfe, J.H., J.D. Mihalov, H.R. Collard, D.D. McKibbin, L.A. Frank, and D.S. Intriligator, Pioneer 10 observations of the solar wind interaction with Jupiter, J. Geophys. Res., 79, 3489, 1974.
- Wolfe, J.H., J.D. Mihalov, H.R. Collard, D.D. McKibben, L.A. Frank, D.S. Intriligator, Preliminary results on the plasma environment of Saturn from the Pioneer 11 plasma analyzer experiment, Science, 207, 403, 1980.

## Figure Captions

1. Histograms of sonic and Alfvénic Mach number based upon Pioneer 10 measurements near Jupiter encounter.
2. Histograms of sonic and Alfvénic Mach number based upon Pioneer 11 measurements near Saturn encounter.
3. Pioneer and Voyager spacecraft trajectories at Jupiter and Saturn encounter in cylindrical planetocentric coordinates.
4. Fits to the Jovian bow shock crossings with and without corrections for upstream dynamic pressure.
5. Fits to the Jovian magnetopause with and without corrections for external pressure.
6. Subsolar location of the Jovian bow shock and magnetopause as functions of upstream dynamic pressure.
7. Fits to the Saturnian bow shock crossings with and without corrections for upstream dynamic pressure.
8. Fits to the Saturnian magnetopause crossings with and without corrections for external pressure.
9. Subsolar location of the Saturnian bow shock and magnetopause as functions of upstream dynamic pressure.
10. Upper and lower limits on the location of the outbound Voyager 1 magnetopause crossing at Saturn after correction is made for external pressure. Dashed line is the extrapolated best fit to the pressure corrected dayside magnetopause surface.
11. A comparison of the shapes of all planetary bow shock and magnetopause surfaces determined thus far.
12. A comparison of magnetosheath boundaries at Earth, Jupiter, and Saturn.
13. Histograms of Pioneer 10 solar wind dynamic pressure measurements near Jupiter encounter and the corresponding magnetopause positions relative to the Galilean satellites.
14. Histograms of Pioneer 11 solar wind dynamic pressure measurements near Saturn encounter and the corresponding magnetopause positions relative to the major satellites and the E-ring.
15. Observational models of the Jovian bow shock and magnetopause are compared with the predictions of high Mach number gasdynamic theory (dashed lines).

16. Observational models of the Saturnian bow shock and magnetopause are compared with the predictions of high Mach number gasdynamic theory (dashed lines).
17. A conceptual representation of magnetopause shape in the terminator plane based upon observations at the Earth, theoretical magnetic field models at Jupiter, and interpretation of gasdynamic modeling results for Saturn.
18. A conceptual picture of the solar wind interaction with Titan when it is directly upstream of Saturn based upon a gasdynamic of the Titan flow pattern.

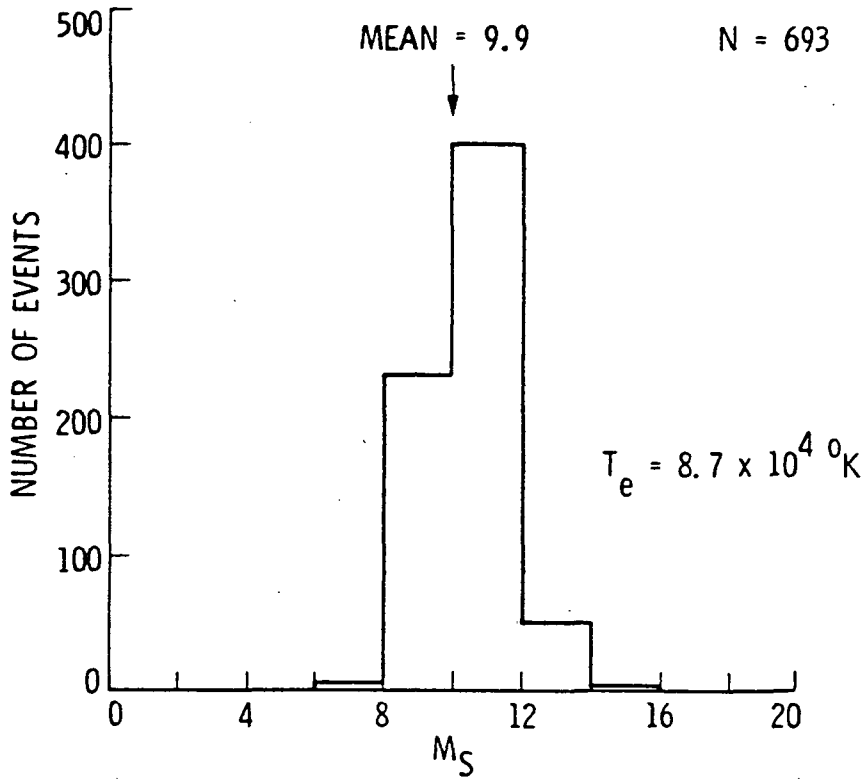
TABLE 1. INTERPLANETARY CONDITIONS

PLANET	R(AU)	V <sub>SW</sub> (KM/S)	N <sub>P</sub> (CM <sup>-3</sup> )	B (NT)	T <sub>P</sub> (10 <sup>4</sup> °K)	T <sub>E</sub> (10 <sup>4</sup> °K)
MERCURY	0.31	430	73.	46.	17.	22.
	0.47	430	32.	21.	13.	19.
VENUS	0.72	430	14.	10.	10.	17.
EARTH	1.0	430	7.0	6.0	8.0	15.
MARS	1.5	430	3.1	3.4	6.1	13.
JUPITER	5.2	430	0.26	0.83	2.7	8.7
SATURN	9.6	430	0.076	0.44	1.8	7.1
URANUS	19.1	430	0.019	0.22	1.1	5.6
NEPTUNE	30.2	430	0.0077	0.14	0.82	4.8
SCALING	----	R <sup>0</sup>	R <sup>-2</sup>	(2R <sup>-2</sup> +2) <sup>1/2</sup> /2R	R <sup>-2/3</sup>	R <sup>-1/3</sup>

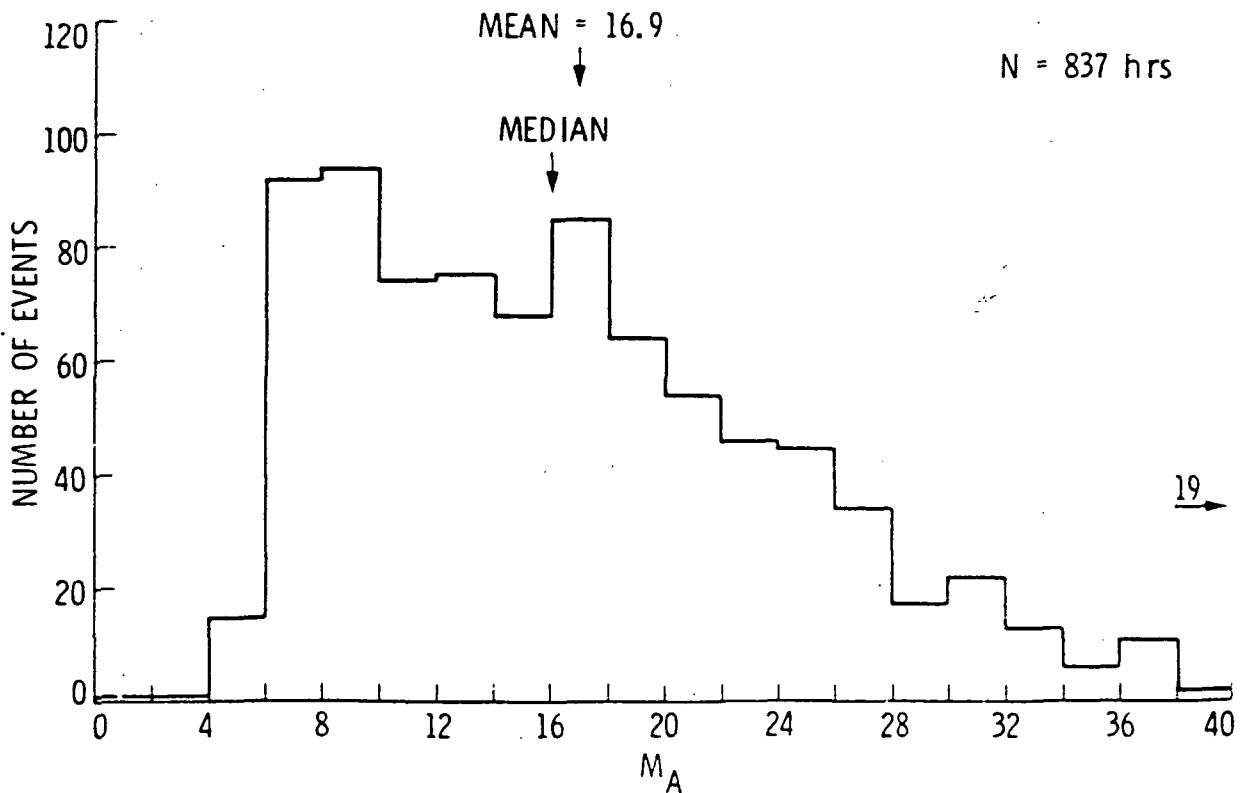
TABLE 2. FLOW PARAMETERS

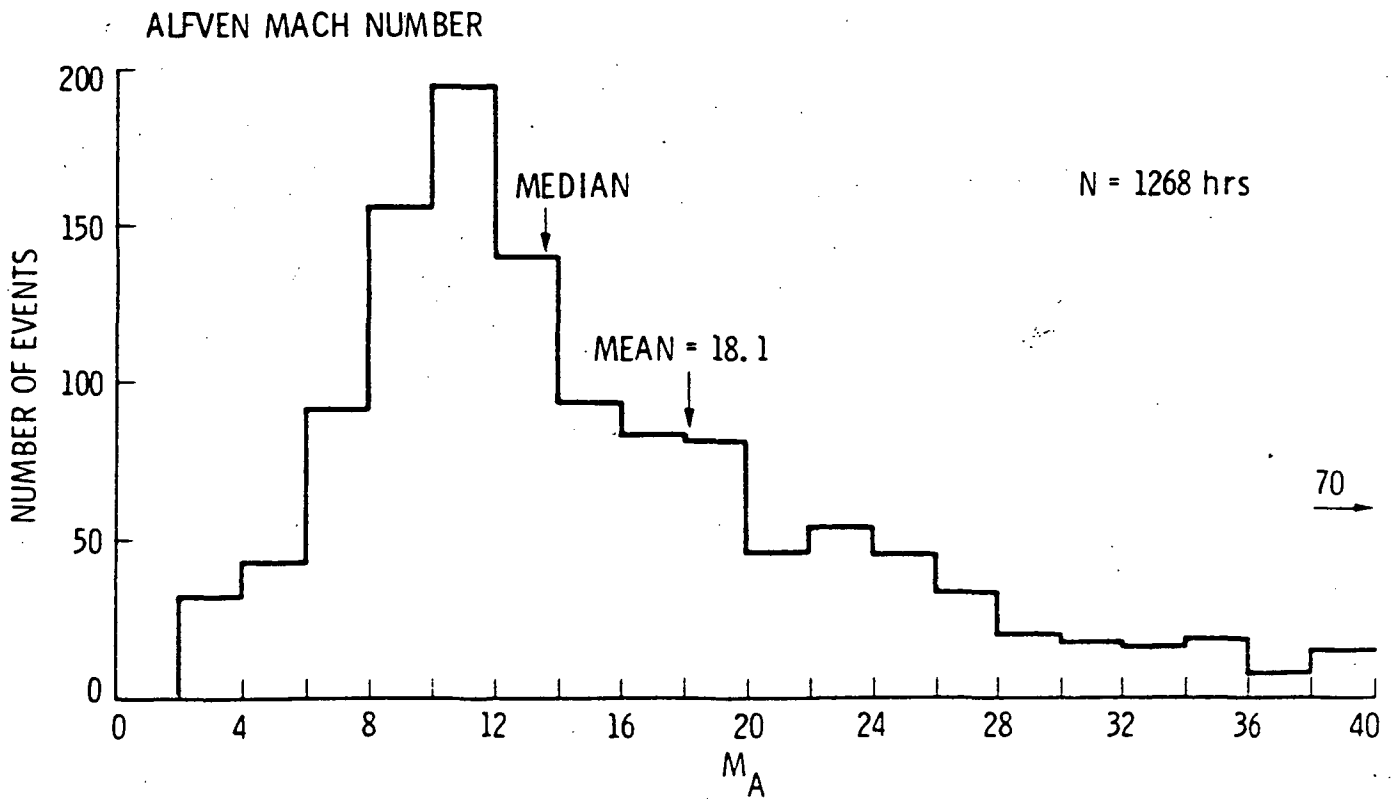
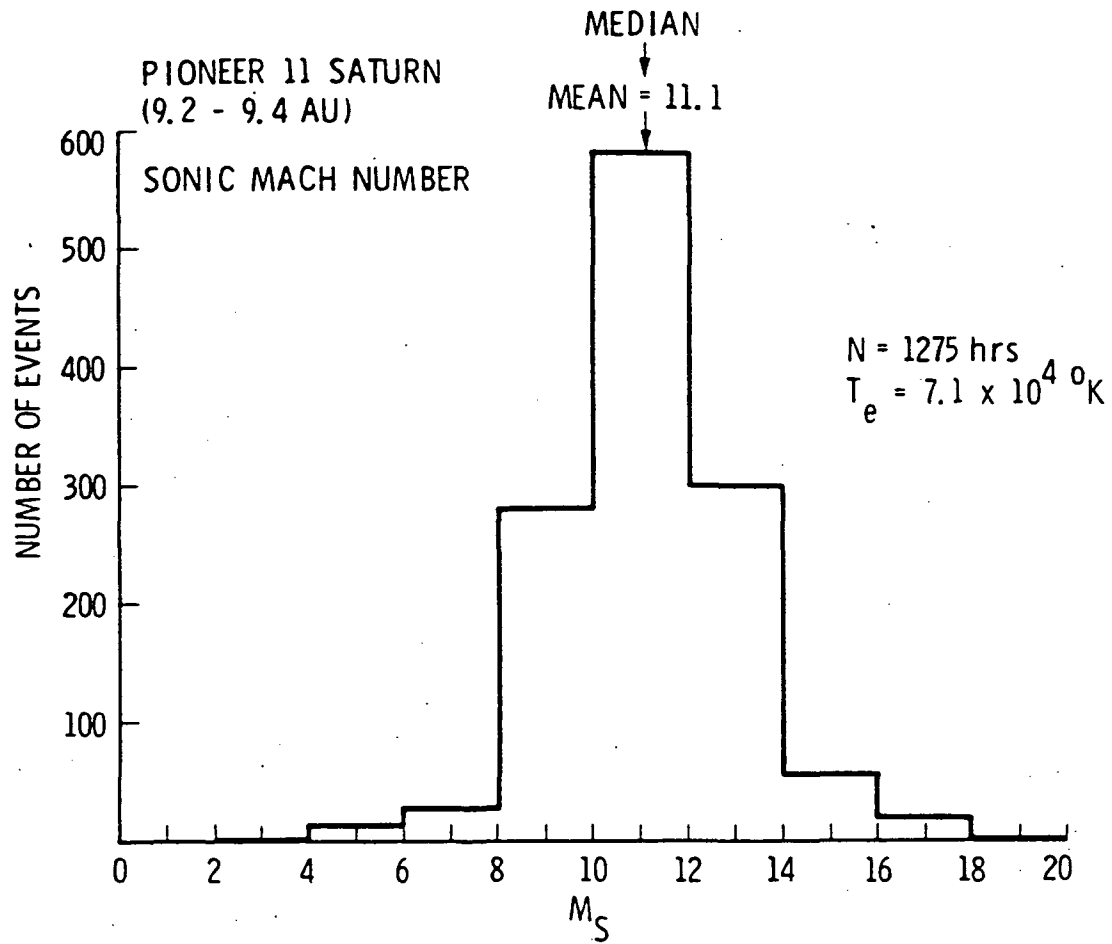
PLANET	R(AU)	$10^{-8} P_{SW}$ (DYNES/CM <sup>2</sup> )	$P_0/P_{SW}$ (%)	$M_S$	$M_A$	SPIRAL ANGLE (°)
MERCURY	0.31	26.	4.9	5.5	3.9	17
	0.47	11.	2.9	6.1	5.7	25
VENUS	0.72	5.	1.9	6.6	7.9	36
EARTH	1.00	2.5	1.5	7.2	9.4	45
MARS	1.52	1.1	1.2	7.9	11.1	57
JUPITER	5.2	0.092	0.78	10.2	13.0	79
SATURN	9.6	0.027	0.65	11.6	13.3	84
URANUS	19.1	0.0069	0.57	13.3	13.3	87
NEPTUNE	30.2	0.0027	0.52	14.6	13.3	88

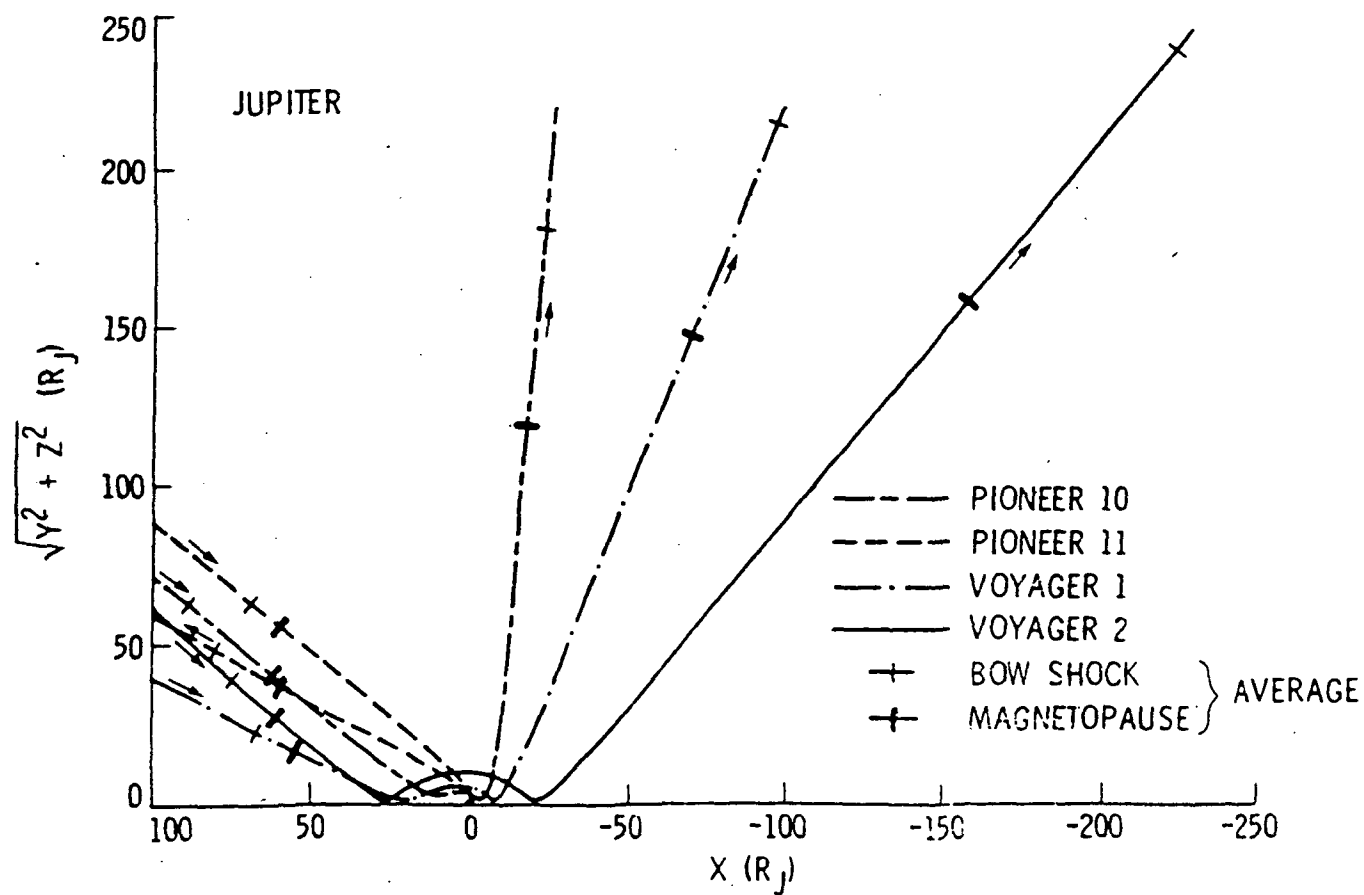
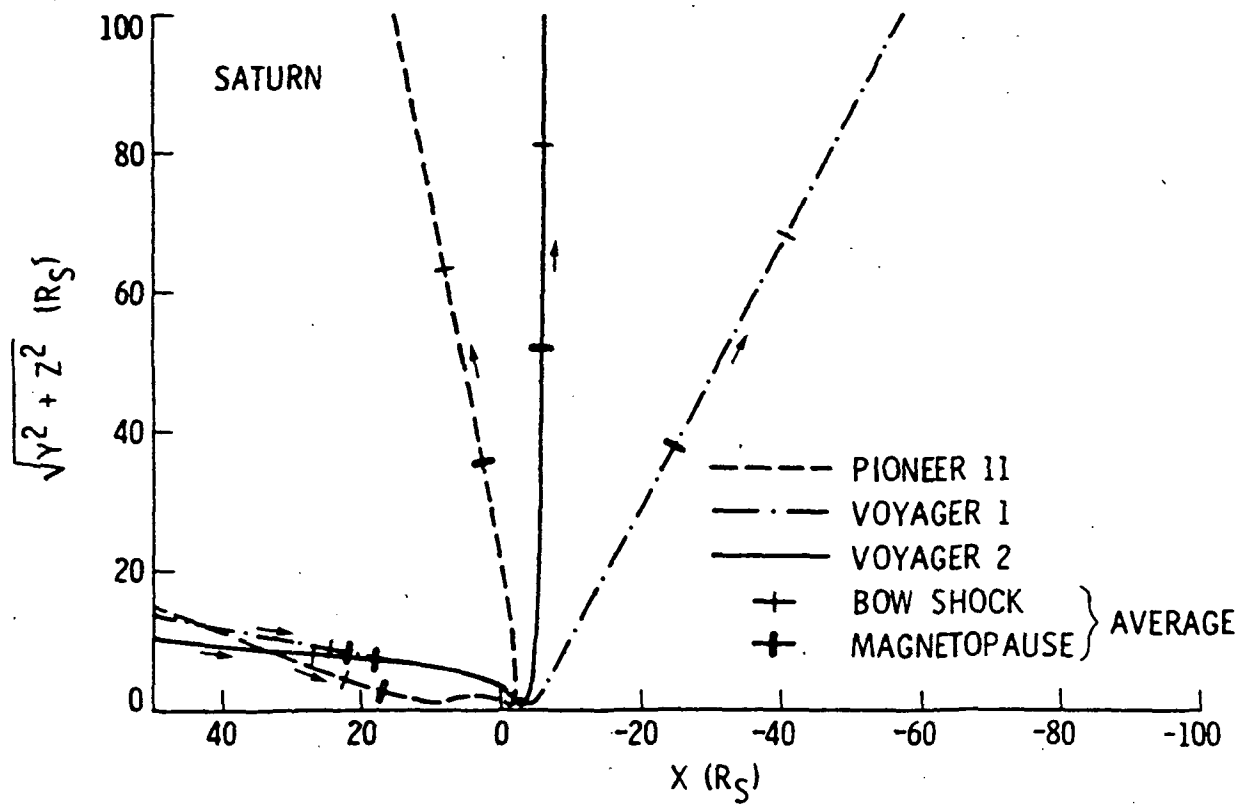
PIONEER 10 JUPITER (4.9 - 5.1 AU)  
SONIC MACH NUMBER

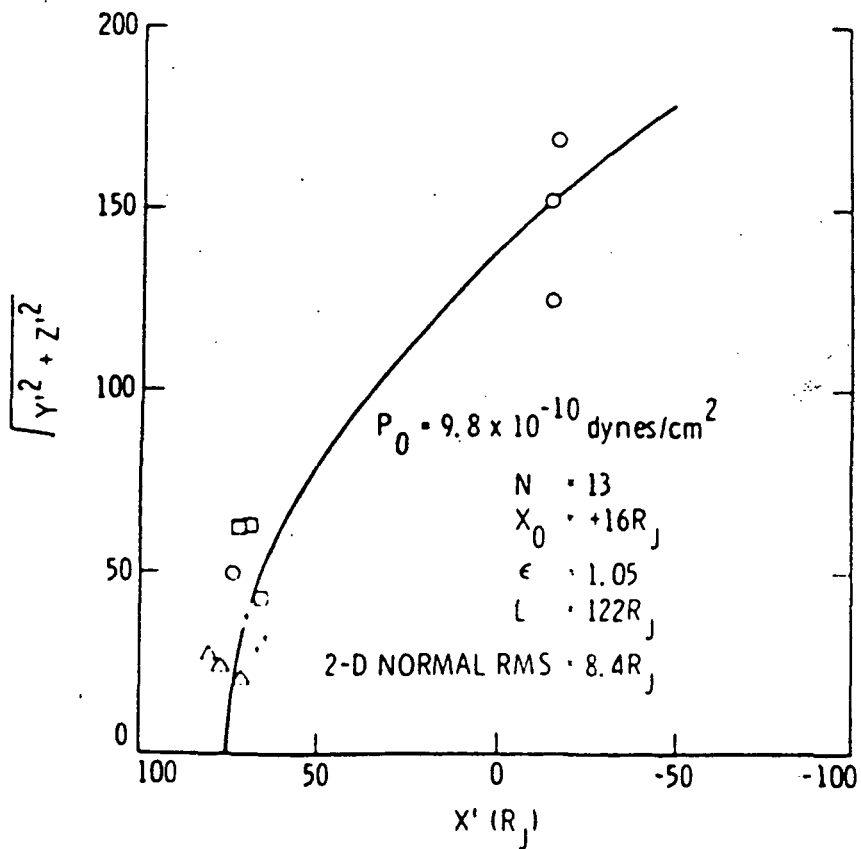
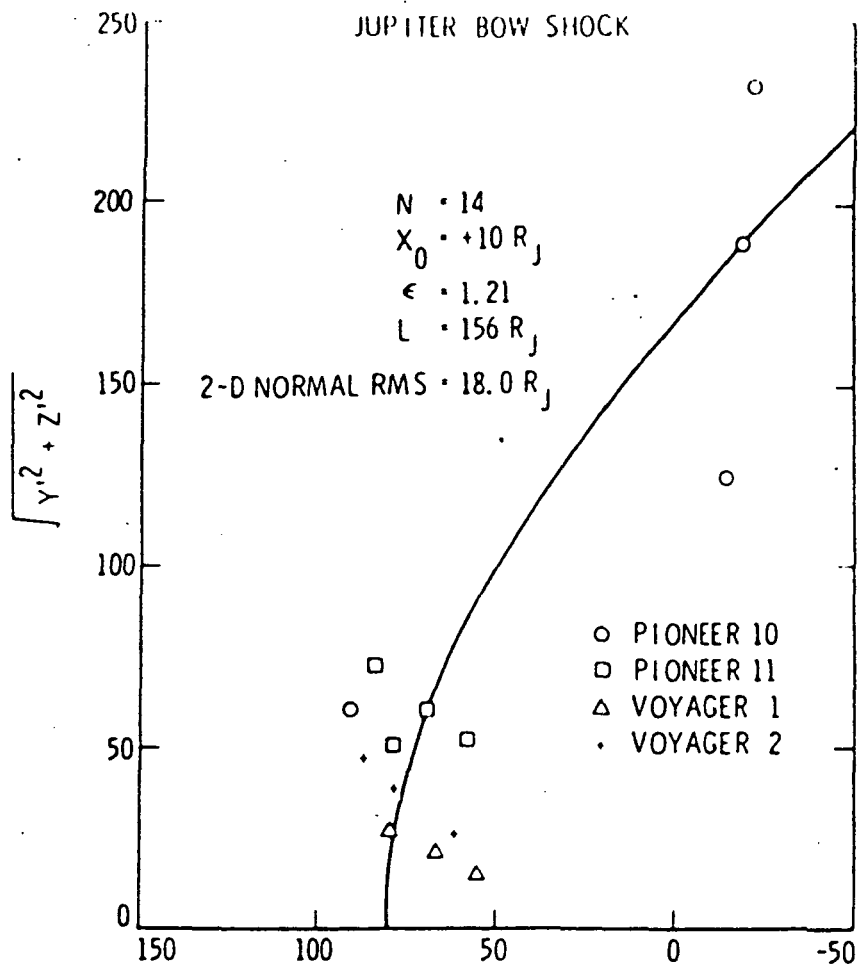


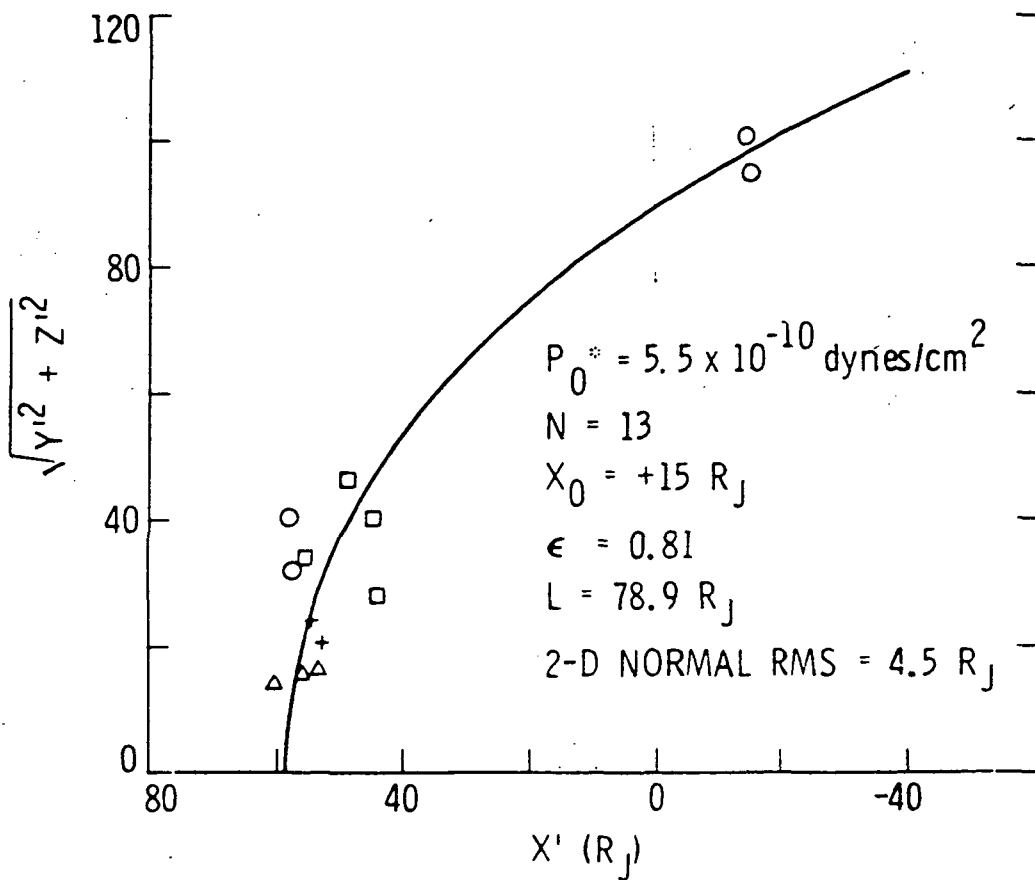
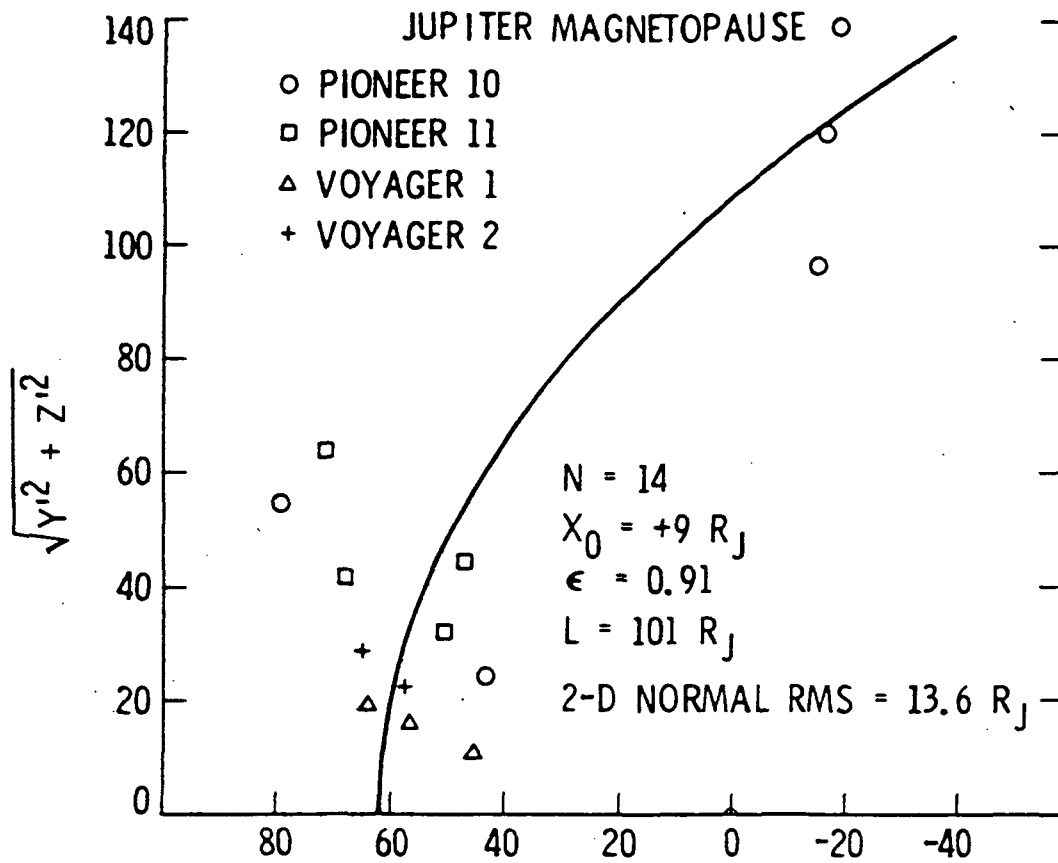
ALFVEN MACH NUMBER

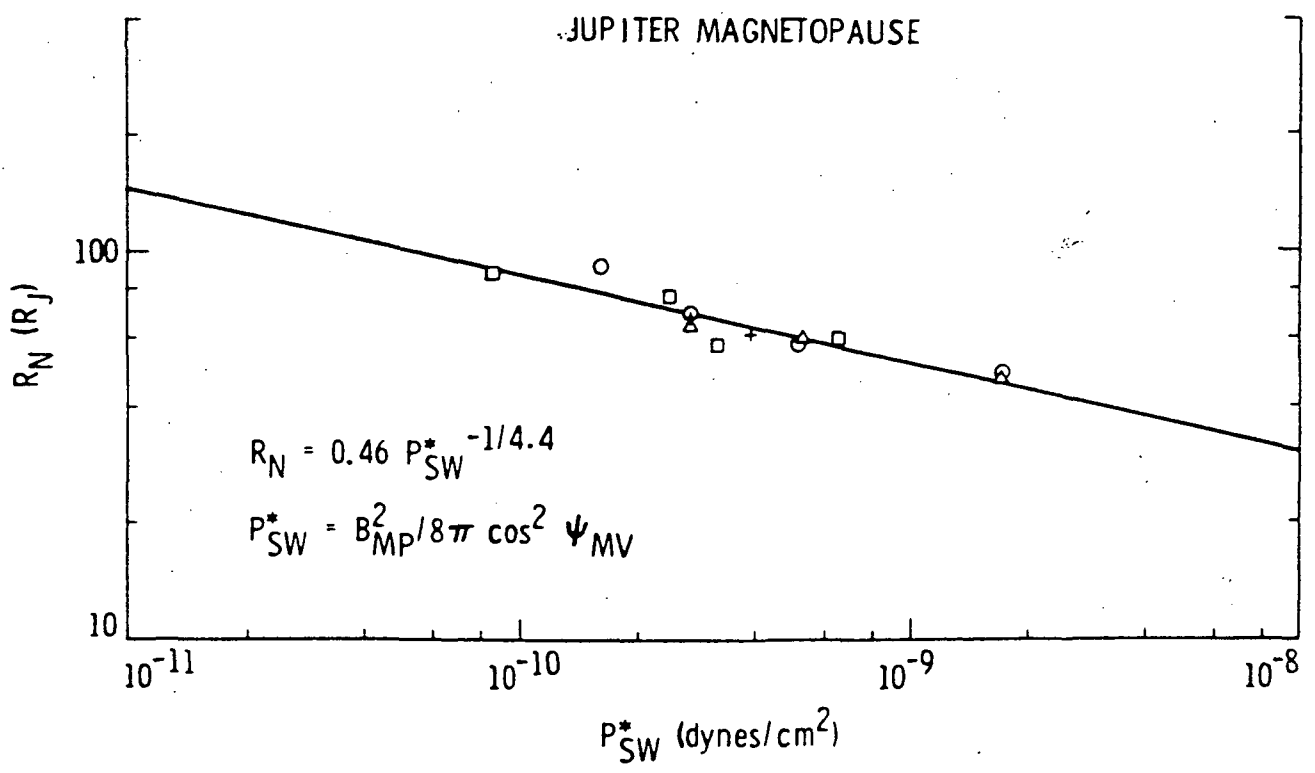
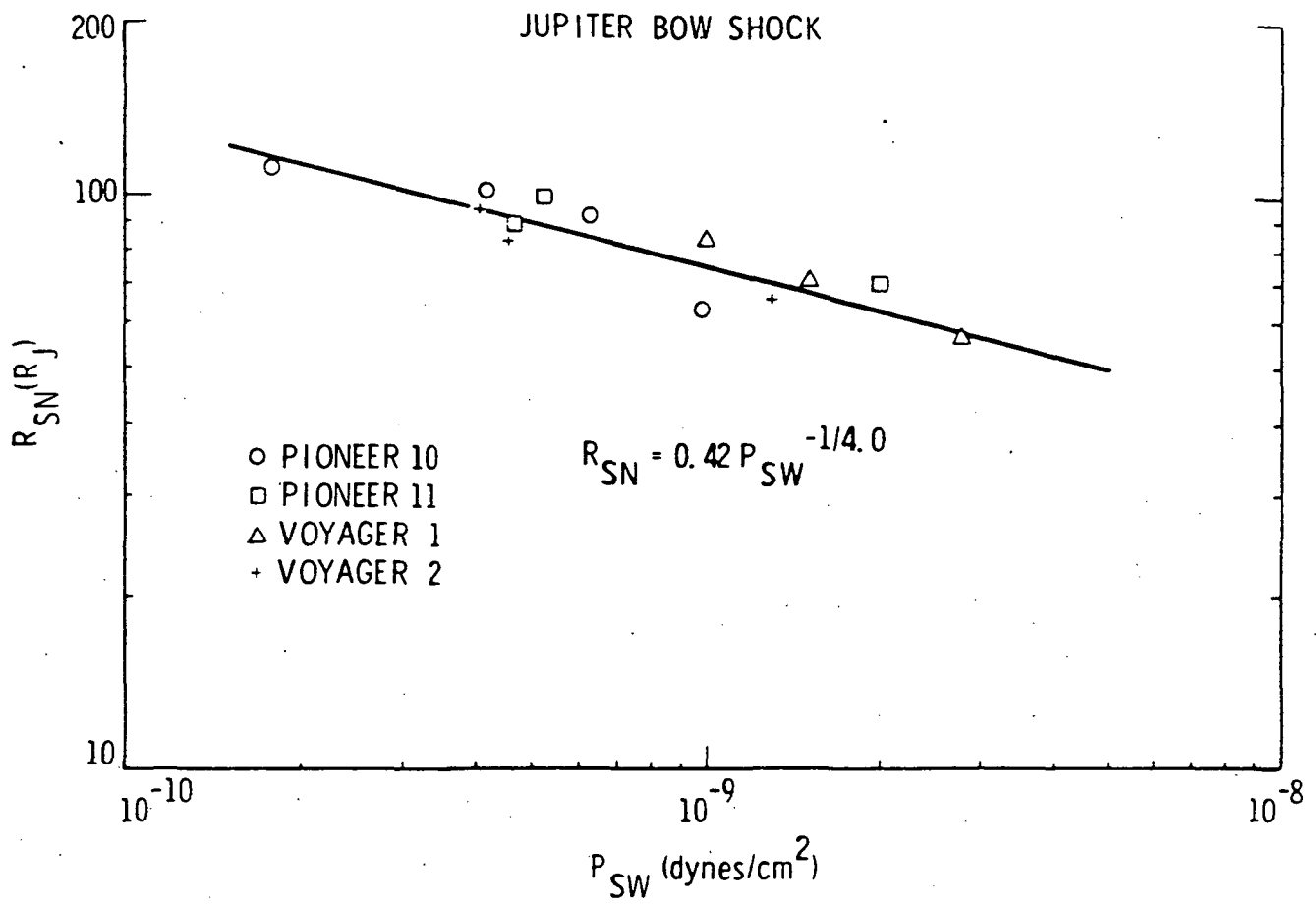


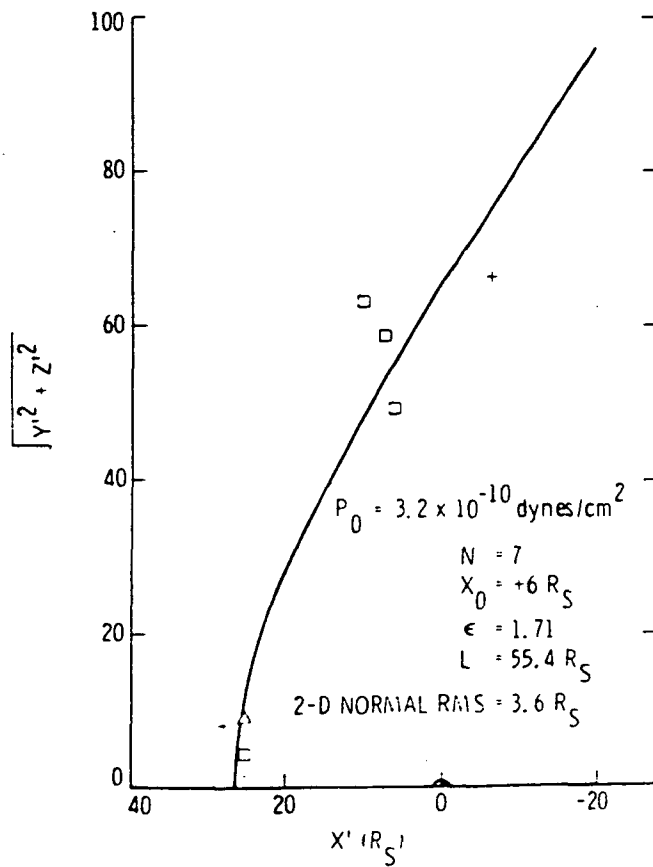
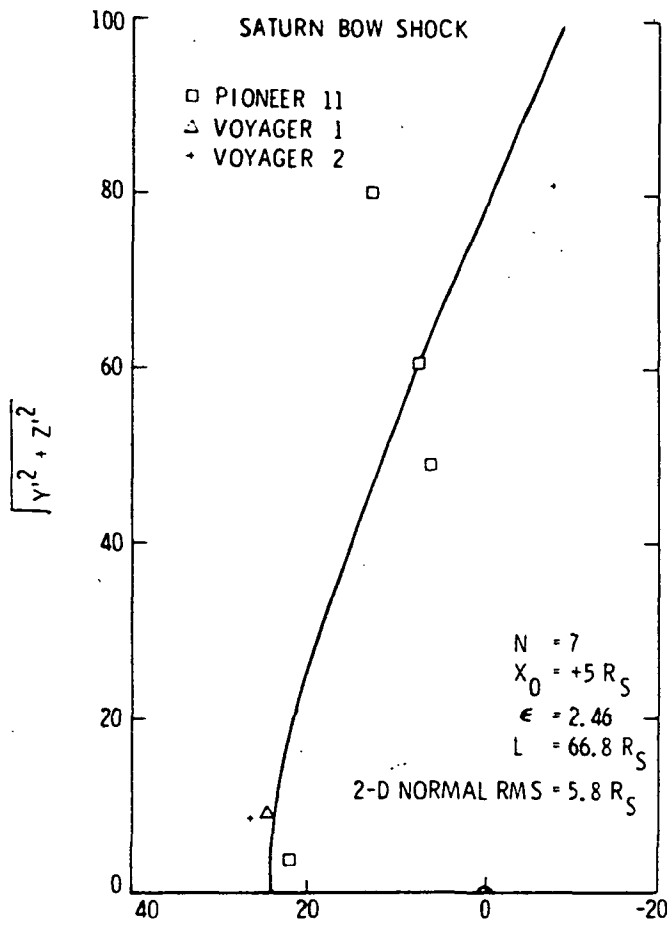


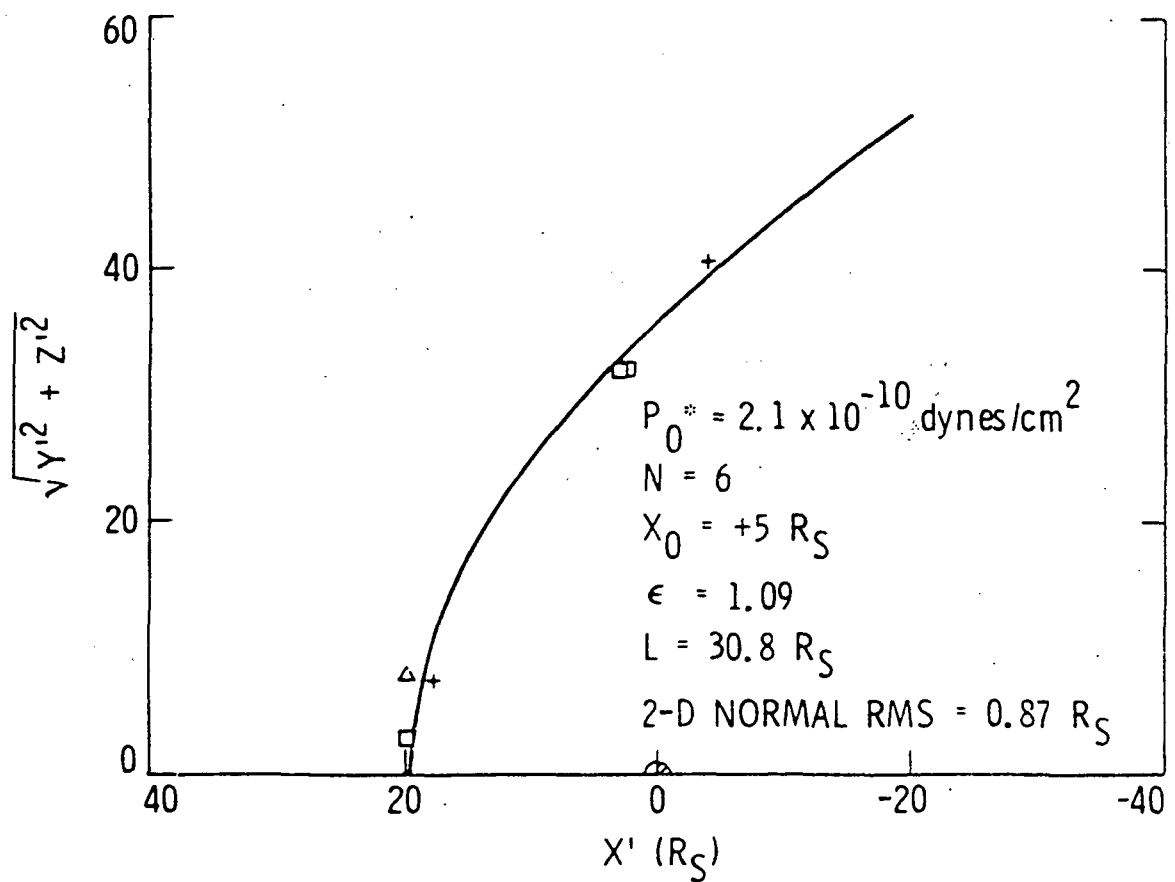
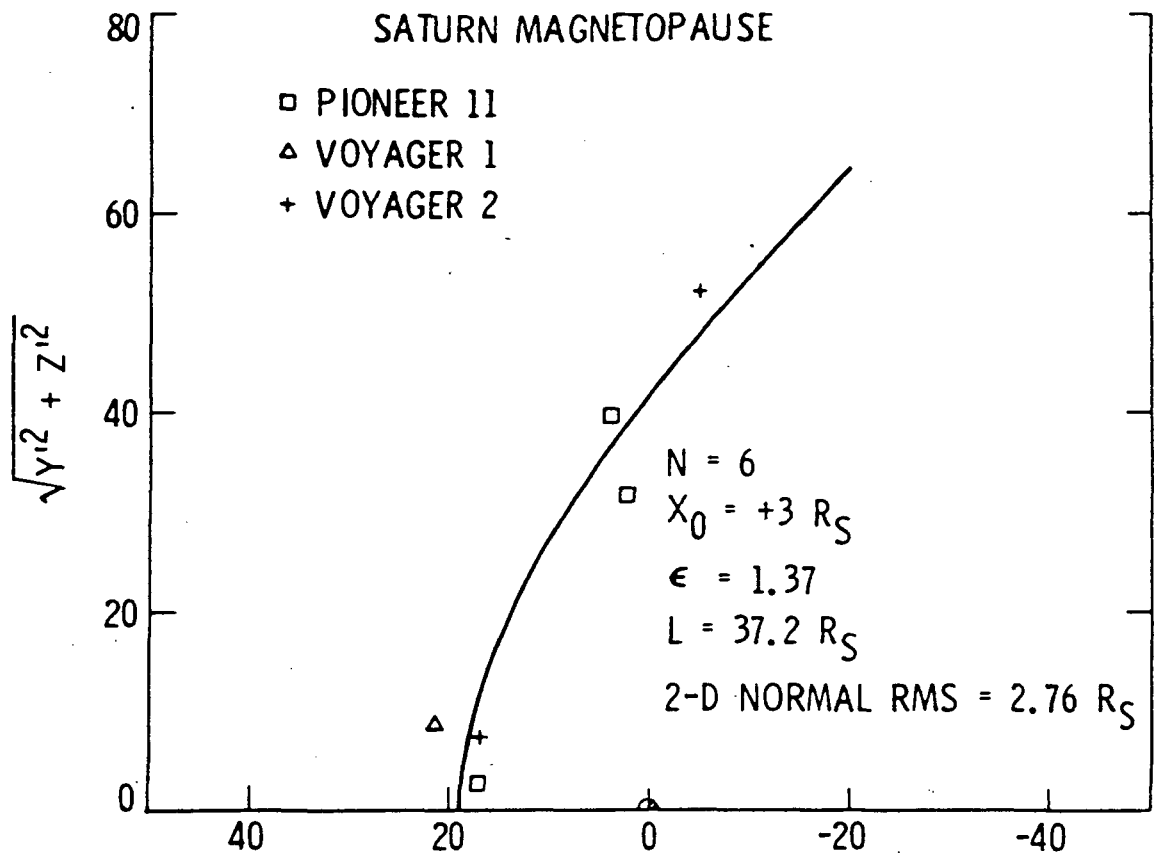


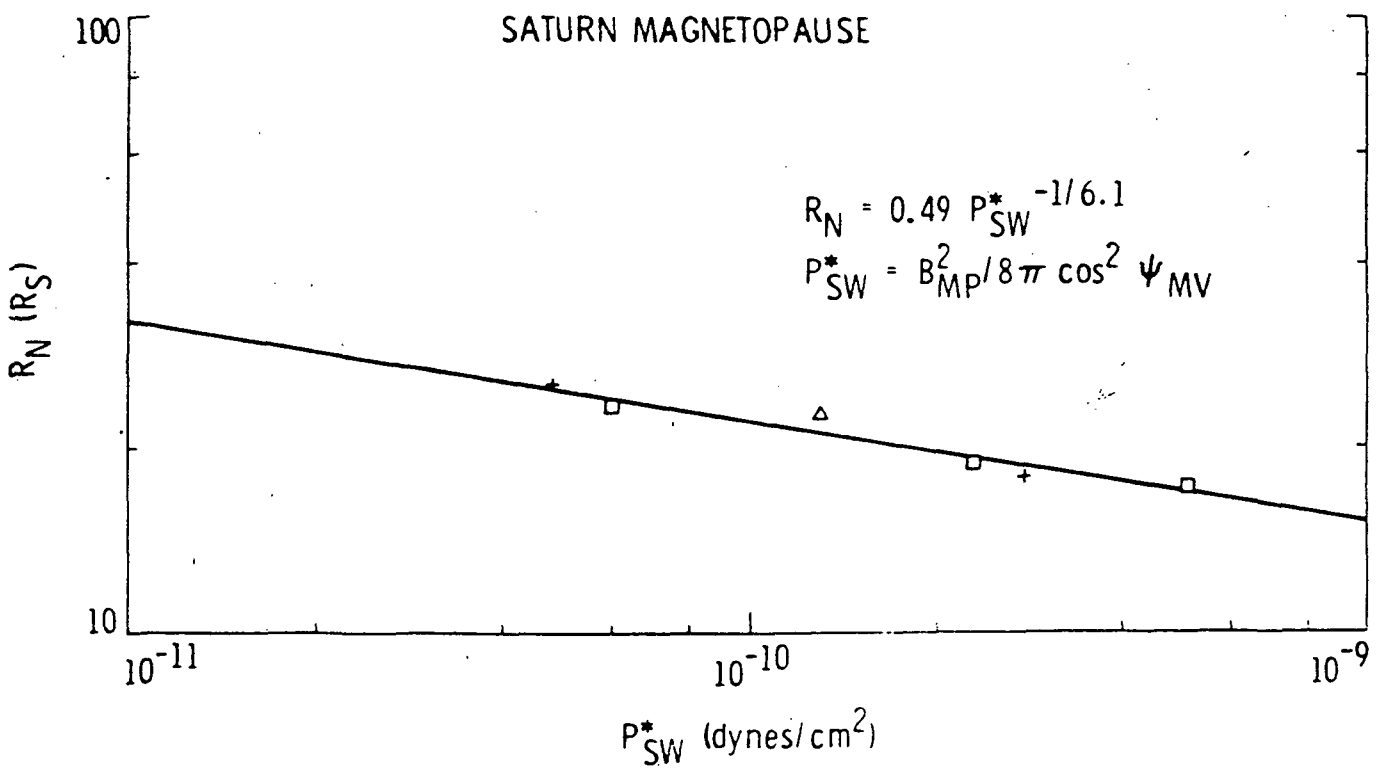
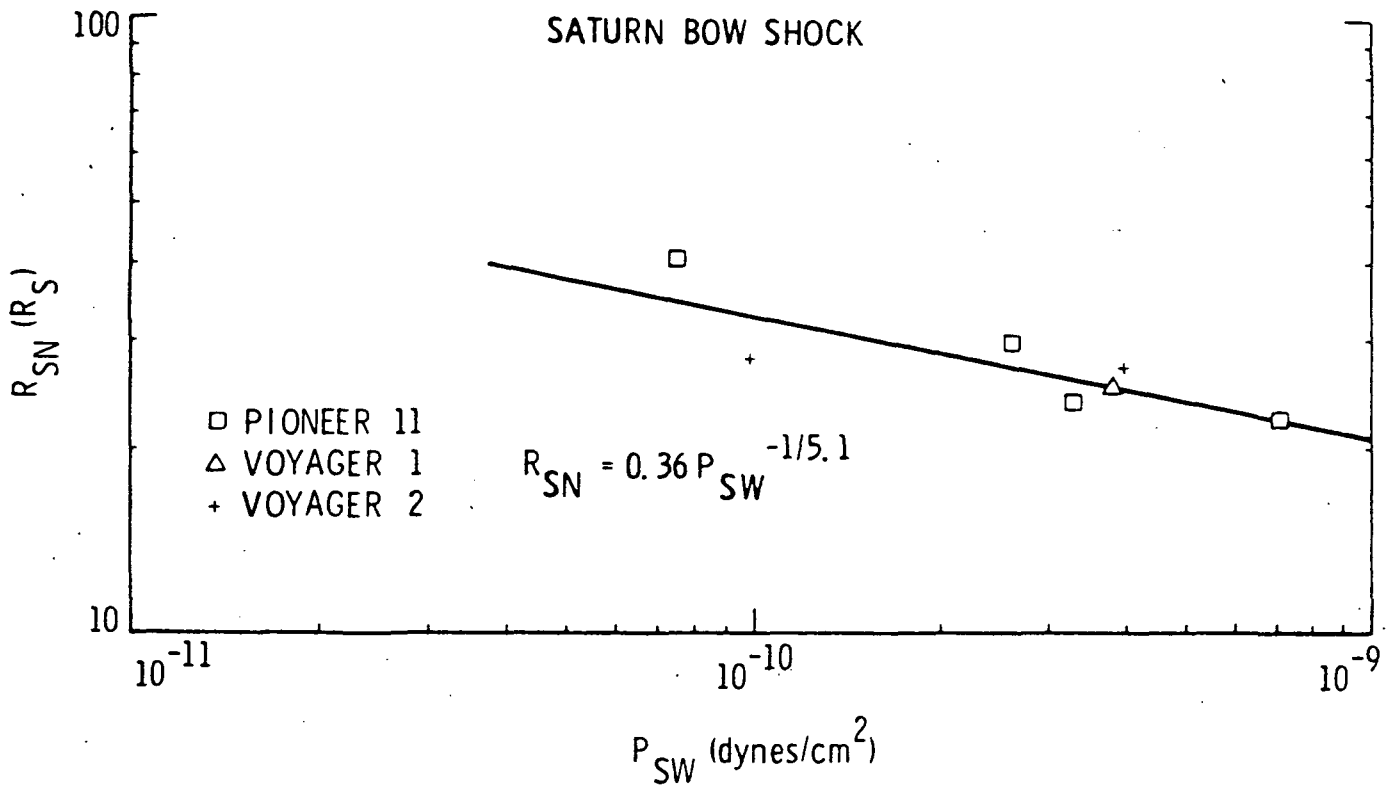


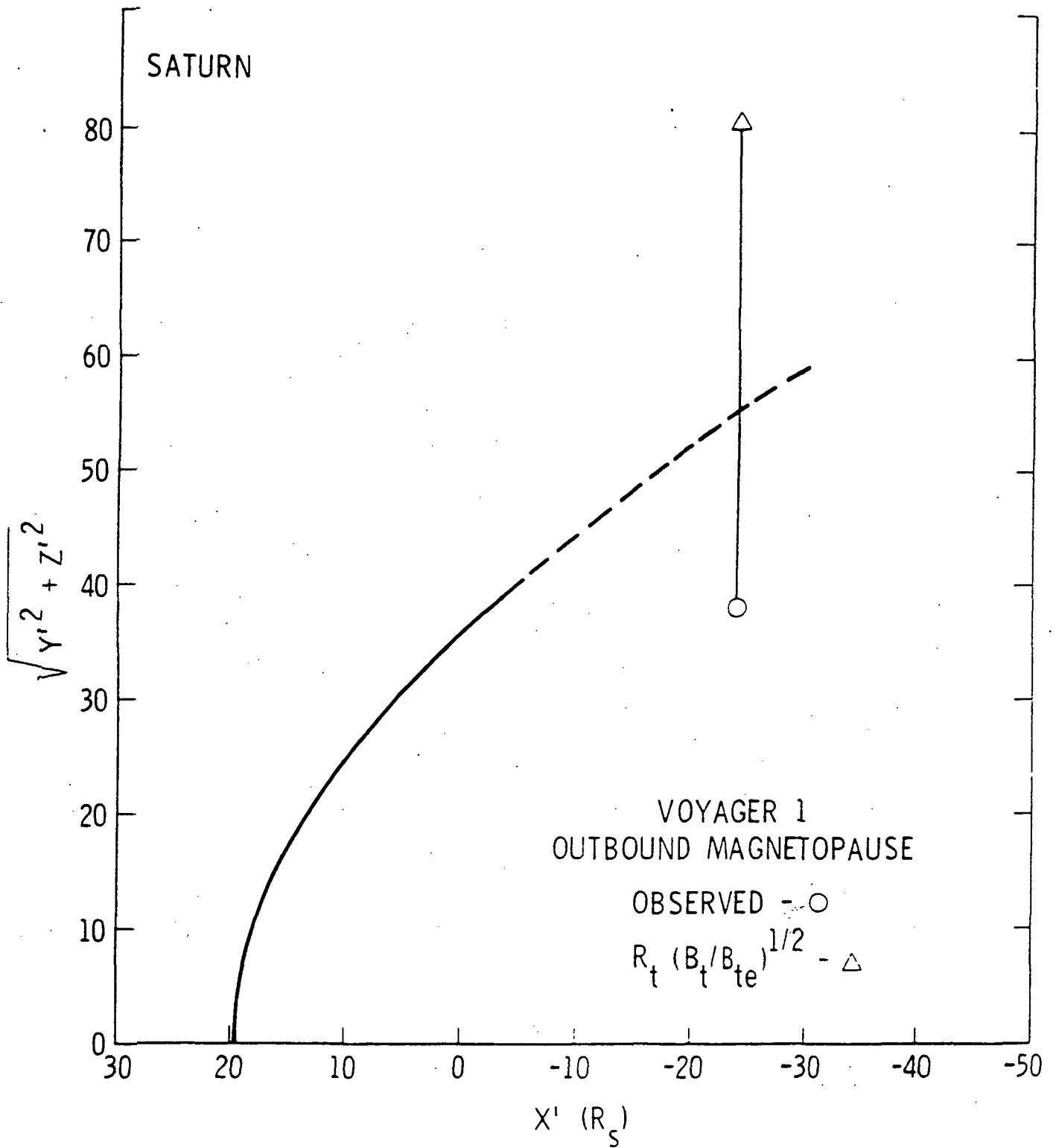


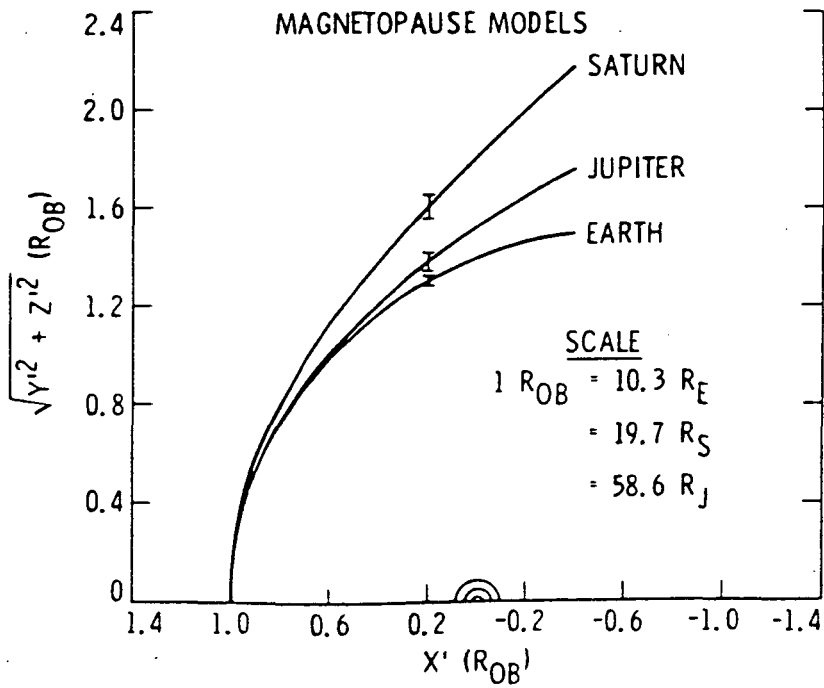
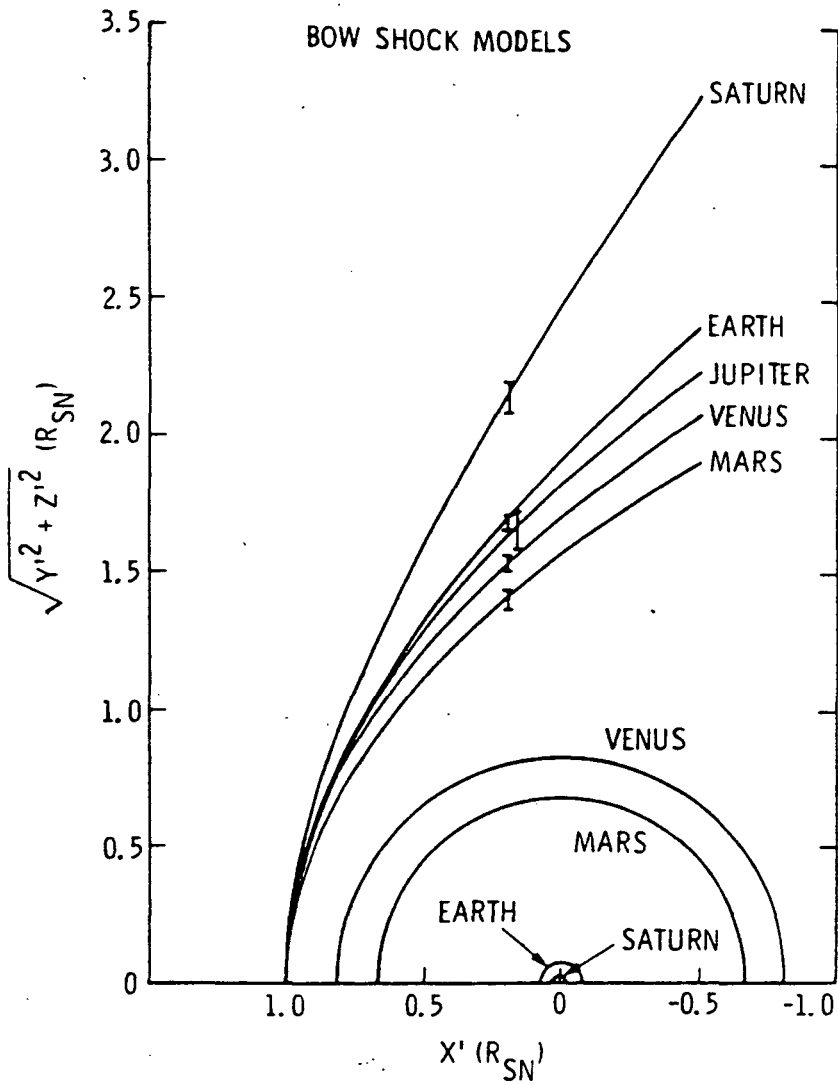




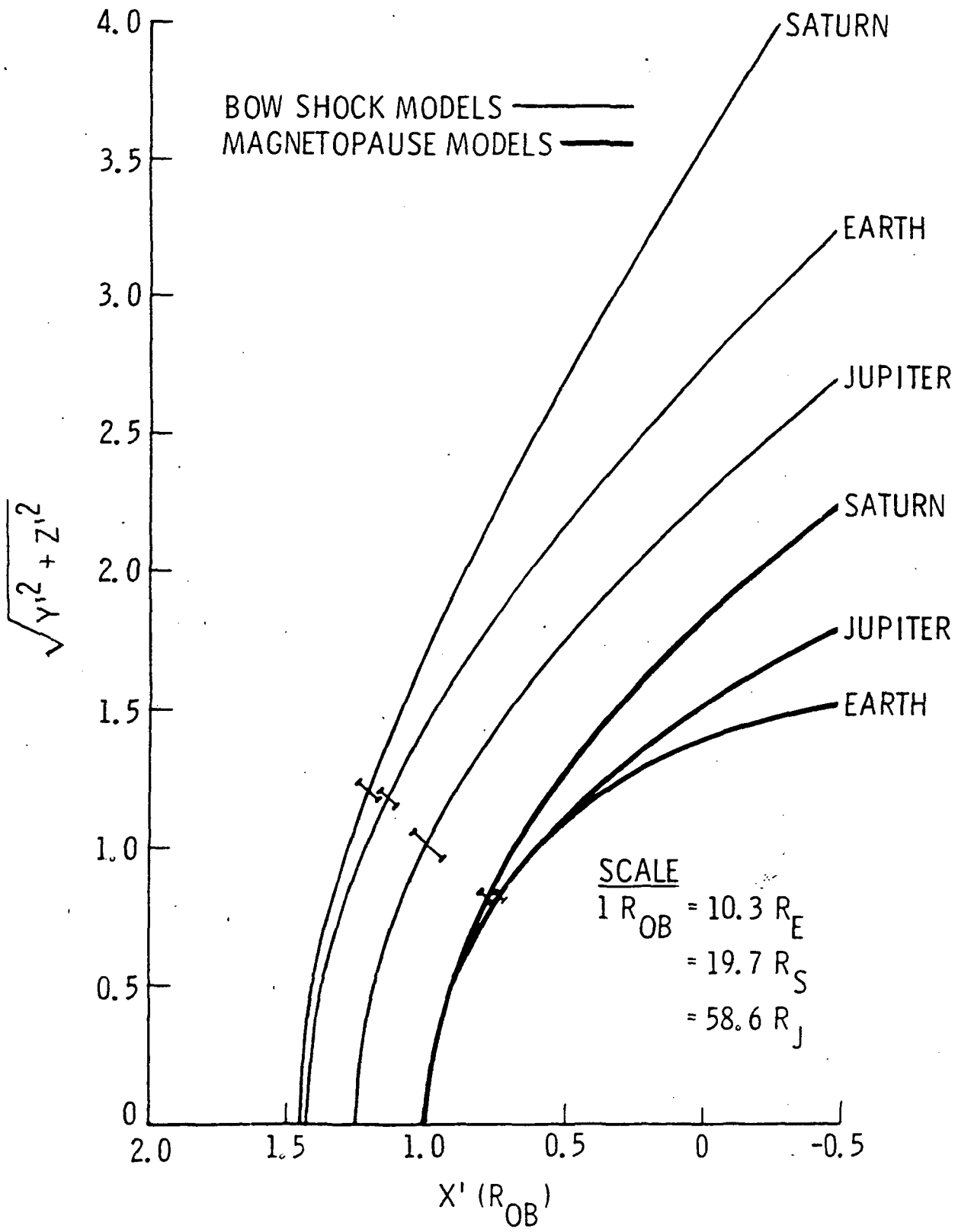




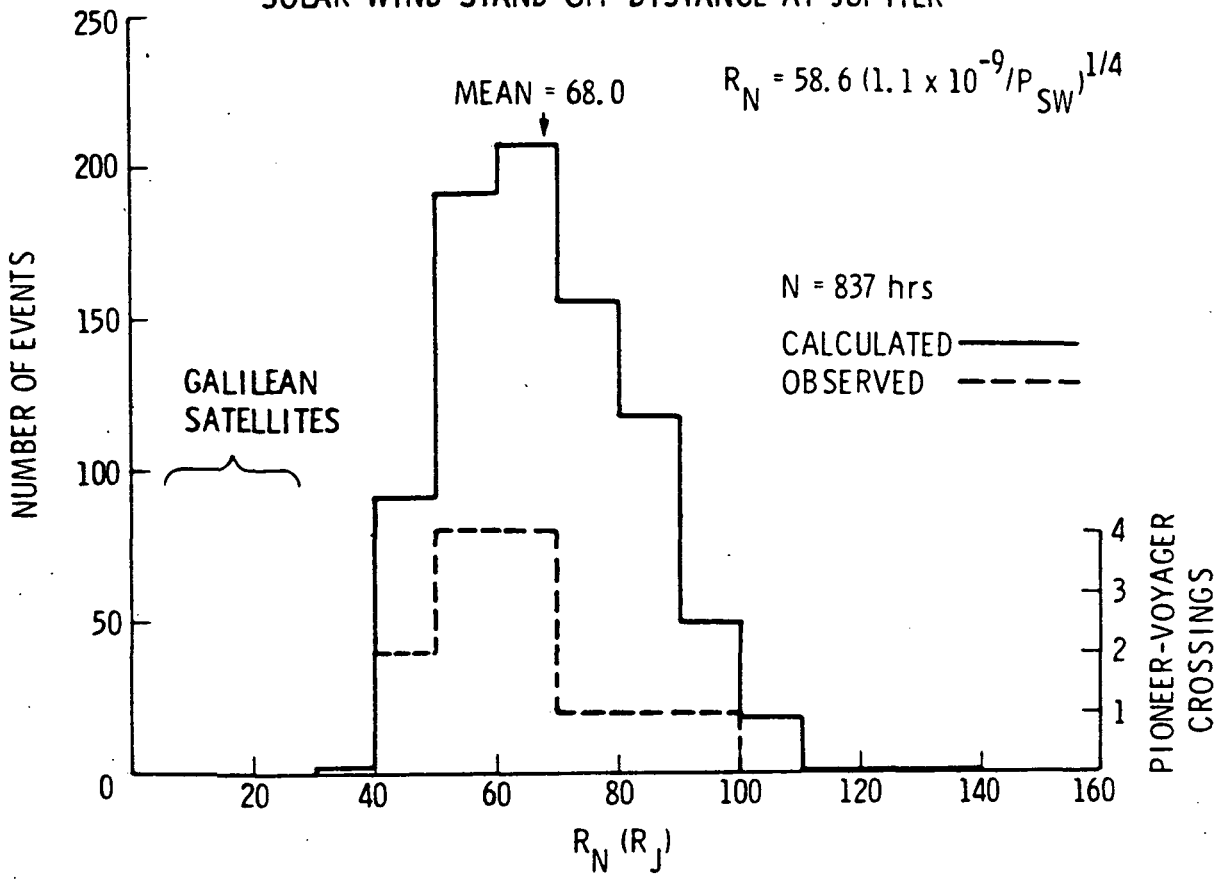




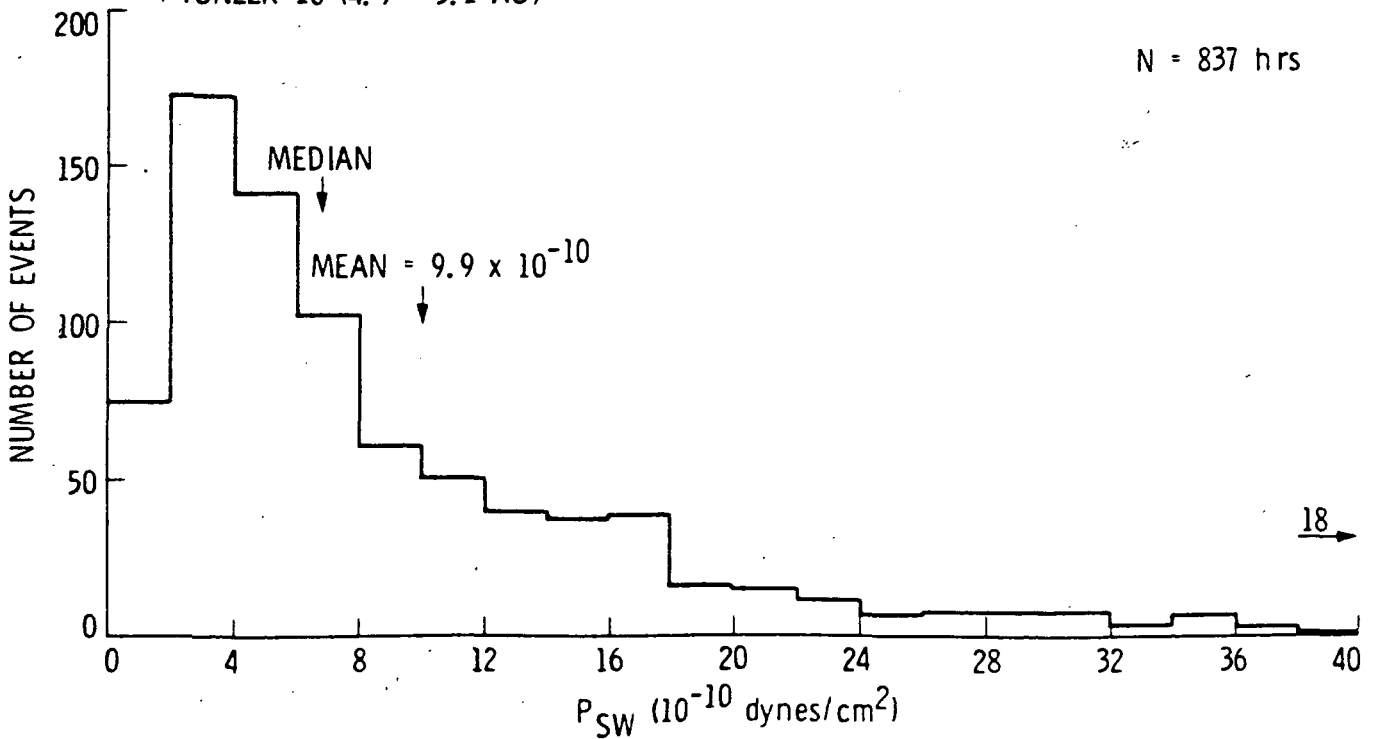
# MAGNETOSHEATH BOUNDARIES

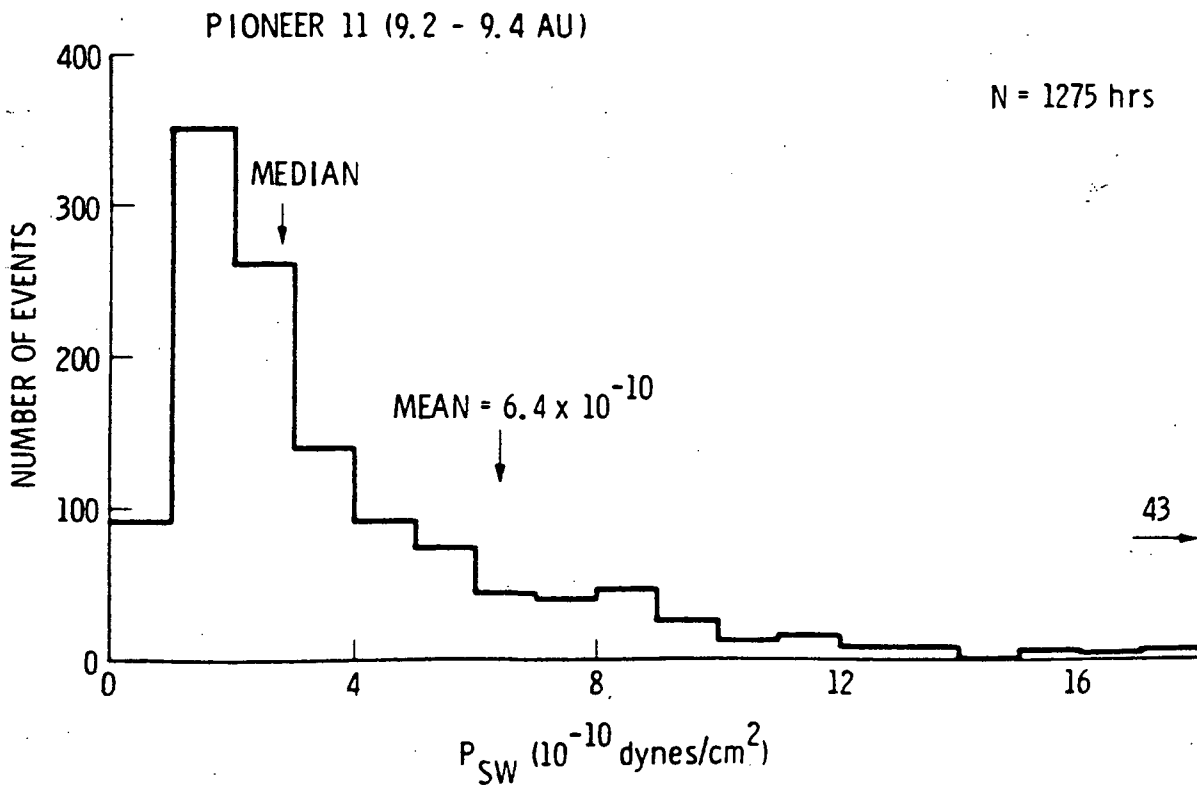
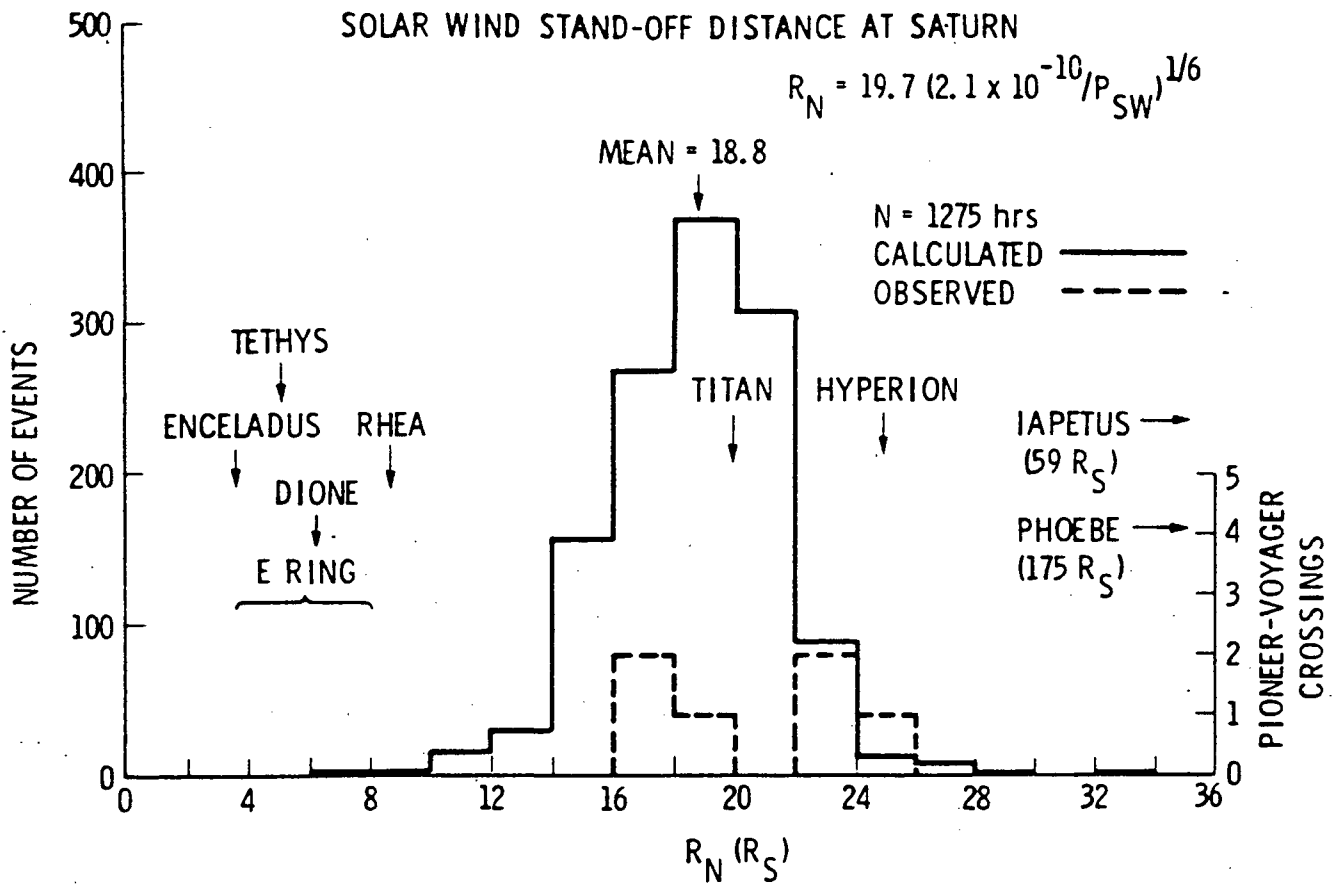


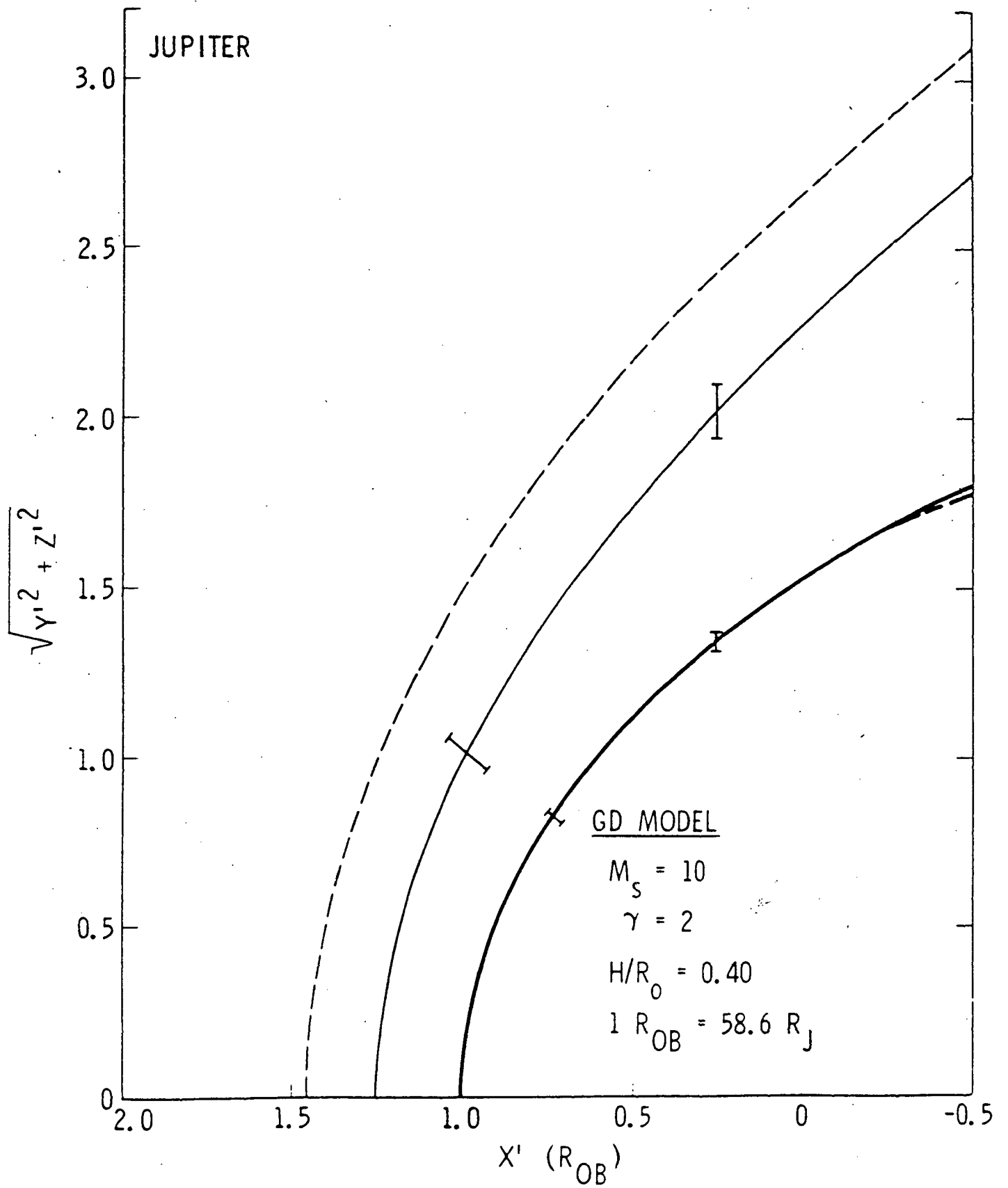
SOLAR WIND STAND-OFF DISTANCE AT JUPITER

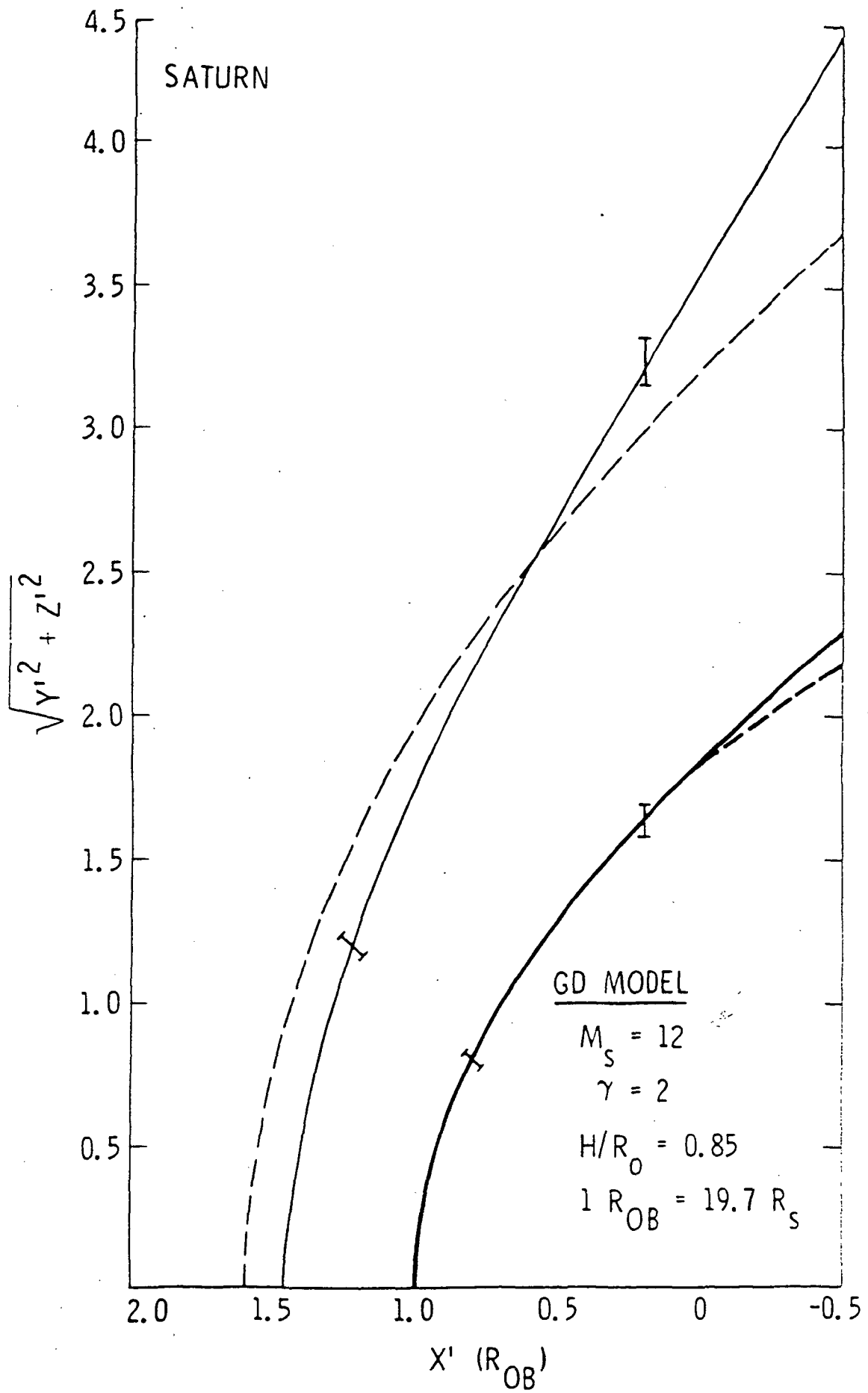


PIONEER 10 (4.9 - 5.1 AU)



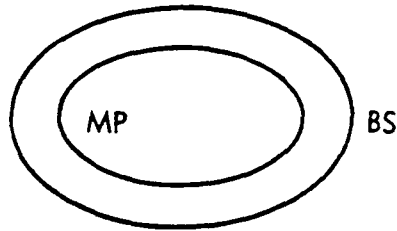






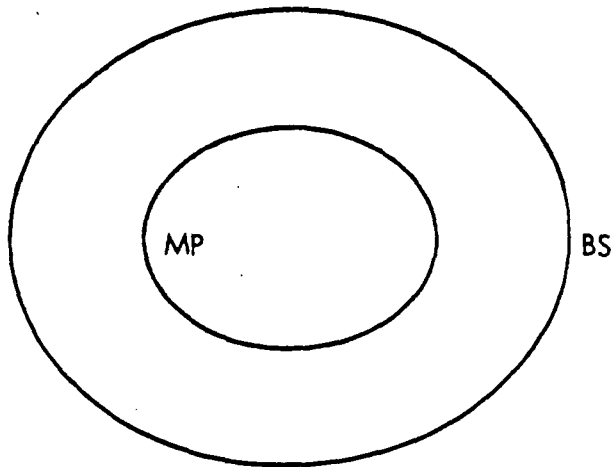
POLAR FLATTENING HIERARCHY

JUPITER



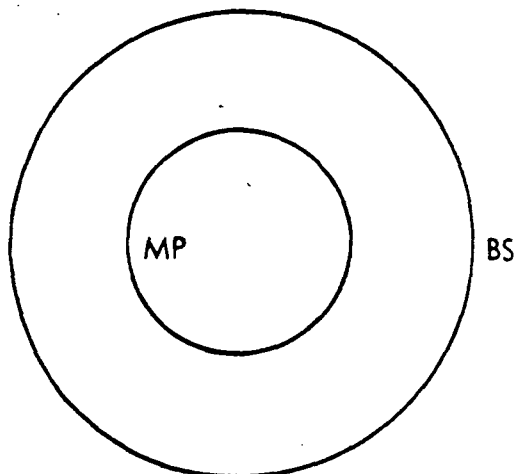
$$\epsilon_J \sim 0.8$$

SATURN



$$\epsilon_E < \epsilon_S < \epsilon_J$$

EARTH



$$\epsilon_E \lesssim 0.2$$

